博士論文

Study on Saturated Flow Boiling CHF using Porous Honeycomb Plate and Irradiation Effect
(ハニカム多孔質体と照射効果を用いた飽和流動沸騰における限界熱流束の研究)

王 来順

STUDY ON SATURATED FLOW BOILING CHF USING POROUS HONEYCOMB PLATE AND IRRADIATION EFFECT

A Thesis

by

Laishun Wang

Submitted to

The University of Tokyo

in partial fulfillment of the requirements for the degree of

Doctor of Philosophy

Department: Nulcear Engineering and Management

August 2017

Contents

Nomenclature

Symbols

$q"$	Surface heat flux [MW/m^2]
k	Thermal conductivity of copper [W/m-K]
ΔT	Temperature difference between different positions [K]
Δx	Distance between different positions [m]
q_{CHF}	Critical heat flux [MW/m^2]
G	Water mass flow flux [kg/m^2-s]
h_{fg}	Heat latent of vaporization [kJ/kg]
ρ_g	Density of vapor [kg/m^3]
ρ_l	Density of liquid [kg/m^3]
σ	Liquid surface tension [N/m]
l	Length of the heater [m]
S_b	Bubble coverage area [m^2]
N	Nucleation sites number
r_a	Average bubble departure diameter [m]
F_D	Drag force [N]
u	Speed of the bubble relative to the fluid [m/s]
C_D	Drag coefficient
A	Cross sectional area [m^2]
u_{max}	Maximum velocity in the channel [m/s]
y	Distance from the channel wall [m]
h	Half of the channel height [m]

List of figures

List of tables

1 Introduction

1.1 Background

1.1.1 In-vessel Retention Strategy

One of the important aims of nuclear power plant safety is to make sure that the high radioactive materials will not escape from the reactor containment and enter outside environment which may throw huge threaten on outside environment and people's health. As is known, nuclear reactor core still needs cooling after the reactor is shut down due to decay heat. However, it may fail to cool down the reactor core after the reactor is shut down due to loss of power or other reasons in some severe accidents conditions. If this happens, nuclear fuel rods in the reactor core may melt down due to lack of effective cooling. The reactor core corium which contains a lot of high radioactive materials may fall down to the bottom of the reactor vessel and then transfers heat to the reactor vessel. When the temperature of reactor vessel exceeds the melting points of its material (usually is carbon steel), the reactor lower head will melt and be damaged at last. Then, the corium will fall the corium will drop down to the concrete base and interact with the concrete, which has happened in Fukushima accidents. This may lead to steam explosion in the containment and increase the risk of radioactive material leakage to outside environment [1]. Besides, the corium may also pollute the underground water. If the reactor core corium can be kept in the Reactor Pressure Vessel which is a closed system during severe accidents, the risk of radioactive material release can be reduced.

In advanced passive pressurized water reactors (such as Westinghouse AP600, AP1000), a key severe accident mitigation strategy is In-vessel Retention (IVR) Strategy. It can also be named as External Reactor Vessel Cooling (ERVC), which means keeping

the integrity of the reactor vessel by external cooling of the reactor pressure vessel. It aims to keep the integrity of the reactor pressure vessel and mitigate the severe accident by building a natural circulation along the out surface of reactor pressure vessel to cool down it. Figure 1-1 is the schematic diagram of IVR. During IVR process, water from In-containment Refueling Water Storage Tank (IRWST) will reach the reactor cavity and submerge lower part of the reactor vessel. As the temperature of reactor vessel out surface is high due to the corium, water will be heated and boil. The density of water will get smaller and water will rise to a higher position as it is heated. So a natural circulation along the out surface of the reactor vessel will be built. As a result, the cooling effective is high enough to cool down the reactor vessel under core melt condition [2].

During IVR process, the most important thing is that Critical Heat Flux (CHF) limit for boiling on the out surface of the reactor vessel should not be reached. If it is reached, it will lead to severe heat transfer degradation. The temperature of reactor vessel will increase dramatically and the reactor vessel will burn out soon. IVR strategy will fail.

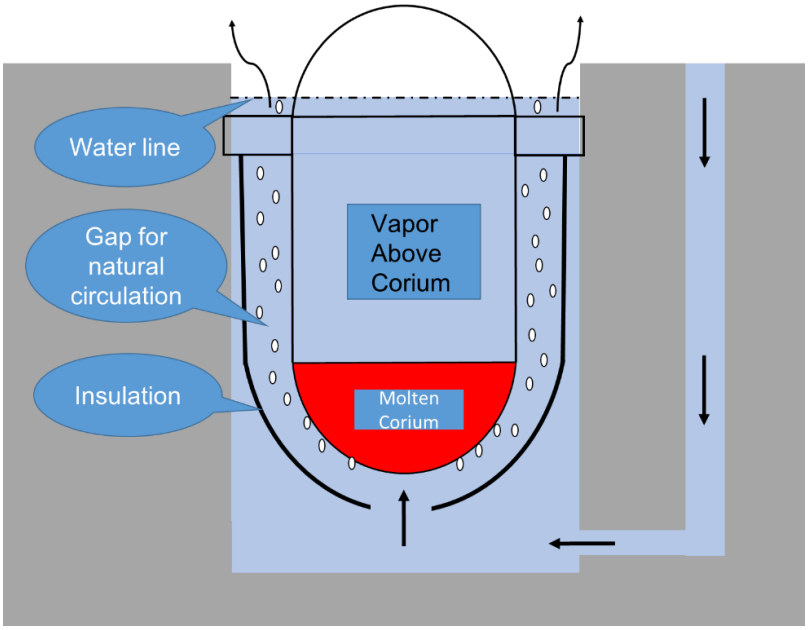

Figure 1-1: Schematic diagram of IVR strategy.

1.1.2 Problem of IVR strategy for future reactors

The IVR strategy is first adopted by Loviisa plant and Westinghouse AP600. To verify the feasibility of IVR in AP600, Theofanous et al. [1] conducted an experimental research in the ULPU facility. Three configurations (Configuration I-III) were adopted. Configuration I only considered part of hemispherical surface (only 0-30°) and pool boiling condition. In Configuration II-III, full curvature (0-90°) of the hemispherical surface and flow boiling condition were considered. Water–steam two-phase flow natural circulation circuit is built outside the heated vessel wall. The scaling of this facility is exact for AP600 except for the slice nature. Experiment results of Configuration II-III shows that the CHF margin is sufficient for AP600.

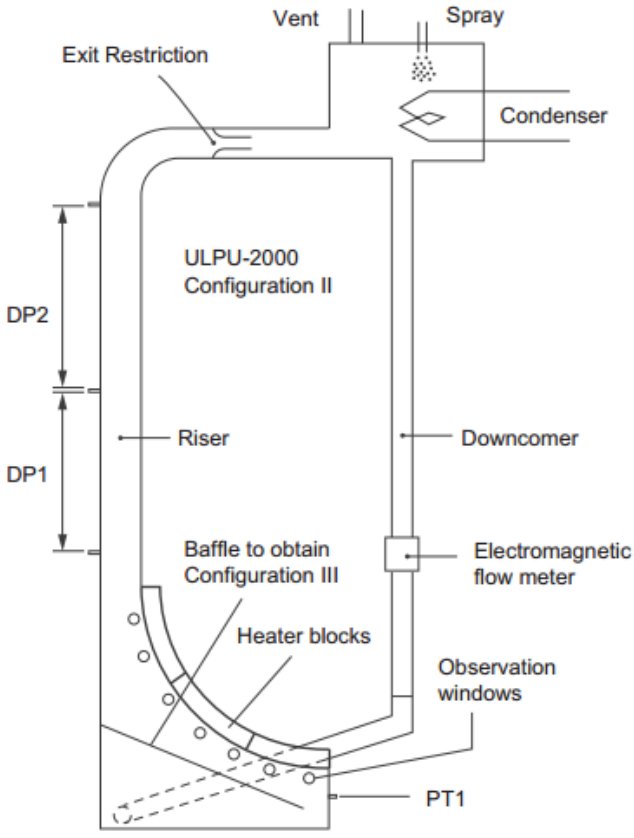

Figure 1-2: Scheme of the ULPU facility: Configuration II and III [1].

The IVR strategy is continually adopted by Westinghouse AP1000. However, for AP1000, as its power is 66% larger than that of AP600 whereas there is no commensurate increase in vessel surface area, there is a need to increase the CHF. Configuration IV and V in ULPU facility were then designed to research the CHF margin for AP1000 is enough or not. The way adopted in configuration IV and V to increase CHF is shaping the flow circuit to increase flow velocity to increase CHF value. Configuration IV for AP1000 got a maximum value of CHF-1.8MW/m^2. This value cannot provide sufficient margin. So configuration V were made with detailed shaping the flow path to have a further increase in CHF. Experimental results of configuration V shows that the CHF margin for AP1000 may be enough by detailed shaping the flow path.

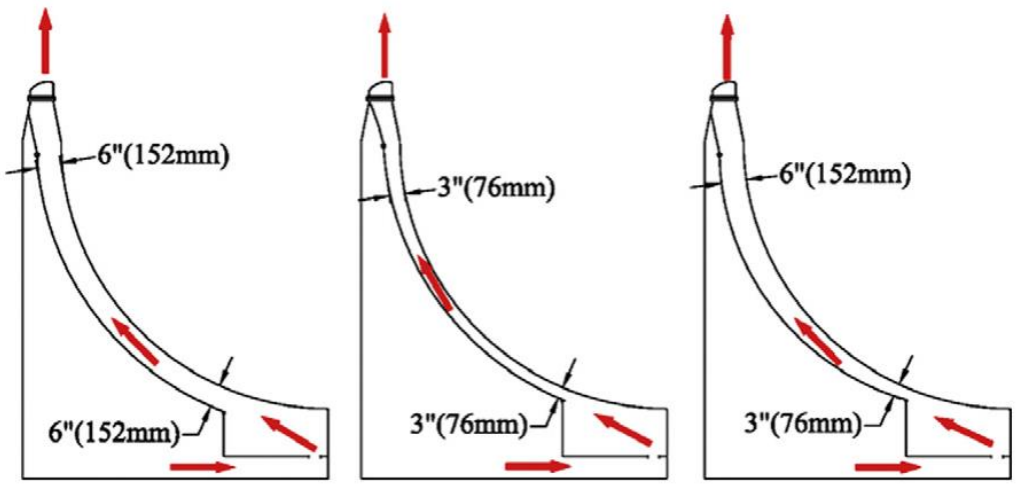

Figure 1-3: Three baffle configurations in ULPU-V [3].

Although the ULPU tests seem CHF margin for AP1000 is enough and it has got the license, it is not clear the CHF margin of IVR is enough or not for a reactor plant with a higher power. In recent years, the power plant power increase due to economy pressure. IVR is still adopted by a higher power plant like Korea APR1400 and China CAP1400. Larger power means more fuel and larger decay heat. When these materials melt and drop

down to the bottom of the reactor vessel, more heat flux will be produced. To keep the integrity of the Reactor Pressure Vessel, the critical heat flux for out surface should be increased to give enough safety margin as the nuclear plant power increase. There is a strong need to find a way to enhance the CHF of IVR in addition to shaping the flow path.

1.2 Critical heat flux

Figure 1-4 shows a typical boiling curve. At very low heat flux, it is convection heat transfer region. As the heat flux increases, more and more bubbles will be generated. Bubbles will coalesce with each other near the heat surface and prevent fresh water to the heat surface. There is a key point which is called Critical Heat Flux. When the heat flux exceeds it, a vapor film will cover the heat surface, the efficiency of heat transfer will suddenly decrease and temperature of heat surface will increase dramatically. Usually it can lead to the melt of the heat surface in a very short time. To avoid this, critical heat flux should not be exceeded.

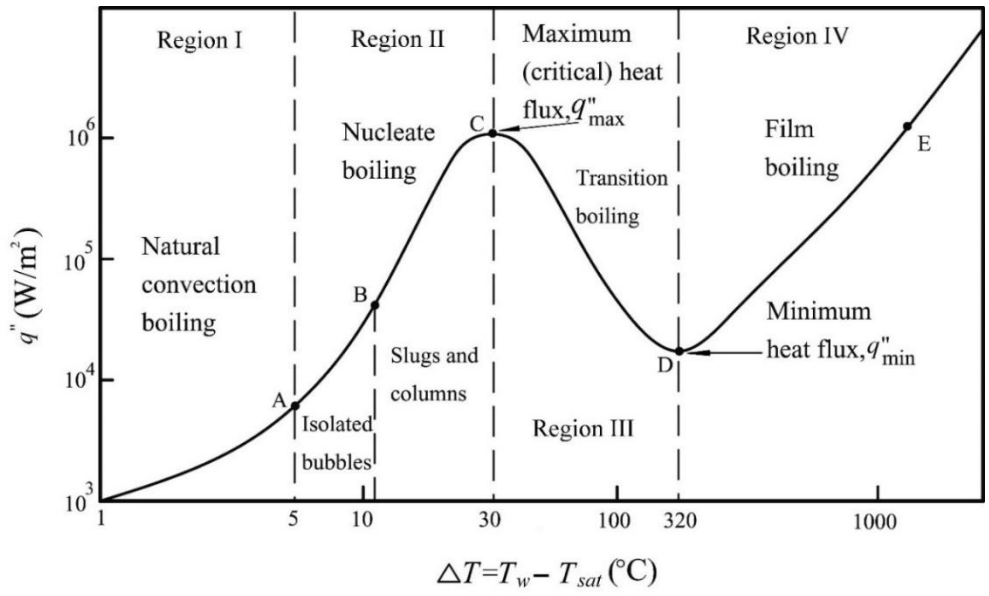

Figure 1-4: A typical boiling curve.

So far, there are four main CHF theories. The first theory is hydrodynamic instability theory firstly developed by Zuber [4]. This theory assumes that CHF is dominated by the hydrodynamic of countercurrent flow of vapor and liquid. When the flow become instable, CHF happens. According to this theory, CHF is related with fluid properties. The second theory is macrolayer dryout theory developed by Haramura and Katto [5]. This theory assumes that there is a liquid macrolayer near the heat surface. If the macrolayer dries out, CHF occurs. According to this theory, CHF is related with surface wettability as it can influence the thickness of the macrolayer. The third theory is hot/dry spot theory developed by Theofanous and Dinh [6]. This theory assumes that there are some hot/dry spots on the heat surface during boiling. These spots can be reversible or irreversible. At high heat flux, when the rewetting of the hot/spots does not occur, CHF happens. According to this theory, CHF is also related with surface wettability. The fourth is Bubble interaction theory developed by Rosenhow and Griffith [7]. This theory assumes that CHF occurs when bubbles coalesce radially, preventing liquid access to the surface. According to this theory, CHF is also related with surface wettability. Among these four main theories, three theories show that CHF are related with the surface wettability.

1.3 Previous critical heat flux enhancement research

Many methods have been investigated to enhance the CHF. It can mainly be divided into two ways. One way is using nanofluid, the other is using surface modifications.

Since You [8] first conducted the pool boiling experiment using nanofluids to enhance CHF, using nanofluids to enhance CHF has been a research hotspot in recent years. Many experimental studies about enhancing CHF using nanofluids have been conducted. Most of these researches were conducted for upward-facing pool boiling condition while there

are also some researches for flow boiling condition. In general, the reported CHF enhancement is approximately from 30% to 200% for pool boiling and approximately 20% to 100% for flow boiling [9-12]. As for the enhancement mechanism, most articles attributed CHF enhancement to nanoparticle deposition on the surface, modifying the surface wettability and enhancing CHF. The flow boiling condition is far more complicated compared with pool boiling condition, the mechanism for flow boiling condition is not so clear by far. Besides, there is a problem for actual application of nanofluids which is the stability problem of nanofluids. The stability is essential in practical applications of nanofluids. In bad cases, the agglomeration of nanoparticles may occur, resulting in clogging of channels and consequently causing failure of thermal systems.

At the same time, numerous research about using various surface modifications to enhance CHF were conducted [13-19]. These surface modifications can be divided into uniform porous coating, modulated porous coating and structures fabricated/installed on the heated surface. The method of using uniform porous coating is to produce a uniform thickness porous coating on the heating surface by sintering, electrolytic deposition, plasma spraying or so on. The thickness of the uniform layer is usually at micrometer magnitude. Many researches about using uniform porous coating have proven that it can enhance CHF effectively in pool boiling condition. Mori summarized the CHF enhancement research using uniform porous coating in pool boiling condition [20]. In general, using uniform porous coating can get a 1.5-3 times CHF enhancement in pool boiling. But most of these researches are about upward-facing pool boiling condition using a relatively smaller heater size. It is noted that the CHF enhancement ratio is related with the heater size. For a larger size, the enhancement ratio may decrease.

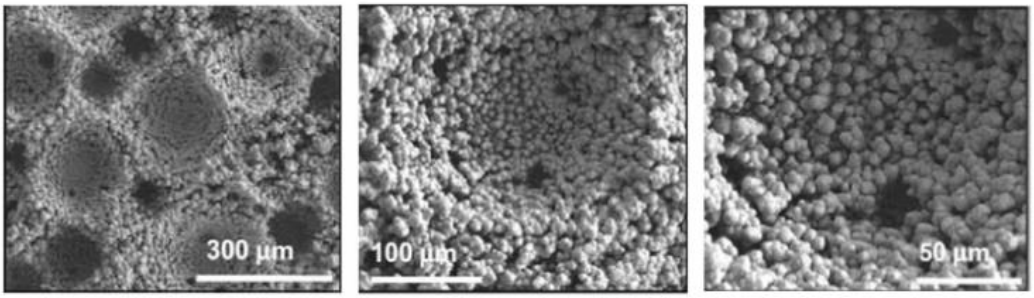

Figure 1-5: Scanning electron microscopy images of a micro-porous surface layer fabricated by electrical deposition [20].

The CHF enhancement effect of using a uniform porous coating may be due to additional nucleation sites, increase in hydrophilicity/wettability, increase in heat transfer area, capillary wicking or wavelength decreased based on modified hydrodynamic stability CHF model. Further clarification is needed for the enhancement mechanism of structured surfaces. The exact contribution of each effect has not yet been clarified.

Liter et al. used modulated (periodically, non-uniform thickness) porous layer coatings to enhance pool boiling CHF [21]. The CHF obtained was nearly three times greater than the bare surface. They stated that the strong enhancement effect is partly due to the separation in the liquid and vapor flow paths resulting from the modulated coatings which reduces the vapor-liquid counter flow resistance. They suggested that completely separating liquid and vapor flow paths can result in further enhancement.

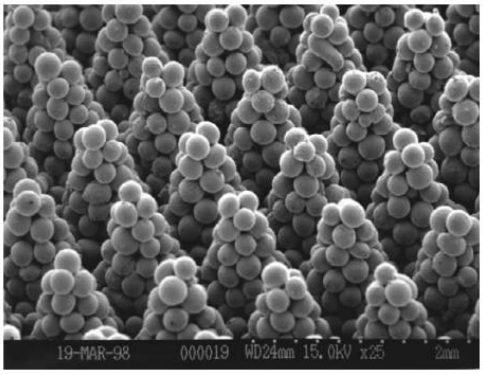

Figure 1-6: Scanning electron microscopy images of modulated porous coating [21].

Besides porous coating, some researchers tried to enhance CHF using structures fabricated or installed on the heat surface. Jaikumar et al. enhanced the CHF during their pool boiling experiments using a copper surface which had open channels with porous fin tops in FC-87 [22]. A maximum CHF enhancement of 270% was achieved compared to a plain chip surface. They believed that the reason for CHF enhancement was due to the generation of bubbles from the porous fin tops which allowed for separated vapor-liquid pathways.

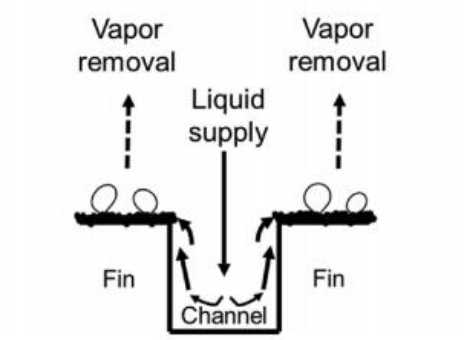

Figure 1-7: Schematic of porous fin tops on open microchannel [22].

Mori et al. researched enhancement of CHF by attaching of a ceramic honeycomb plate on the upward-facing plain heated surface under saturated pool boiling conditions [23]. Three ceramic porous honeycomb plates with different heights (1.2 mm, 5.0 mm and 10mm) were used. As seen in Figure 1-9, the measured CHF increases with the decrease of the height in the honeycomb porous plates. The highest CHF is approximately 2.5 times that of a plain surface. This is a relatively big enhancement. CHF enhancement is believed to be due to liquid supply by the capillary force through the pores of the material and reduction in the vapor flow resistance due to separation of water and vapor flow.

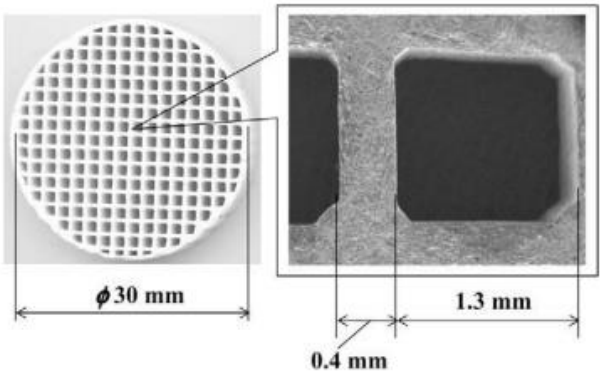

Figure 1-8: Shape of the ceramic porous honeycomb plate.

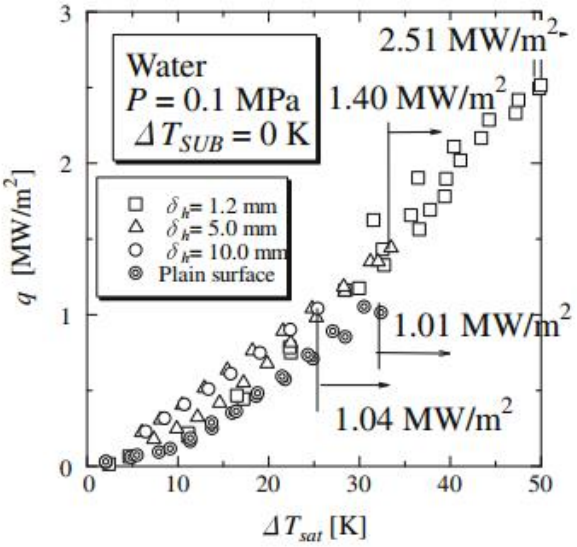

Figure 1-9: Boiling curves for honeycomb porous plates of different heights [23].

They developed a simplified one-dimensional model based on capillary limit which is similar to the capillary limit model for a conventional heat pipe. There is a totally separation of water and vapor as seen in figure 1-10. CHF is assumed to occur when the maximum capillary pressure in the porous media equals to the sum of the pressure losses along the vapor-liquid path. Figure 1-11 shows the relationship between the vapor escape channel widths and predicted CHF according to their model.

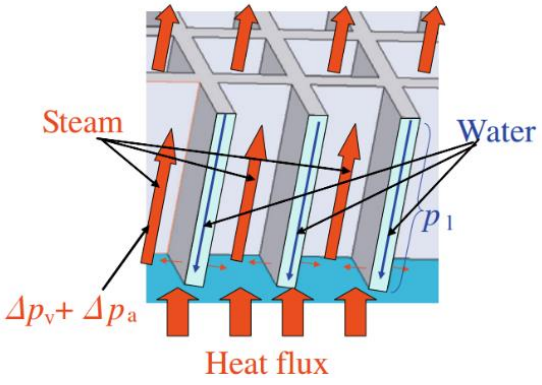

Figure 1-10: Schematic diagram of flows in a ceramic honeycomb porous plate [23].

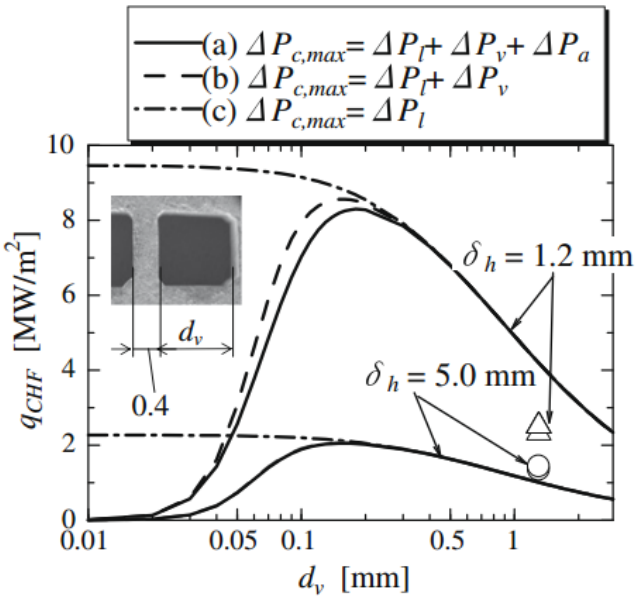

Figure 1-11: Predicted CHFs change as vapor escape channel widths [23].

Research about enhancing CHF in flow boiling using surface modifications in large size channels is really rare. Rainey et al. conducted subcooled flow boiling experiments using an upward-facing 1 cm^2 microporous-coated copper surface in pure FC-72 [24]. They found that the porous surface can enhance the CHF compared to bare surface but the enhancement effect decreases as water flow rate increases as seen in figure 1-12.

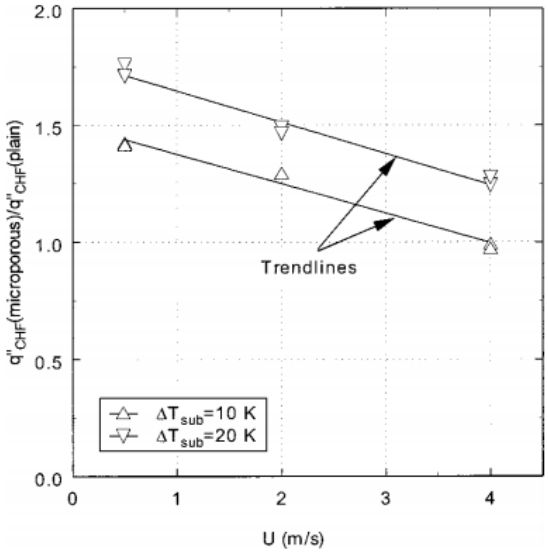

Figure 1-12: Effect of velocity and subcooling on microporous coating effectiveness [24].

Besides nanofluid and surface modifications, some researchers found that gamma-ray irradiation can significantly increase the surface wettability of metals and oxides, which named as Radiation Induced Surface Activation (RISA) effect. For example, RISA effect has shown an increase in wettability in titanium dioxide, copper, and SUS-304 [25-26]. The reason is assumed to be oxygen vacancies produced on the surface due to the cathodic and anodic reactions. They also found that wettability decreases after irradiation as the time passes. As mentioned above, increase in surface wettability is believed to enhance CHF. Based on these, Okamoto et al. [27] conducted pool boiling experiment using irradiated SUS304 foil with plasma oxidized surface and obtained CHF enhancement of ~20%. Gong et al [28] research using Gamma-ray irradiation (around 1000 kGy) to enhance CHF in downward-facing pool boiling condition. The boiling condition is saturated and atmospheric condition. The inclination of the downward-facing is 5 degree. The boiling area is 30mm by 30mm and boiling material is copper. They found that the surface wettability increase a lot after the Gamma-ray irradiation and the CHF increases while the superheat also increase as seen in figure 1-13.

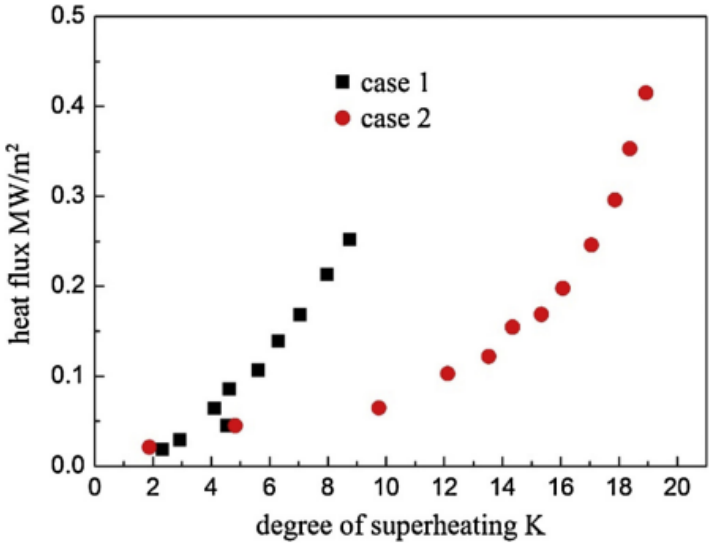

Figure 1-13: Boiling curve for cases 1 (non-irradiation) and 2 (irradiation) [28].

In summary, most previous experimental works, especially relating to surface modifications, were based on pool boiling and upward-facing surface conditions. The research about downward-facing sutured flow boiling is really rare.

1.4 Focus of this study

As mentioned above, there is a strong need to find a way to enhance CHF for out surface of the reactor vessel bottom head which is hemispheric downward-facing condition and natural circulation flow boiling condition. Most of previous CHF enhancement about using nanofluids or surface modifications are about upward-facing and pool boiling conditions. Research about enhancing the CHF in downward-facing flow boiling condition is really rare. However, there is unique characteristic of downward-facing flow boiling which is different with upward-facing or pool boiling conditions.

Figure 1-14 shows the difference between upward-facing and downward-facing conditions in flow boiling. For downward-facing condition, when bubbles are generated,

it is hard for them to leave the heat surface due to the buoyance force. It depends on water flow to remove the bubbles from the heat surface. If the mass flow rate is low, vapor will soon cover the heat surface and prevent water supply to the heat surface, CHF happens. As the flow rate increases, due to the stronger ability to take away bubbles and stronger turbulence, CHF increases. The research about CHF in downward-facing flow boiling is rare. Zhang [29] found CHF was very sensitive to orientation for flow velocities below 0.2 m/s and near-saturated flow conditions and CHF values for downward-facing heated surface were much smaller than for upward-facing surface orientations. For downward-facing condition, especially at low liquid velocity condition, more important thing is let the bubble leave the heat surface quickly and leave space for fresh water to the heat surface.

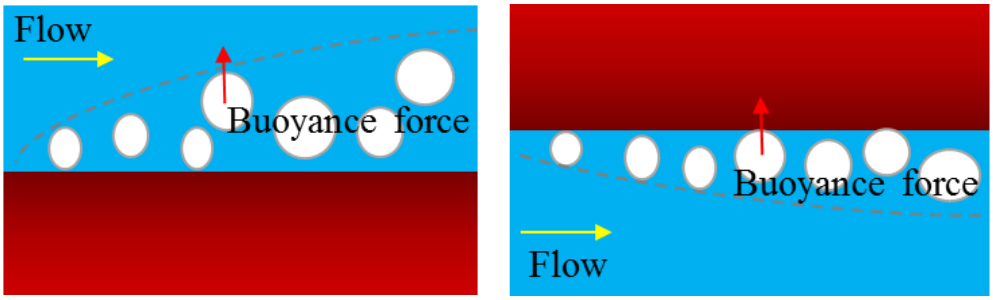

Figure 1-14: Upward-facing and Downward-facing flow boiling conditions.

Firstly, based on Mori's research [23] about using ceramic porous honeycomb plate to enhance CHF in upward-facing pool boiling, this study focuses on enhancing CHF in downward-facing saturated flow using a metal porous honeycomb plate. It is believed that the porous honeycomb structure which could let water-vapor separate is very beneficial for enhancing CHF in downward-facing flow boiling condition. The material of the porous honeycomb plate chosen in this study is stainless steel metal porous plate, which is stronger for actual application than ceramic porous honeycomb plate and has a

strong corrosion resistance in water. A wide water mass flow rate (160-1280 kg/m^2-s) were used, so we can research the CHF enhancement effect from low flow rate to high flow rate, and investigate the CHF increase ratio changes as flow rate changes.

Secondly, this study also focuses on irradiation effect on CHF in downward-facing flow boiling condition. As it is known, various type of radiations are emitted in nuclear reactors in the form of neutron radiation, alpha radiation, beta radiation, and gamma radiation. Many studies have shown that these radiation types can change the mechanical properties of metallic materials, such as a change in hardness, ductility, embrittlement and susceptibility to environmentally induced cracking [30-31]. For the sake of ease, most of experimental researches about heat transfer and CHF related to the nuclear reactors were conducted using an electric heater without any irradiation. Therefore, the effect of the irradiation on heat transfer and CHF has not received sufficient attention even though it is vital to the reactor safety. During IVR condition, the environment will be under high irradiation condition, and previous research show that Gamma-ray irradiation can increase the surface wettability of metal and thus increasing the CHF in pool boiling condition. So secondly, this study focuses on irradiation effect on the saturated downward-facing flow boiling condition to investigate can RISA effect enhance CHF in downward-facing saturated flow boiling condition or is there any other irradiation effects on heat transfer and critical heat flux in downward-facing flow boiling condition.

2 Objective

Based on the characteristic of downward-facing flow boiling condition in IVR and previous CHF enhancement research, two ways are chosen in this study to enhance the CHF in saturated downward-facing flow boiling condition in this study. One way is attaching a metal porous honeycomb plate on the heat surface, the other way is using irradiation effect.

2.1 Objective of honeycomb plate experiment

The main objective of the honeycomb experiment is to research the CHF enhancement effect of metal porous honeycomb plates in downward-facing flow boiling. It includes several aims:

1. To research the CHF enhancement effect of metal porous honeycomb plate under different flow rates;
2. To find the CHF enhancement mechanism of using a metal porous plate in saturated downward-facing flow boiling;
3. To find a honeycomb structure which can enhance downward-facing flow boiling CHF to the largest extent.

2.2 Objective of irradiation experiment

The main objective of the irradiation experiment is to research irradiation effect on CHF in saturated downward-facing flow boiling condition. It includes below aims.

1. To research whether downward-facing flow boiling CHF of bare surface can be

enhanced through increasing surface wettability by RISA effect;

2. To research whether downward-facing flow boiling CHF of a porous honeycomb plate can be further enhanced through increasing surface wettability by RISA effect;

3. To find is there any difference on CHF in downward-facing flow boing between different kinds of irradiation sources (Gamma-ray irradiation and electron beam irradiation).

4. To find is there any other irradiation effect in addition to RISA effect on heat transfer and CHF in downward-facing flow boiling condition.

3 Experiment loop and Data post-processing

3.1 Experiment loop

The saturated downward-facing flow boiling experiments were conducted using an experimental loop as shown in Figure 3-1. It mainly consists of a pump, an electromagnetic flow meter, two tanks-upstream tank and downstream tank (a pre-heater is placed in the downstream tank), a flow channel and a test section. The details of each part are described in the following sections. Distilled water is used in the test loop as the working fluid. During the experiment, the valve of the upstream tank is closed. Water enters into the flow channel from the upstream tank. The experiment facility is a closed loop. Experiments were conducted after the flow rate reached to steady-state condition. Under this condition, mass flow rate should be same at every location due to the mass conservation of incompressible fluid. So the flow rate in the flow channel should equal to the flow rate at the measured position during the experiment. As the valve at the top of the downstream tank is open during the experiment process, the loop pressure is atmospheric pressure. The test section is installed on the top of the channel, so the heated surface is downward-facing. A condenser is installed on the top of the downstream tank to cool the steam produced during the experiment. A 2kW pre-heater is installed at the bottom of the downstream tank to heat the water to saturation temperature before starting the experiment. Two K-type thermocouples are used in the upstream and downstream tanks to monitor the temperature of water during the experiment. During the experiment process, the temperature of water in the upstream tank and downstream tank is kept at 100±0.5℃.

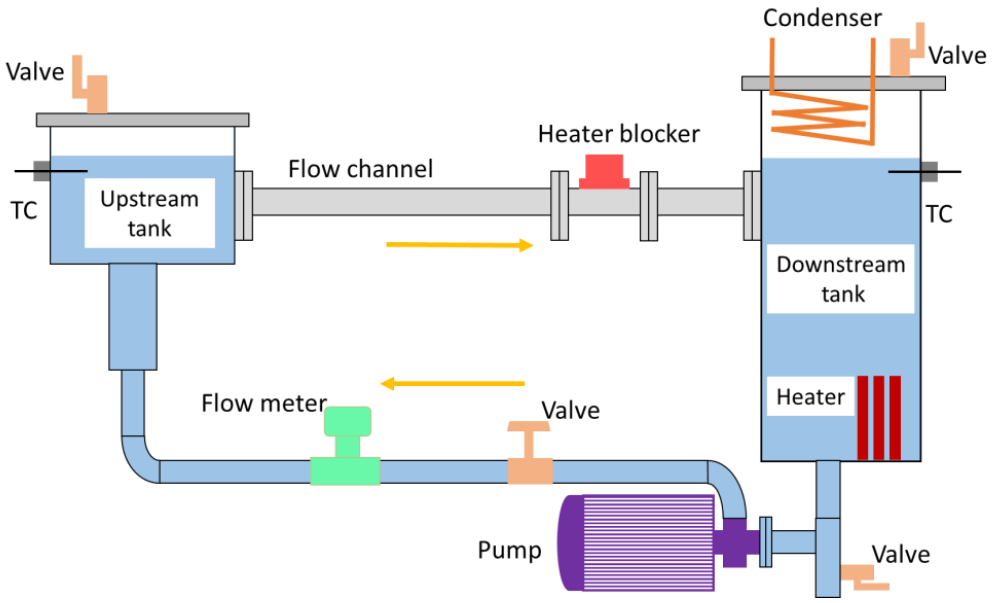

Figure 3-1: Schematic diagram of the flow loop.

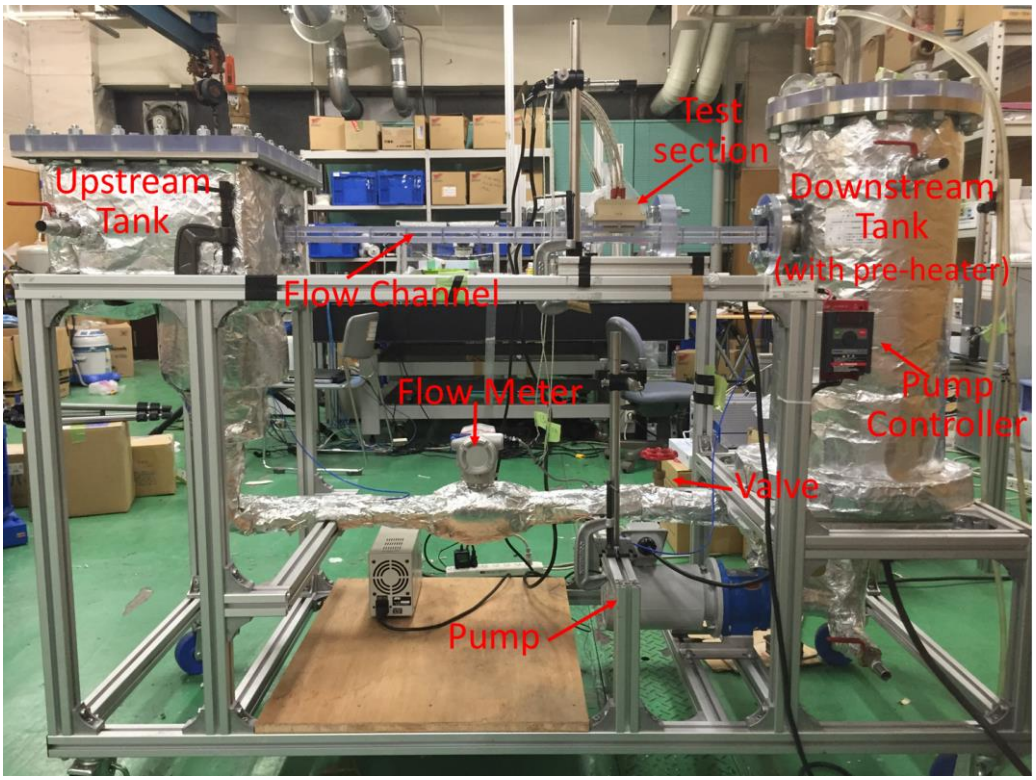

Figure 3-2: Photo of the experiment loop.

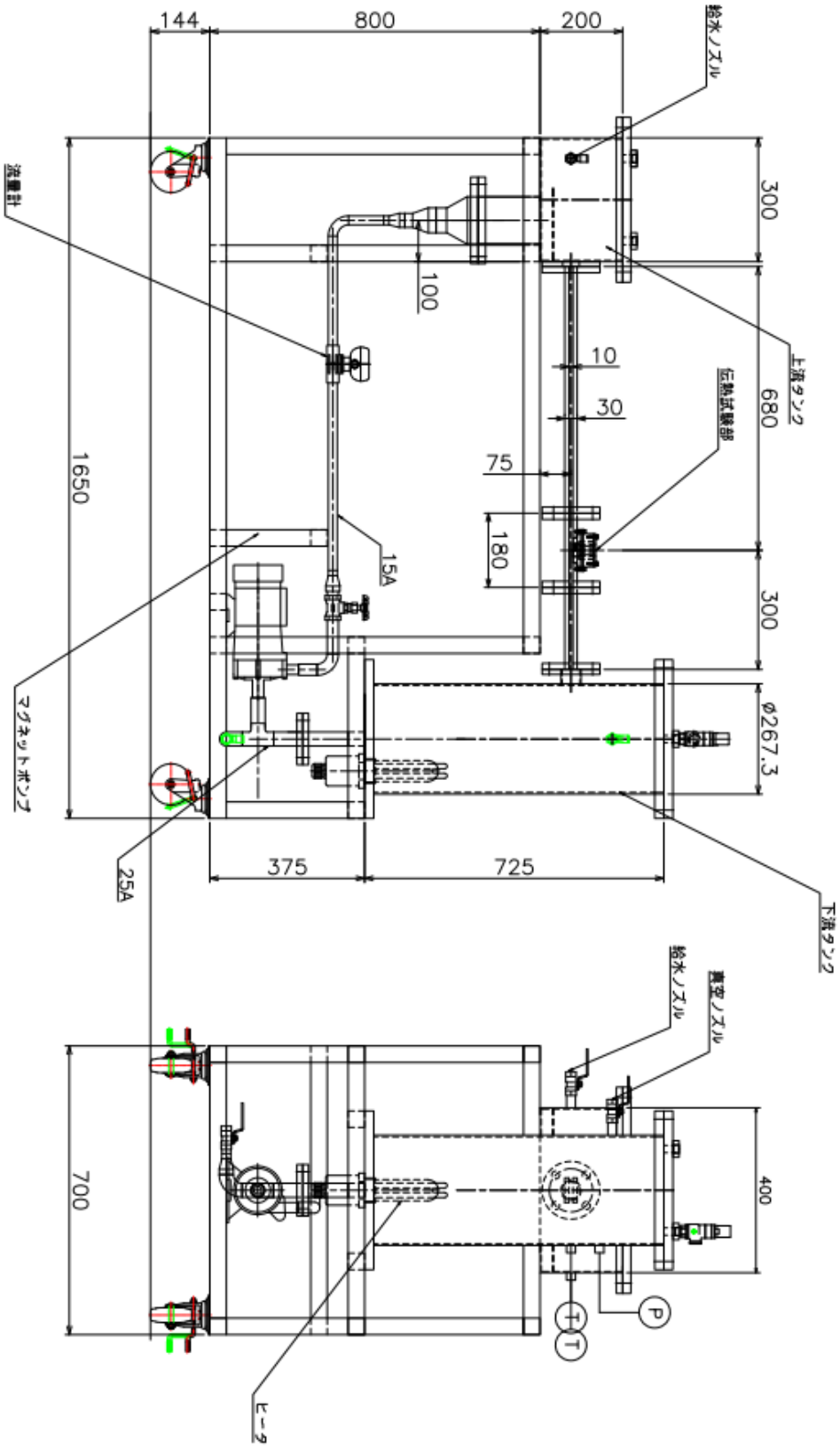

Figure 3-3: CAD design of the experiment loop (dimensions in mm).

3.1.1 Pump

A centrifugal type pump manufactured by Sanwa Hydrotech Corporation was installed near the downstream tank to supply the forced circulation. The maximum capacity of the pump is 3 m^3/h (50 L/min). The highest flow rate used in the experiment is 32 L/min. It can stand with a high temperature for a long time . The specification of the pump is shown in Table 3-1. The pump has a controller which can be used to set different flow rates. It is also used to keep the flow rate stable during the experiment process slightly.

Table 3-1: Specification of the pump

SPEED	2920RPM
MAX. HEAD	8m
MAX. CAPACITY	3m^3/h (50L/min)
MAX. LIQUD TEMP.	150℃

Figure 3-4: Photo of the pump controller.

3.1.2 Flow meter

The flow meter is an electromagnetic flow meter. The measurement range of the flowmeter is 0 to 40 L/min. There is a display screen on the flow meter which can show the flow rate in real time. The flow rate was monitored from the display screen during the experiment process. A 24V DC power is used to supply power to the electromagnetic pump.

Figure 3-5: Photo of the electromagnetic flow meter.

3.1.3 Flow channel

The flow channel was fabricated by polycarbonate material to withstand saturated temperatures during the experiments. The cross-section of the flow channel is rectangular, with a length of 980mm. The width and height of the flow cross-section is 40mm and 10mm, respectively. The distance from channel inlet to the upstream edge of the test section is 680 mm. It is long enough for stable flow.

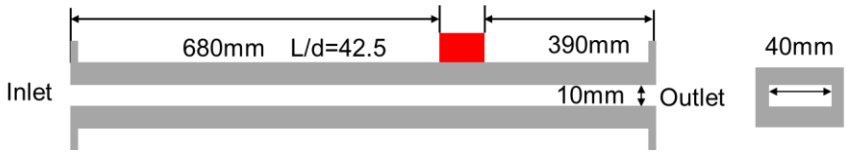

Figure 3-6: Size of the flow channel.

3.1.4 Test sections

In order to observe the enhancement from the honeycomb-structured plate, the bare surface experiment was also conducted for comparison. Therefore, two different test sections were manufactured. One is for bare surface experiment, the other is for honeycomb experiment.

Figure 3-7 shows the structure of the test section of the bare surface. Copper was chosen as the heating material as it has a very high thermal conductivity. The copper boiling surface area is 30mm×30mm. The insulation material is PEEK (polyether ether ketone). Nine electric cartridge heaters were used to heat the copper block. The heating power supplied to the cartridge heaters was controlled by the slidac. Three K-type thermocouples (0.5 mm diameter) are placed in the center line of the copper blocks. They are connected to the data acquisition system, so the temperature of the thermocouples were acquired by computer. The distance between each thermocouple is 3mm. The distance between the boiling surface and the bottommost thermocouple is also 3mm. We calculated the temperature and the heat flux of the boiling surface using the temperature of the three thermocouples according to Fourier's law.

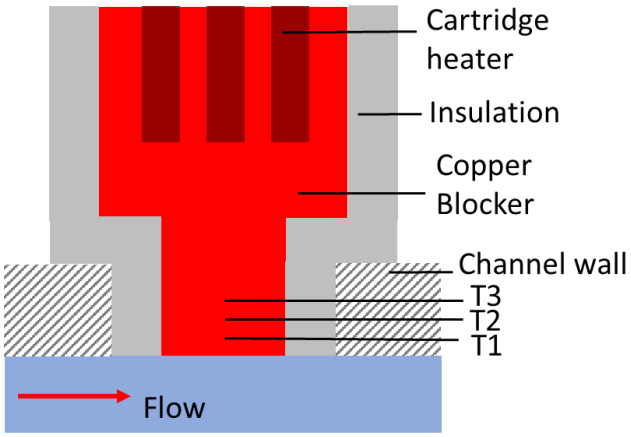

Figure 3-7: Schematic diagram of the bare surface test section.

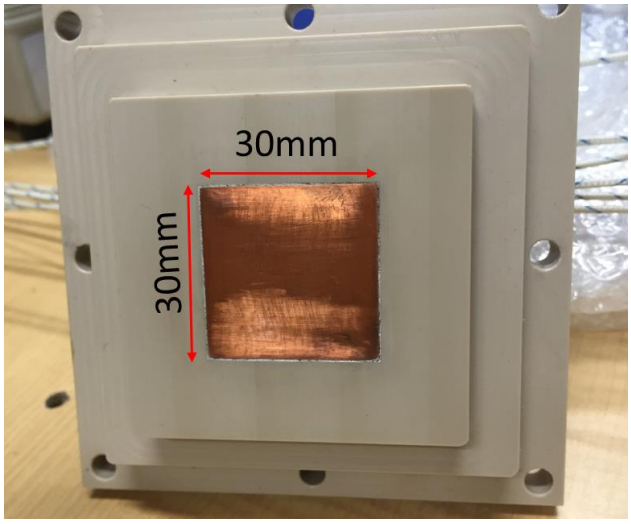

Figure 3-8: Photo of the bare surface.

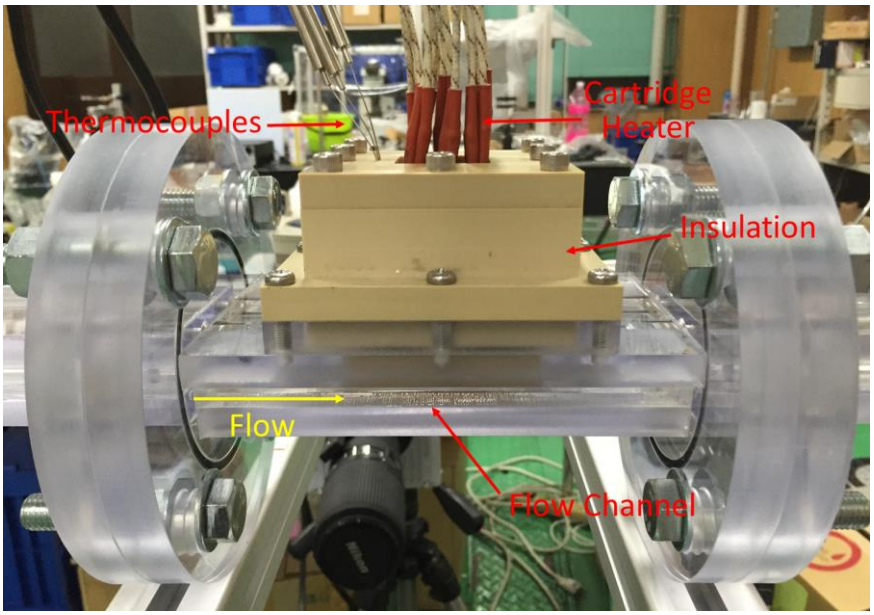

Figure 3-9: Photo of the test section on the flow channel.

Figure 3-10 shows the structure of honeycomb test section. The structure is very similar to that of bare surface test section. The difference between the bare surface test section and the honeycomb test section is that there is a region which is 1mm lower than surrounding PEEK on the surface of the honeycomb test section. This region is for installing the honeycomb plate. The honeycomb plate was attached to the boiling surface

by fixing it into the PEEK. The length and width of the region is 50mm and 34mm, respectively. The total size of the area containing holes is the same size as the copper boiling surface as seen in Figure 3-11. The four holes on the edges are for securing the plate into the PEEK.

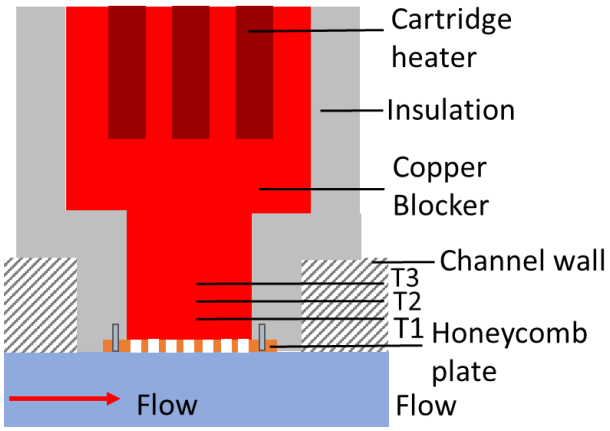

Figure 3-10: Schematic diagram of the honeycomb test section.

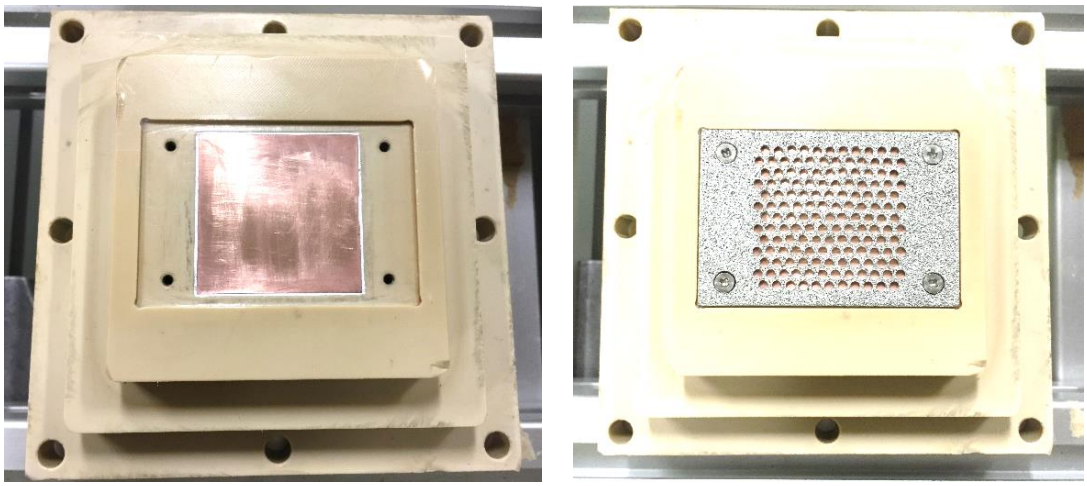

Figure 3-11: Photo of the honeycomb test section with and without honeycomb plate.

3.1.5 Cartridge Heaters

Nine cartridge heaters which were inserted to the holes from the top of the test sections were used to heat the test sections during the experiment. The other head of the cartridge heaters was connected to a slidac. During the experiment, the heat from the cartridge

heaters was changing by modifying the slidac which will change the voltage of the cartridge heaters. As a result, the heat flux to the heat surface can be changed. As the minimum scale of the slidac is 20V which is too large and not so accurate, we use a tester which is connected with the slidac to measure the out voltage of the slidac.

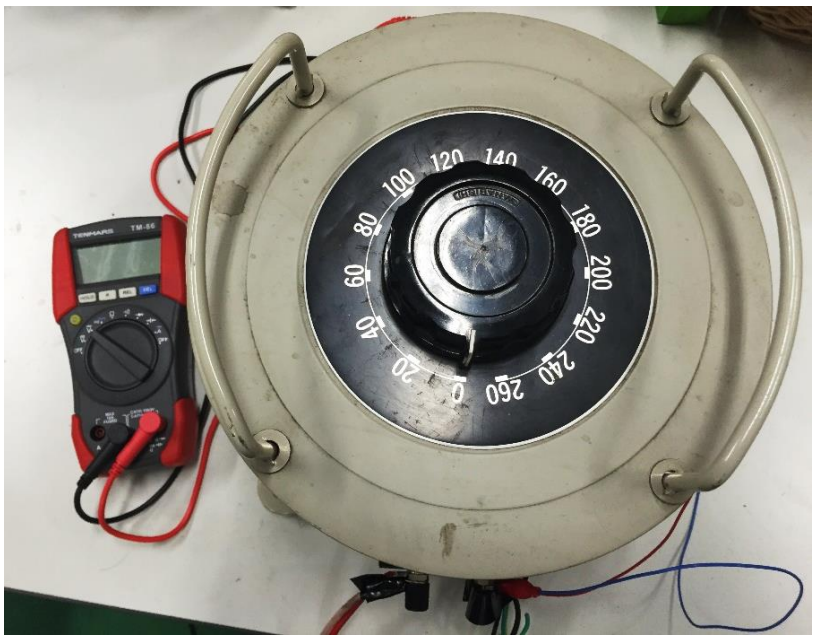

Figure 3-12: Photo of the slidac and tester.

3.1.6 Experiment Visualization

To observe the boiling phenomenon during the experiment which is very important for understanding CHF in downward-facing flow boiling condition, a Photron SA5 high speed camera was used during the experiment to observe and record the boiling phenomena at different heat fluxes conditions. As the boiling surface is downward-facing, a mirror was installed below the test section to reflect the heat surface, so the camera can be located horizontally. The frame rate used is 1000 frames per second.

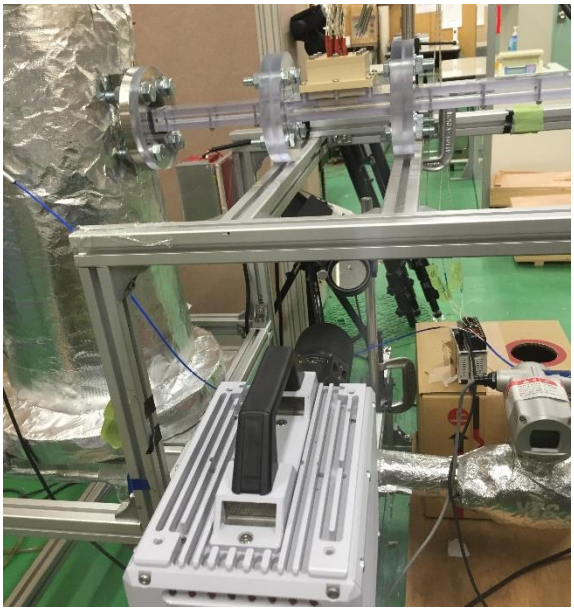

Figure 3-13: Photo of the camera and mirror.

3.2 Data post-processing

As mentioned in section 3.1.4, three K-type thermocouples were placed in the center line of the test section. The interval of each two thermocouples is 3 mm. The distance between the bottommost thermocouple and the heat surface is also 3 mm. The temperatures of these three thermocouples during experiments are used to calculate the heat surface superheat and heat flux.

According to Fourier's one-dimensional thermal conduction law:

$$q'' = k\frac{\Delta T}{\Delta x} \tag{3-1}$$

Where:

q'' = surface heat flux [MW/m^2]

k = thermal conductivity of copper [W/m-K]

ΔT = temperature difference between different positions [K]

Δx = distance between different positions [m]

At certain heat flux, as we know the thermocouple temperature difference between the top thermocouple and the bottom thermocouple and the distance between them, the exact value of heat flux can be calculated.

Besides, at certain heat flux, the temperature distribution along the axial direction of the test section had a linearity relation with the distance as the thermal conductivity of copper is a fixed value. As we know the temperatures of the three thermocouples and the distance between them and the heat surface, we can get the temperature of the copper surface using extrapolation method.

4 Experiments of bare surface

As mentioned before, bare surface experiments were conducted first for comparison. Experiment of bare surface under four flow rates (160 kg/m^2-s, 320 kg/m^2-s, 640 kg/m^2-s, 1280 kg/m^2-s) were conducted. The flow parameters is as seen in Table 4-1.

Table 4-1: Flow rate parameters of the experiments

Mass Flux	Velocity	Reynold number
160 kg/m^{2}s	0.17 m/s	0.74×10^4
320 kg/m^{2}s	0.33 m/s	1.48×10^4
640 kg/m^{2}s	0.67 m/s	2.97×10^4
1280 kg/m^{2}s	1.33 m/s	5.93×10^4

4.1 Experiment procedure of bare surface experiment

For the bare surface experiments, the experiment procedure is as blew:

1. Polishing the copper surface of the bare surface test section using P1200 sandpaper; cleaning it using acetone and distilled water.
2. Installing the bare surface test section on the flow channel.
3. Adding distilled water into the loop, heating the water to saturation condition and degassing for 30 minutes.
4. Adjusting the flow rate to target flow rate using the pump controller.
5. Increasing the output voltage of the slidac (Increasing the heat flux) step by step and keeping each stable state for at least 4 minutes;
6. CHF happens; shut down the heater power of the test section; saving data.

4.2 Experimental results of bare surface

Figure 4-1 shows the boiling curves of bare surface under four different flow rates. As it can been, there is a big difference in CHF while there is no big difference in wall superheat at CHF condition. CHF value at lowest flow rate is around 0.4 Mw/m^2 while

CHF value at highest flow rate is around 1.4 Mw/m^2. CHF values increase as flow rate increases.

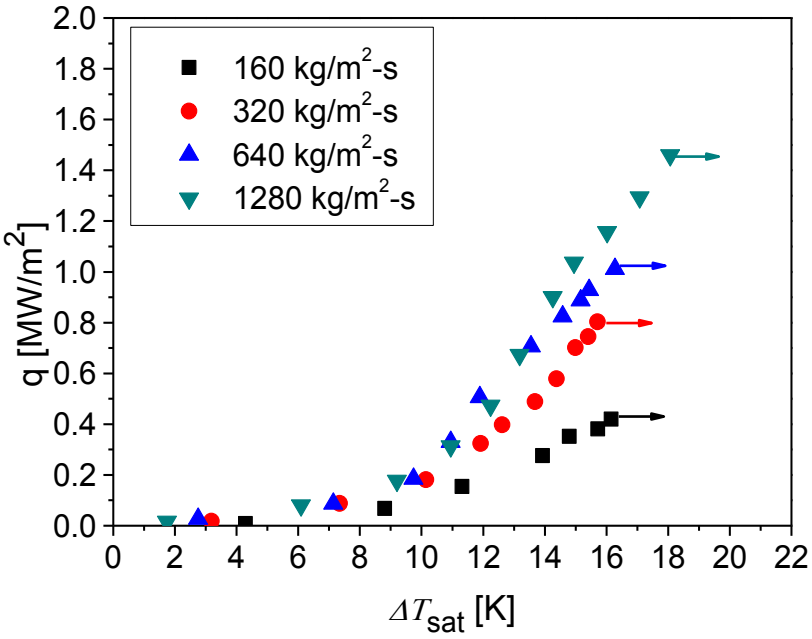

Figure 4-1: Boiling curves of bare surface at different flow rates.

Katto's CHF correlation for convective flow was chosen for comparison [32]. The correlation was developed based on his flow boiling experiments about a vertical heated surface of 10, 15, and 20 mm in length and a velocity of 1.5–10 m/s using saturated water and R-113 at atmospheric pressure. Figure 4-3 shows the schematic diagram of the katto's experimental flow loop

The equation is expressed as:

$$\frac{q_{CHF}}{Gh_{fg}} = 0.186\left(\frac{\rho_g}{\rho_l}\right)^{0.559}\left(\frac{\sigma\rho_l}{G^2 l}\right)^{0.264} \qquad (4\text{-}1)$$

Where:

q_{CHF} = critical heat flux [MW/m^2]

G = water mass flow flux [kg/m^2-s]

h_{fg} = heat latent of vaporization [kJ/kg]

ρ_g = density of vapor [kg/m^3]

ρ_l = density of liquid [kg/m^3]

σ = liquid surface tension [N/m]

l = length of the heater [m]

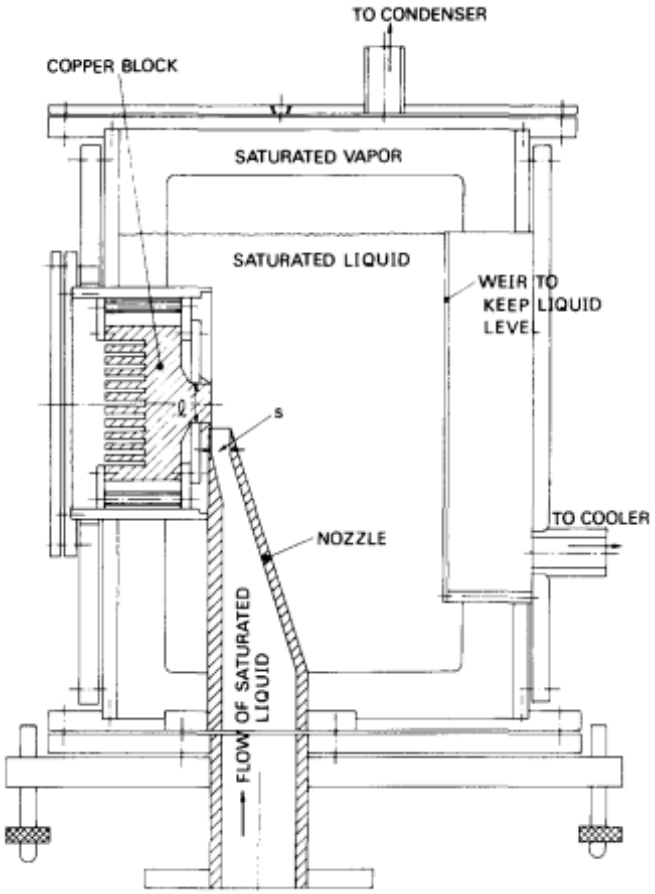

Figure 4-2: Schematic diagram of the katto's experimental flow loop [32].

Figure 4-3 shows the CHF values change as water flow rate increases and comparison with Katto's CHF correlation. As it can be seen, even though the water flow velocity range in our experiments is lower than that of the Katto's experiment and our boiling

surface is downward-facing, our experimental results of bare surface show good agreement with the correlation except experiment result at the lowest flow velocity condition. This means that there is no big difference in CHF between vertical surface flow boiling condition and downward-facing surface flow boiling condition when the flow rate beyond some value. The CHF values at lowest water velocity in our experiment is lower than that of Katto's correlation.

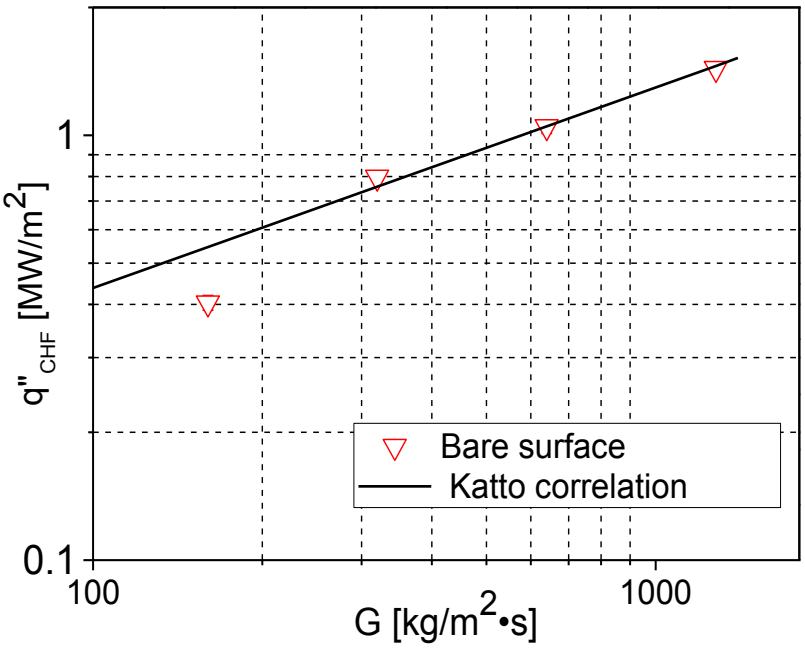

Figure 4-3: CHF values of bare surface change as flow rates.

Figure 4-4 to Figure 4-7 shows the boiling phenomena change as heat flux increase of the bare surface at four flow different flow rates. The flow direction is from left to right. From these figures we can clearly see the boiling process and understand the boiling characteristics of downward-facing flow boiling better. In general, more and more bubbles are generated and coalesce near the heat surface as heat flux increases. The area of the heat surface which has not been covered by bubbles get smaller and smaller as heat flux increases. When all heat surface is covered by the bubbles, water cannot supplied to the heat surface and CHF will happen soon. At the lowest flow rate condition, bubbles

cannot be removed quickly, bubbles will totally cover the surface soon as heat flux increases which we can see clearly from figure 4-4, CHF happens. So Katto's correlation which is based on vertical surface does not give so good prediction at the lowest flow rate. As the flow rate increases, CHF will be delayed due to the stronger drag force and turbulence induced by water flow.

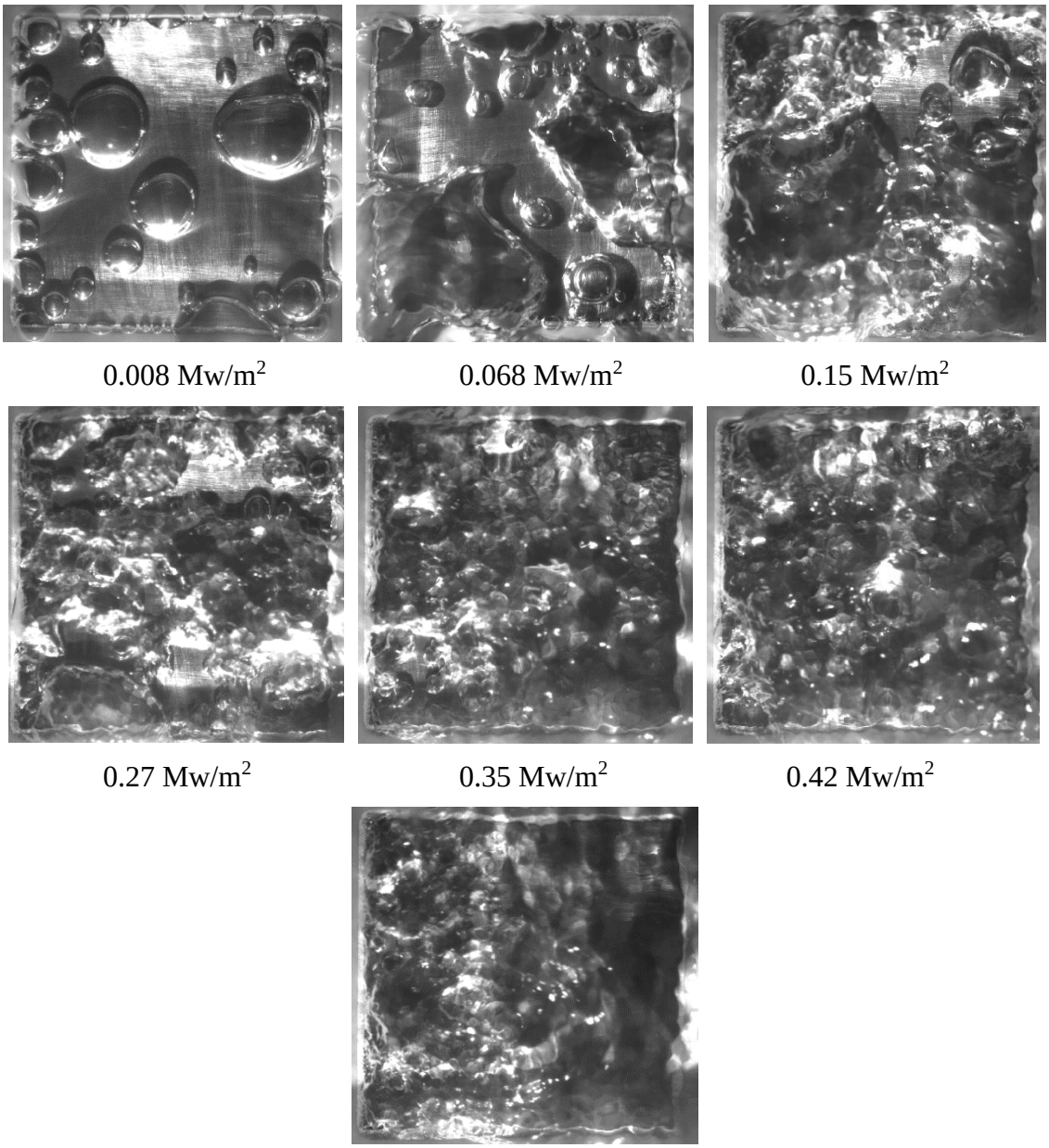

0.008 Mw/m^2 0.068 Mw/m^2 0.15 Mw/m^2

0.27 Mw/m^2 0.35 Mw/m^2 0.42 Mw/m^2

CHF

Figure 4-4: Boiling process of bare surface at 160 kg/m^2-s.

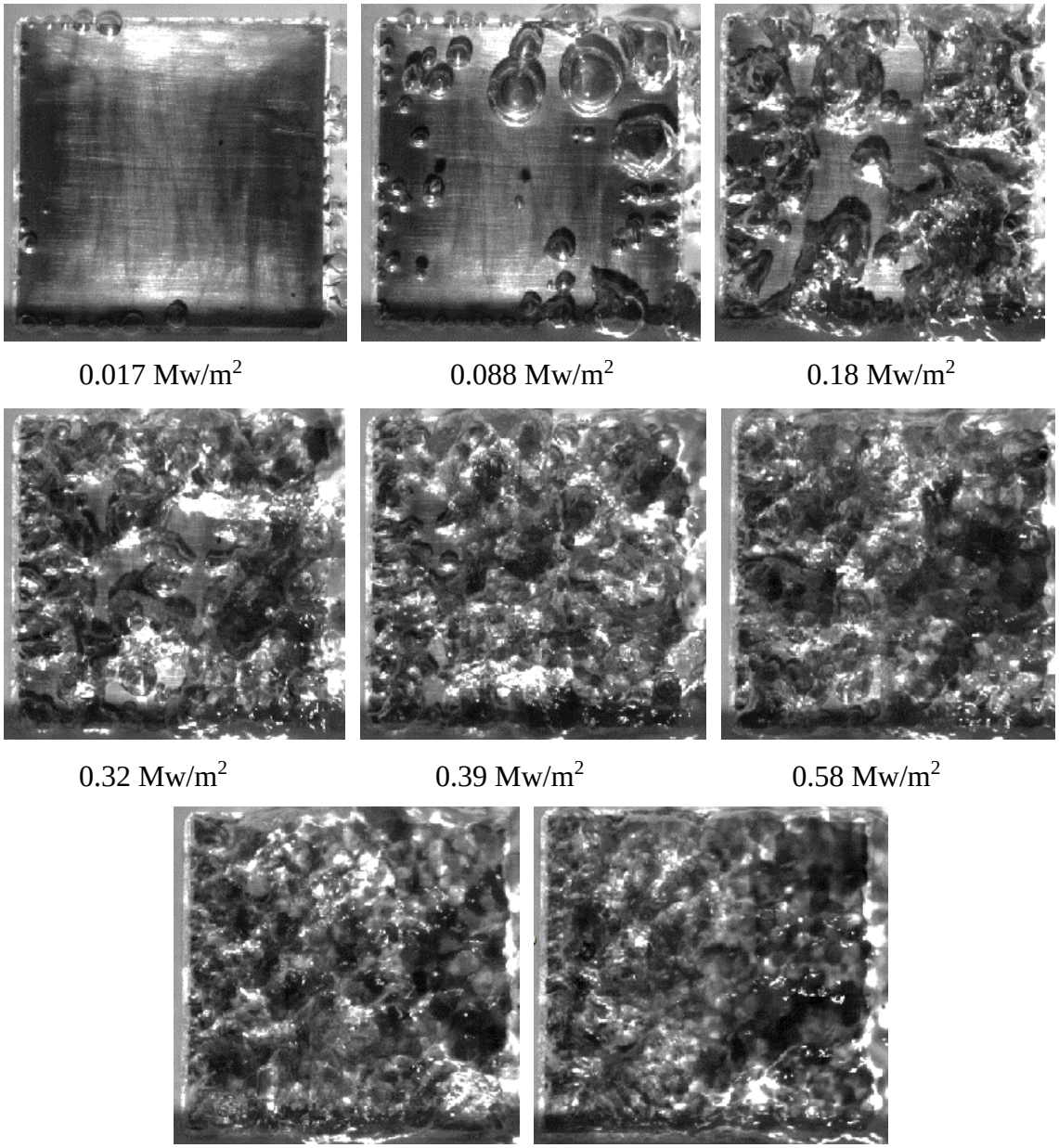

0.017 Mw/m^2 0.088 Mw/m^2 0.18 Mw/m^2

0.32 Mw/m^2 0.39 Mw/m^2 0.58 Mw/m^2

0.74 Mw/m^2 CHF

Figure 4-5: Boiling process of bare surface at 320 kg/m^2-s.

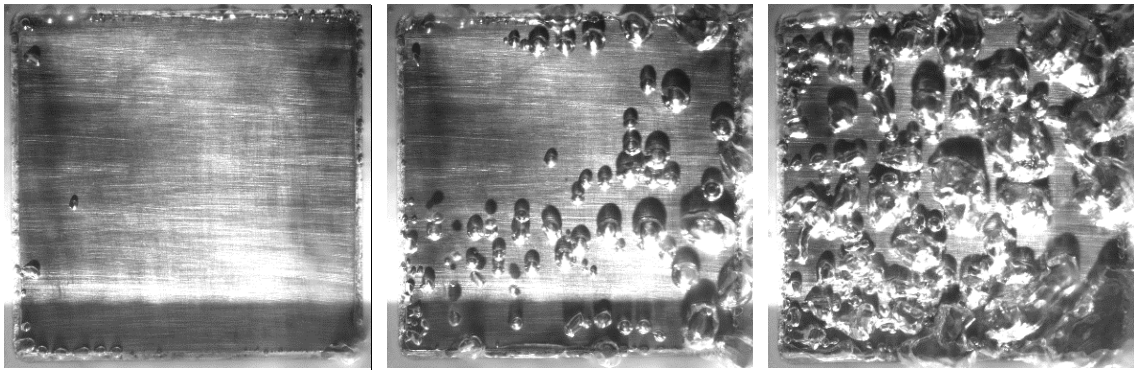

0.027 Mw/m^2 0.086 Mw/m^2 0.18 Mw/m^2

0.32 Mw/m^2 0.51 Mw/m^2 0.71 Mw/m^2

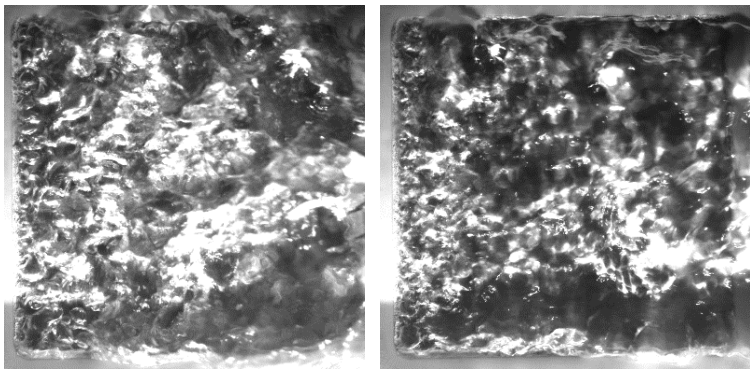

1.0 Mw/m^2 CHF

Figure 4-6: Boiling process of bare surface at 640 kg/m^2-s.

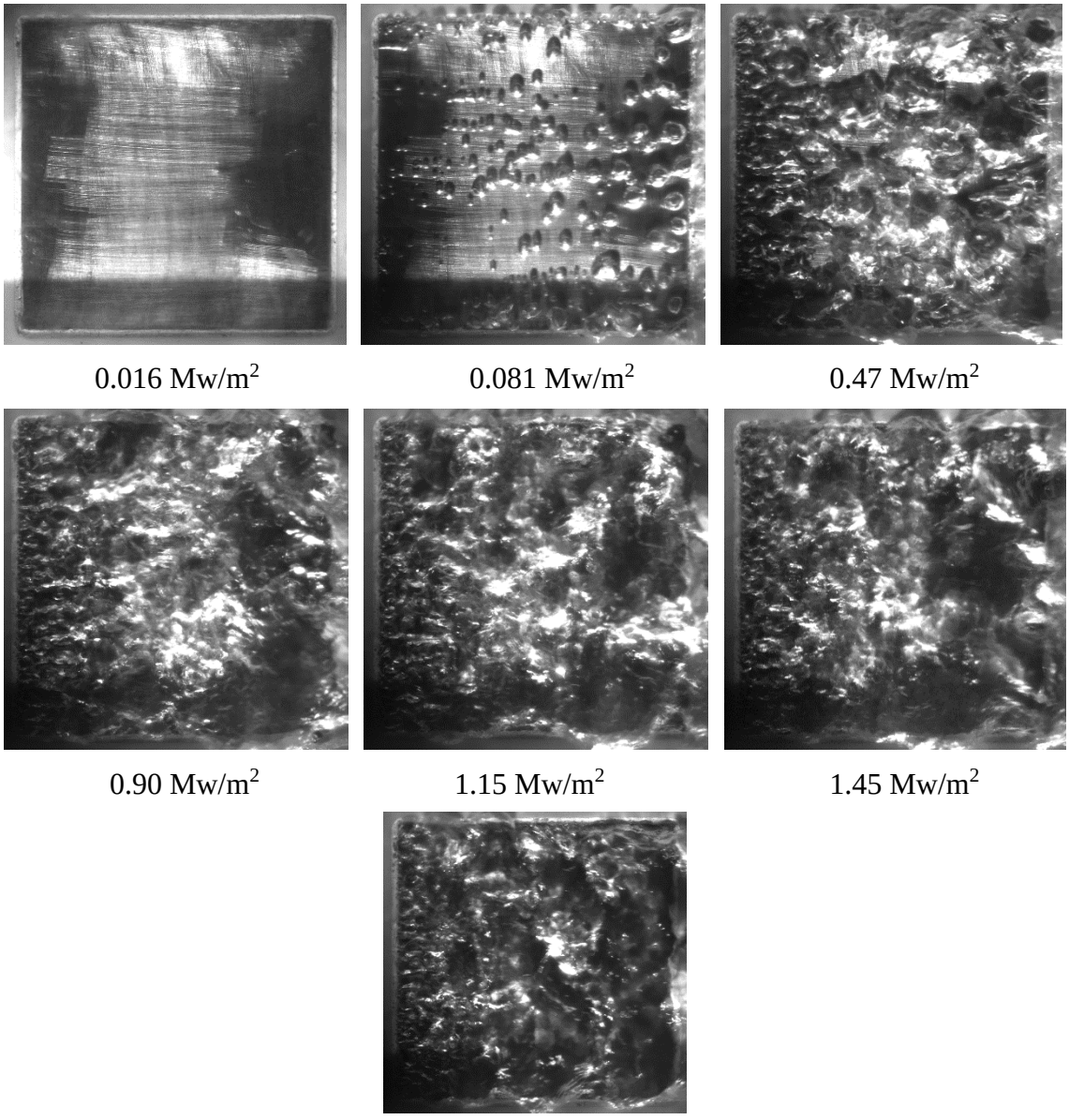

0.016 Mw/m^2 0.081 Mw/m^2 0.47 Mw/m^2

0.90 Mw/m^2 1.15 Mw/m^2 1.45 Mw/m^2

CHF

Figure 4-7: Boiling process of bare surface at 1280 kg/m^2-s.

5 Honeycomb Experiments

5.1 Honeycomb plates

The porous honeycomb plate used in this study is a porous stainless-steel metal plate with small circular holes arranged in a hexagonal (honeycomb) layout shape. The manufacture process of the metal porous honeycomb plate is as shown in Figure 5-1. The stainless steel porous plate was manufactured by sintering stainless steel particles. This kind of porous plate is originally used to filter some particles in air or some kinds of liquid in some applications. Using different sizes of stainless steel particles can produce porous plates with different filtration performances. For example, if the particle size of the raw material is 100μm, solid particle in water with size of 87μm can be removed by the porous medium with an efficiency of 95%. Then, small holes with same diameter were drilled on the porous plate to produce honeycomb plate.

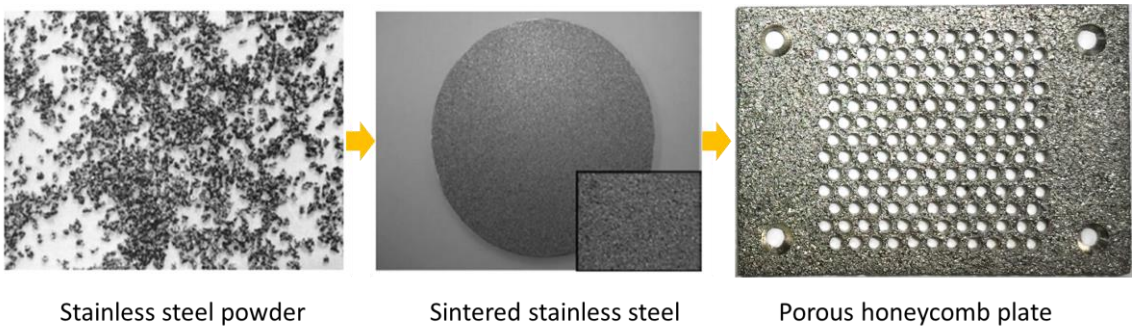

Figure 5-1: Manufacture process of porous honeycomb plate.

As mentioned in chapter 2, the objective of the honeycomb experiment includes investigating the CHF enhancement effect of the porous honeycomb plate under different water flow rates and finding a porous honeycomb plate which can enhance CHF most. For the former, the idea is conducting the downward-facing flow boiling experiments

using the same porous honeycomb plates at different water flow rates. For the latter, the idea is conducting the downward-facing flow boiling experiments using different honeycomb plates at same water flow rate. Thus, several different honeycomb plates were manufactured and used to conduct the downward-facing flow boiling experiments at same water flow rate. These different honeycomb plates can be divided into two kinds. One kind is porous honeycomb plates with different raw particles sizes. The other kind is porous honeycomb plates with different hole diameters and pitches. The details of different porous honeycomb plates are given in below sections.

As mentioned above, the thickness of the all honeycomb plates is 1mm.

5.1.1 Porous honeycomb plates with different raw particle sizes

As mentioned, sintering different raw particles can produce metal porous plate with different permeability and pore sizes. To investigate whether this will lead to difference in water supply ability through metal porous media and CHF values in downward-facing flow boiling condition, three kinds of porous honeycomb plate whose raw metal particle sizes are 5μm, 20μm and 100μm separately were manufactured. The hole diameter and hole pitch of these three porous plates are same, which are 1.7 mm and 2.5 mm, respectively. Table 5-1 show the detail of the three kinds of porous honeycomb plates.

Table 5-1: Specification of the three kinds of porous honeycomb plates.

Nominal Filtration accuracy	Particle sizes can be moved with a efficiency of 95%
5μm	15μm
20μm	31μm
100μm	87μm

Figure 5-2 is the photo of the three kinds of porous honeycomb plates with different raw particle sizes.

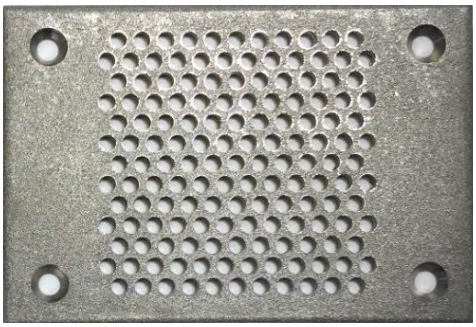

(a) Porous plate (5μm)

(b) Porous plate (20μm)

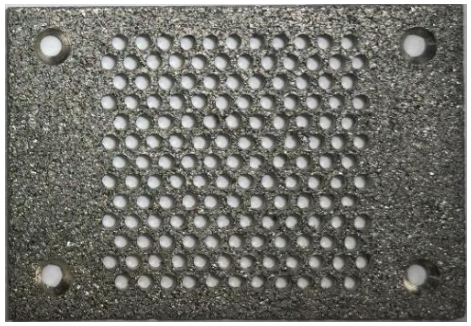

(c) Porous plate (100μm)

Figure 5-2: Three kinds of porous honeycomb plates with different raw particle sizes.

5.1.2 Honeycomb plates with different hole diameters and hole pitches

This kind of porous honeycomb plates have same raw particle size (100 μm) but different hole diameters or hole pitches. To find a honeycomb plate with certain hole diameter and hole pitch which can enhance CHF in downward-facing flow boiling most and investigate the water supply ability through metal porous media, nine porous honeycomb plates with different hole diameters or hole pitches were manufactured as shown in Table 5-2.

Table 5-2: Honeycomb plates with different hole diameters and pitches

Hole Diameter	Pitch	Pitch/Diameter	Number of holes
1.7	2.5	1.47	149
1.0	2.5	2.5	149
1.7	4.0	2.35	67
1.0	1.8	1.8	295
1.7	2.1	1.24	216
2.4	3.2	1.33	85
2.9	4.2	1.45	52
1.7	3.0	1.76	105
2.4	4.2	1.75	52

Among these honeycomb plates, four plates have a 1.7 mm hole diameter but different pitches (2.1 mm, 2.5 mm, 3.0 mm, 4.0 mm) as seen in Figure 5-3. The idea is to investigate for this hole diameter, which plate can enhance CHF to the largest extent since the area of porous media will increase as the pitch increases while the total area of the holes will decrease as the pitch increases.

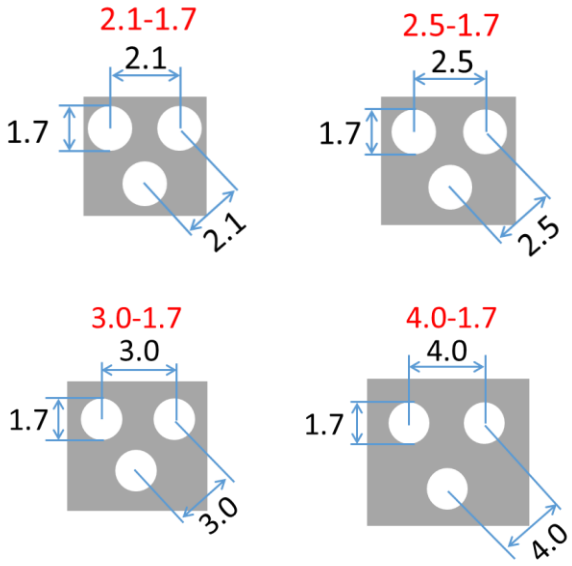

Figure 5-3: Four honeycomb plates with 1.7 mm hole diameter but different pitches.

Besides, two honeycomb plates have same1.0 mm hole diameter but different pitches (1.8mm, 2.5mm) as seen in figure 5-4. We want to investigate which plate with this hole diameter can enhance CHF to the largest extent. Besides, according to Mori's model [23], if the hole pitch is same, CHF will increase by reducing the hole diameter from 1.7 mm to 1.0 mm. The applicability of the model can be checked by comparing the CHF values of the two honeycomb plates which have same hole pitch (2.5 mm) but different hole diameters (1.0 mm, 1.7 mm).

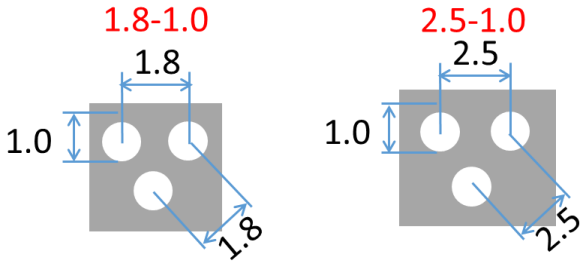

Figure 5-4: Two honeycomb plates with 1.0 mm hole diameter but different pitches.

Two plates have same 2.4 mm hole diameter but different pitches (3.2mm, 4.2mm) as seen in figure 5-5. Using these two plates, we want to investigate CHF values change as the hole pitch increases for a relatively large hole diameter (2.4 mm) condition.

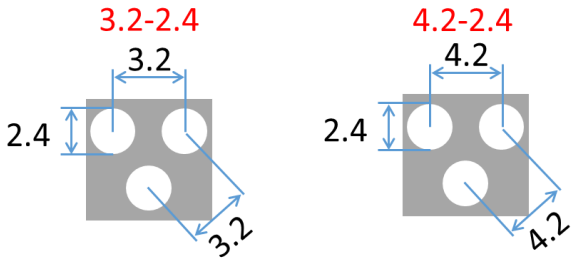

Figure 5-5: Two honeycomb plates with 2.4 mm hole diameter but different pitches.

Besides, three honeycomb plates have same pitch/diameter ratio which is about 1.7, but different hole diameters (2.5-1.0, 2.5-1.7, 4.2-2.4) as seen in figure 5-6.

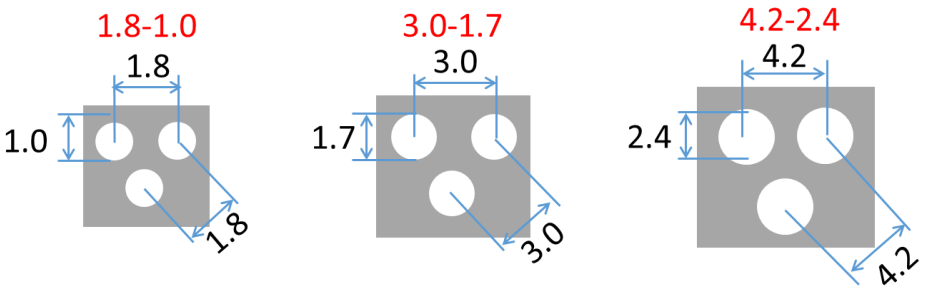

Figure 5-6: Three honeycomb plates with a pitch/diameter of 1.7.

Two honeycomb plates have same pitch/diameter ratio which is about 1.45, but different hole diameters (2.5-1.7, 4.2-2.9) as seen in figure 5-7.

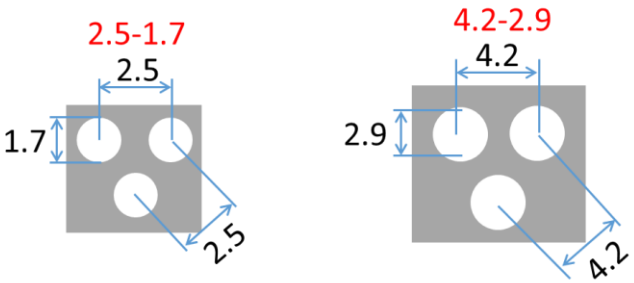

Figure 5-7: Two honeycomb plates with a pitch/diameter of 1.45.

5.1.3 Solid honeycomb plate

As mentioned before, it is assumed that water will be supplied to the boiling surface through porous media for porous honeycomb plate. To clarify the effect of honeycomb structure and water supply through the porous media, we also manufacture solid plate for each kind of porous plate, which is a stainless steel plate with small holes (not porous). The idea is to investigate the water supply ability through porous media by comparing the CHF values of porous plate and solid plate which have same hole diameter and hole pitch.

Stronger water supply ability through the porous media, larger difference in CHF values between the two kinds of honeycomb plate.

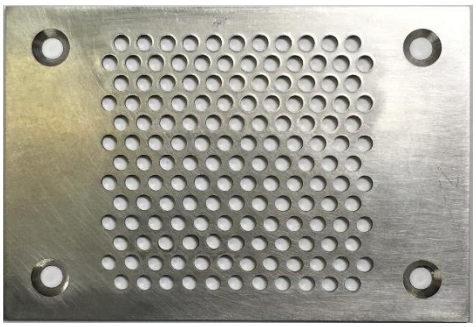

Figure 5-8: Photo of the solid honeycomb plate with 1.7mm hole diameter and 2.5 mm pitch.

5.2 Experiment procedure

For honeycomb experiments, the experiment procedure is as below:

1 Polishing the copper surface of the honeycomb test section using P1200 sandpaper; cleaning it using acetone and distilled water.
2 Installing the honeycomb test section on the flow channel.
3 Adding distilled water into the loop, heating the water to saturation condition and degassing for 30 minutes.
4 Adjusting the flow rate to target flow rate using the pump controller.
5 Increasing the output voltage of the slidac (Increasing the heat flux) step by step and keeping each stable state for at least 4 minutes;
6 CHF happens; shut down the heater power of the test section; saving data.

5.3 CHF values of honeycomb plates at different flow rates.

To research the enhancement effect of the honeycomb plate at different flow rates, four different flow rates were applied: 160, 320, 640, and 1280 kg/m^2-s same as bare

surface conditions. Porous plate and solid plate with same hole diameter (1.7 mm) and hole pitch (2.5 mm) are used to conduct the experiments to analyze the water supply ability through the porous media. The raw particle size of the porous plates are all 100 μm as seen in Table 5-3.

Table 5-3: Three kinds of surfaces and four different flow rates.

Surface kinds	Specification of honeycomb plate	Mass flow rates
Bare surface		160, 320, 640, and 1280 kg/m^2-s
Solid honeycomb	2.5-1.7 (pitch-diamter)	160, 320, 640, and 1280 kg/m^2-s
Porous honeycomb	2.5-1.7 (pitch-diamter) (raw particle size: 100 μm)	160, 320, 640, and 1280 kg/m^2-s

Figure 5-9 to Figure 5-12 shows the boiling curves of the bare, solid honeycomb, and porous honeycomb surfaces under different flow rates. We can see that the heat transfer from the solid honeycomb is slightly greater than that on the bare surface at low flow rates but is almost the same as that at high flow rates, whereas the heat transfer from the porous honeycomb plate is greater than that of the bare and solid honeycomb surfaces at all four flow rates. When the solid honeycomb and bare surfaces was compared, three factors were considered that may affect the heat transfer: thermal resistance, boiling surface area, and turbulence. The thermal conductivity of stainless steel [16 W/(m·K)] is much lower than that of copper (391 W/m·K), and a thermal contact resistance exists between the copper surface and honeycomb plate. Figure 5-13 shows images of the boiling phenomena on the bare, solid honeycomb, and porous honeycomb surfaces at

similar heat flux and near CHF condition under same flow rate. For the bare surface, bubbles were produced on the boiling surface, and CHF soon occurred after all the bubbles covered the boiling surface due to lack of water supply. During the boiling using the honeycomb test sections, all bubbles nucleated and departed from the holes and then coalesced and covered the outer surface of the honeycomb. No bubble nucleated on the honeycomb plates. A reduction in the actual boiling surface area occurred in the honeycomb case because the total area of the holes was less than that of the bare surface. These two factors negatively affect the heat transfer. At the same time, the honeycomb structure could increase the flow turbulence and enhanced the heat transfer, but the enhancement effect would become insignificant as flow rate increased. This condition explains why, at a low flow rate, the heat transfer from the solid honeycomb was greater than that of the bare surface but slightly lower at the highest flow rate. The heat transfer increase from the porous honeycomb is attributed mainly to the water supply through the porous media. An increase in the water-supply ability to the heated surface implies greater heat removal and wetting the contact area between copper surface and honeycomb plate. As a result, the slope of the porous honeycomb boiling curve is largest in the three surfaces under all four flow rates.

Under near-CHF conditions, the superheat of the bare surface and the porous honeycomb plate, which was approximately 13 °C, almost did not change as the water flow rate increased. The same was not observed in the solid honeycomb where the superheat increased as the flow rate increased from 15 °C at 160 kg/(m^2·s) to approximately 21 °C at 1280 kg/(m^2·s). For the solid honeycomb, even though the heat transfer was almost the same as that in the bare surface, the CHF was higher under the same water flow rate. The reason believed for the increase in CHF from solid honeycomb

is due to the honeycomb structure. For solid honeycomb, bubbles would nucleate and emerge from the holes and then coalesce outside of the honeycomb. This process delays bubbles coalescing and covering the boiling surface. The increased turbulence caused by water flow over the honeycomb structure also delays the process of bubbles coalescing and covering the surface.

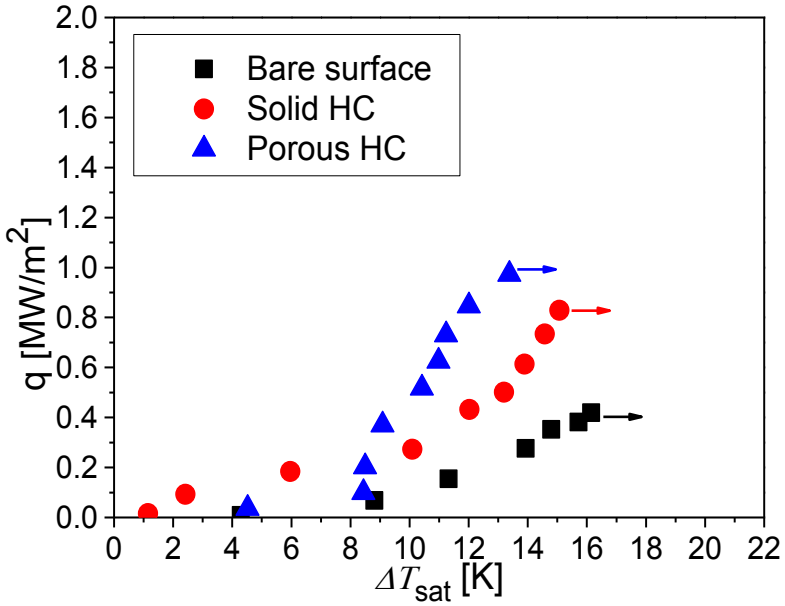

Figure 5-9: Boiling curves of three surfaces at 160 kg/m^{2}s.

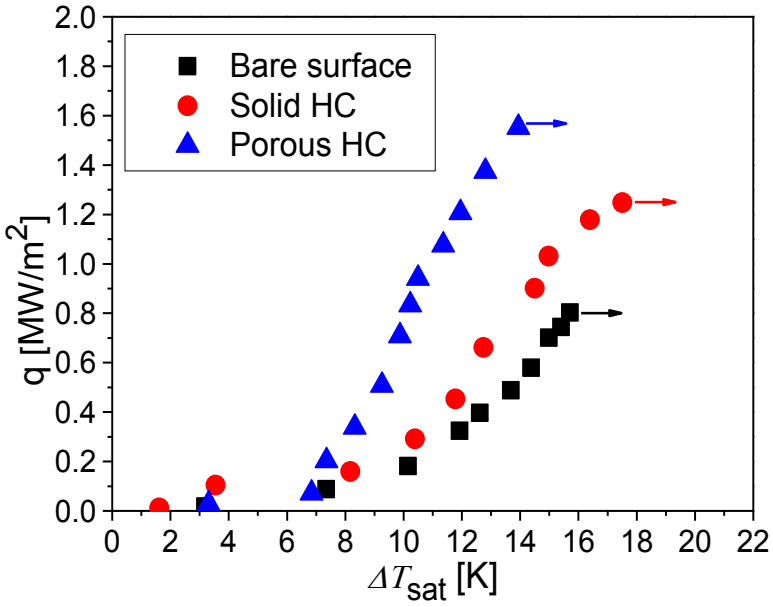

Figure 5-10: Boiling curves of three surfaces at 320 kg/m^{2}s.

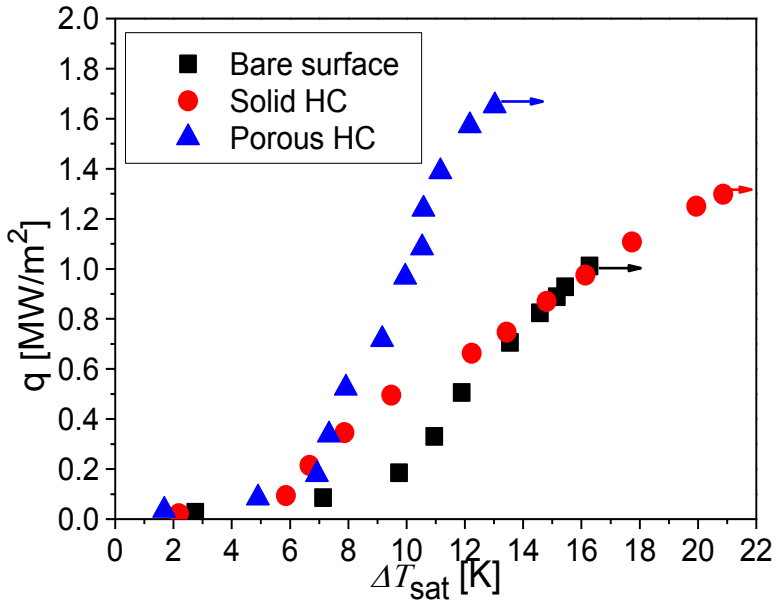

Figure 5-11: Boiling curves of three surfaces at 640 kg/m^{2}s.

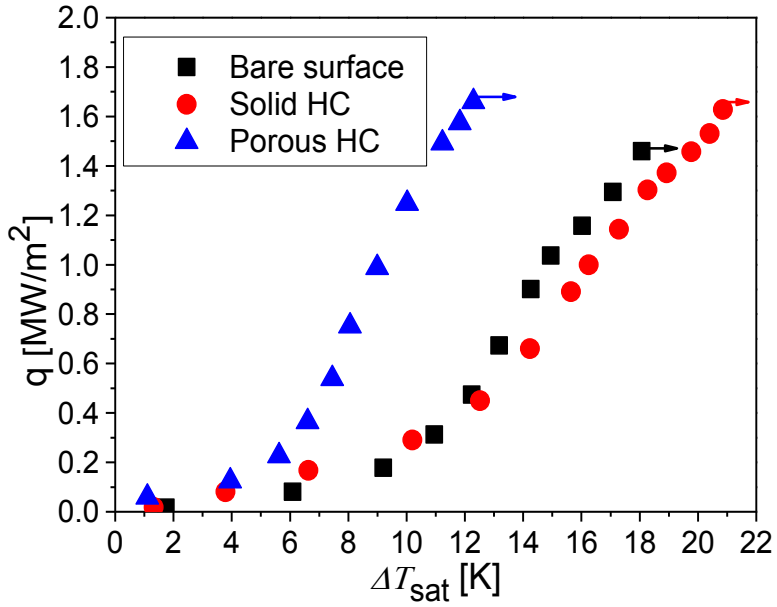

Figure 5-12: Boiling curves of three surfaces at 1280 kg/m^{2}s.

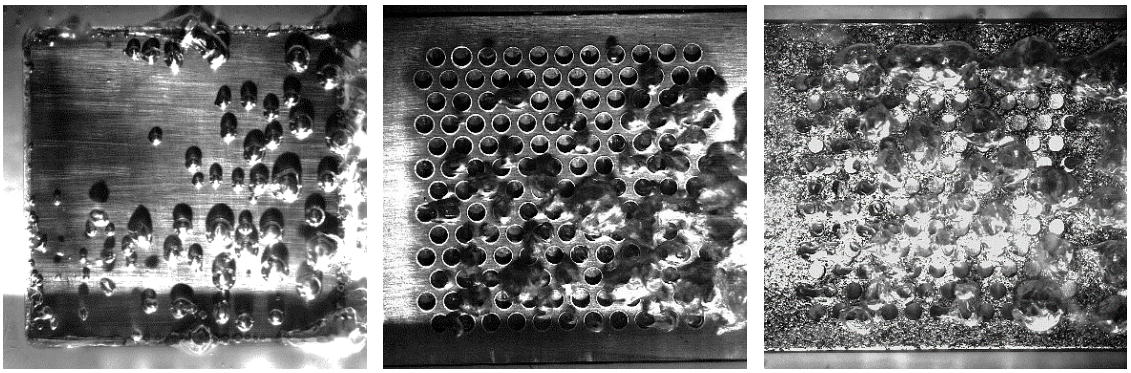

0.08 Mw/m^2 | 0.09 Mw/m^2 | 0.08 Mw/m^2

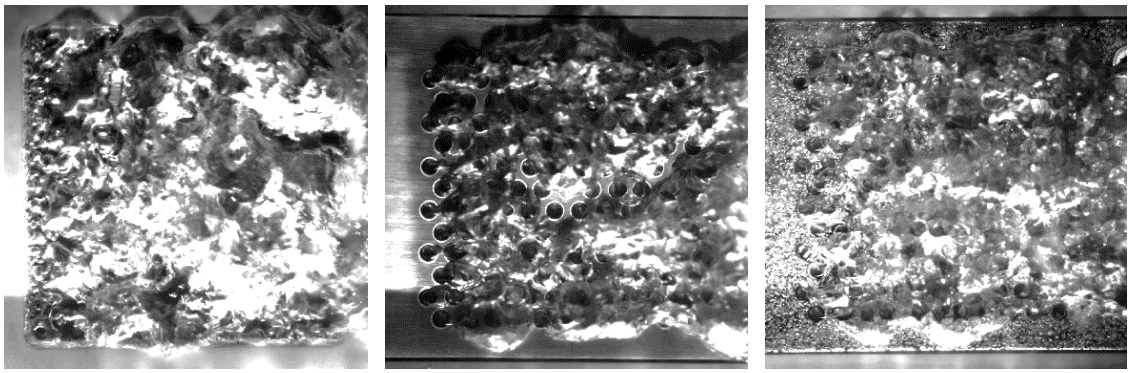

0.51 Mw/m^2 | 0.50 Mw/m^2 | 0.52 Mw/m^2

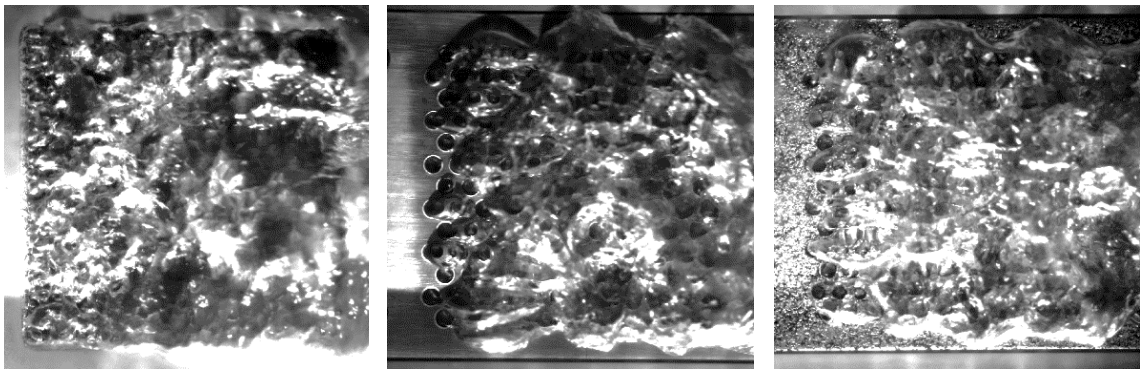

1.01 Mw/m^2 - near CHF | 1.30 Mw/m^2 - near CHF | 1.65 Mw/m^2 - near CHF

a) Bare surface | b) Solid honeycomb | c) Porous honeycomb

Figure 5-13: Boiling phenomena of the bare and honeycomb surfaces at 640 kg/(m^2·s).

Figure 5-14 shows the CHF values for all three surfaces under four different flow rates. It can been seen that CHF values increase under all four flow rates for the solid and porous honeycomb surfaces compared with that in the bare surface. The CHF of the solid honeycomb test section is larger than that of the bare surface and lower than that of the porous honeycomb plates. For the solid honeycomb surface, the enhancement is due to the honeycomb structure. For the porous honeycomb surface, the additional enhancement is due to the water supply through the porous media. Note that when the flow rate increases beyond 320 kg/(m^2·s), no significant increase occurs in the CHF value for the porous honeycomb. The CHF value at a flow rate of 640 kg/(m^2·s) is approximately the same as that at 1280 kg/(m^2·s), implying that the porous honeycomb surface has reached a limit. Even though the porous honeycomb plate shows enhancement in the CHF compared with the bare surface at 160 kg/(m^2·s) flow rate, the CHF value is approximately 60% less than that at 320 kg/(m^2·s). The difference in the CHF values for the other three flow rates is relatively small compared with that at 160 kg/(m^2·s).

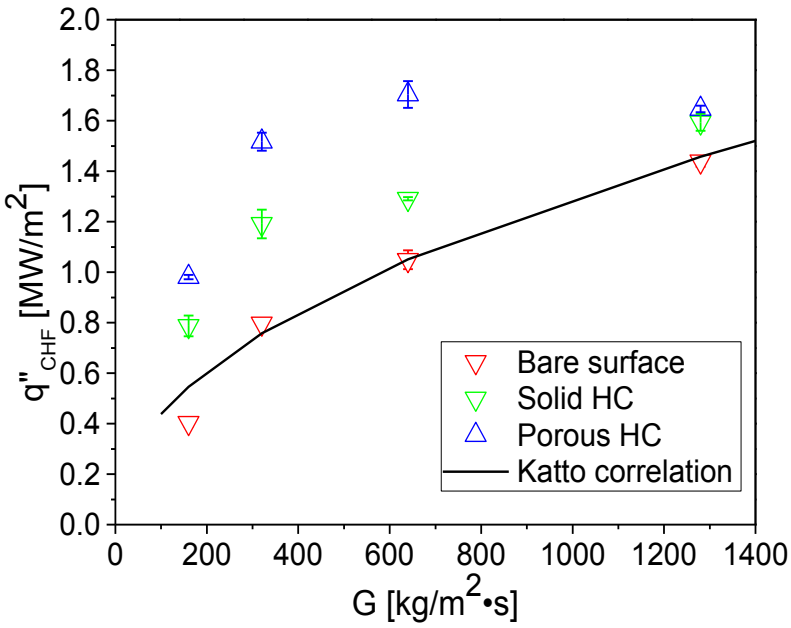

Figure 5-14: CHF values of three surfaces at different water flow rates.

Figure 5-15 shows the boiling phenomenon near the CHF at the 160 kg/(m^2·s) flow rate. Because of the low flow rate conditions, the bubbles coalesce and cover the honeycomb surface when they emerge from the holes. A big vapor film will be produced on the honeycomb plate. Therefore, water cannot be supplied to the boiling surface and CHF happens at a relatively low heat flux. For flow rates beyond 320 kg/(m2·s), a sufficient inertial force is available to remove the bubbles, causing an increase in the CHF.

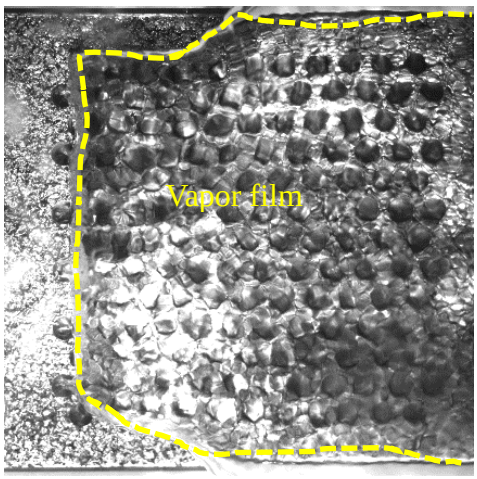

Figure 5-15: Boiling phenomena near the CHF at a flow rate of 160 kg/(m^2·s).

Figure 5-16 shows the increase ratios of the honeycomb plates (q''_{hc}-CHF) compared with those of the bare surface (q''_{b}-CHF). The increase ratios decrease as the flow rate increases. The ratio is approximately 2.4 for the porous honeycomb at 160 kg/(m^2·s) and decreases to nearly 1.1 for both honeycombs at 1280 kg/(m^2·s). The main reason is that as the flow rate increases, the increase in the bare surface CHF is greater than that in the honeycomb surface CHF, which means that the water-supply effect has reached a limit as the flow rate increases. At a flow rate of 1280 kg/(m^2·s), the water-supply ability and the honeycomb structure effect are almost insignificant.

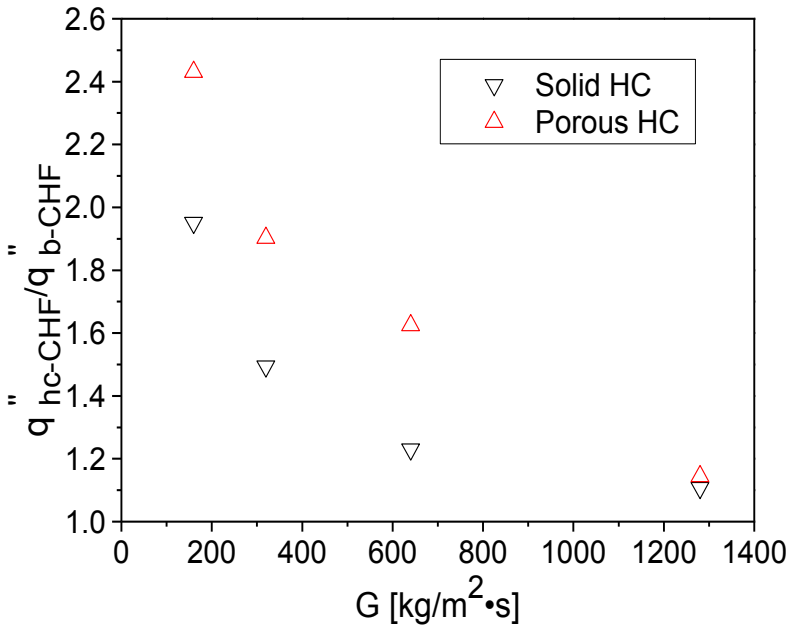

Figure 5-16: CHF increase ratios at different water flow rates.

In the work of Mori [23], they believed that water can only be supplied to the boiling surface through ceramic porous media and CHF will occur when the maximum capillary force is equal to the total pressure drop along the liquid–vapor path. There is a total separation of water–vapor flow. For the solid stainless steel honeycomb plate in this study, water cannot be supplied to the boiling surface through the porous media (not porous) and can only be supplied through the perimeter of the holes at the moment the vapor escapes. For the porous honeycomb plate, additional water is supplied through the porous media. As the CHF values of solid honeycomb plate in this study are also very high compared to that of bare surface, it can be concluded that water supply through the perimeter of the holes is also an important water supply way. A schematic of the water-supply mechanism is proposed as shown in figure 5-17 for both types of honeycomb plates. The stronger the water-supply ability through the porous media is, the greater is the CHF enhancement compared with the solid honeycomb plate.

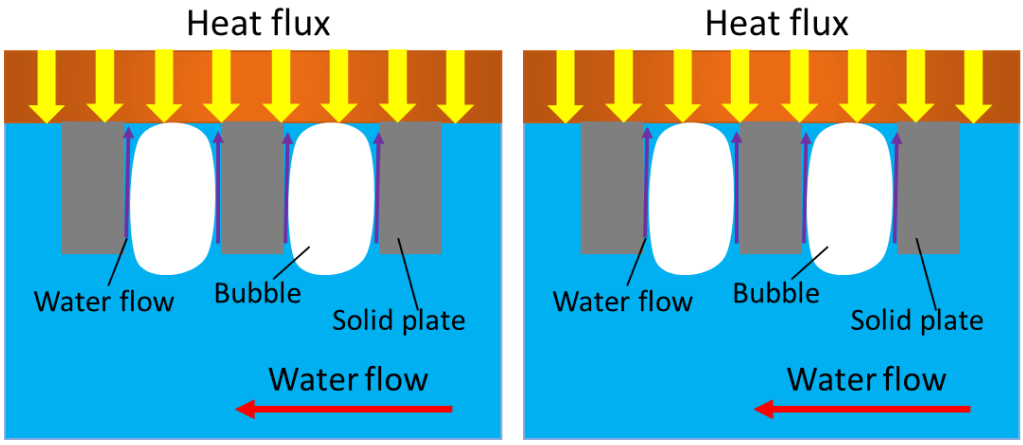

Figure 5-17: Water supply mode of two types of honeycomb plates.

Based on this water supply model, for the porous plate, percentage of water supplied through the porous media near CHF conditions at different water flow rates can be can be calculated. Percentage of water supplied by the holes equals the ratio of $q_{CHF-solid}$ and $q_{CHF-porous}$ at the same flow rate. The rest percentage of water is assumed to being supplied from the metal porous media. Figure 5-18 shows the percentage of water supply through two supply ways of porous plate at different water flow rates. It can be seen that more water is supplied through the perimeter of the holes compared to the pores of the porous honeycomb for downward-facing flow boiling conditions. For example, the lowest flow rate only shows an additional 24% enhancement through the water supply by the pores (for the porous honeycomb), which is not as significant as the water supplied by the perimeter of the holes (solid honeycomb). For the highest flow rate condition the CHF for the solid and porous honeycombs are approximately the same, implying that the water is supplied to the boiling surface almost all by the perimeter of the holes.

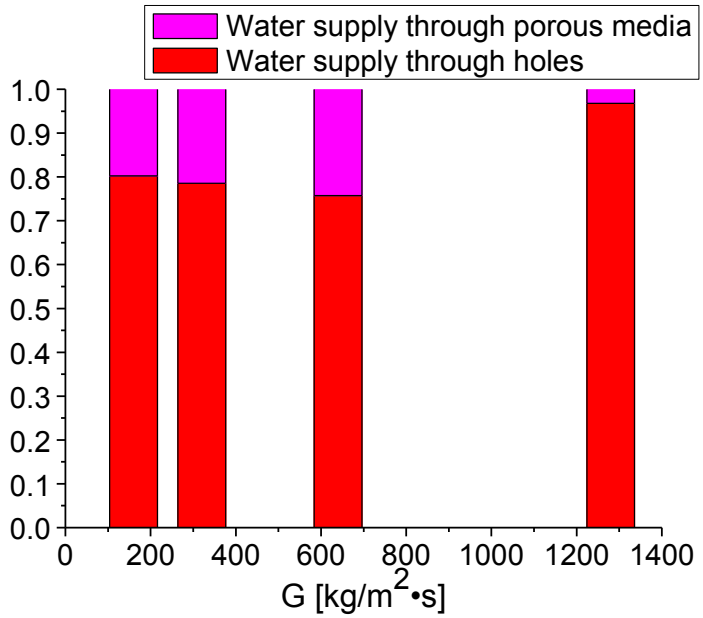

Figure 5-18: Percentage of water supply though two ways for porous plate.

5.4 CHF values of honeycomb plates at same flow rate

To find a honeycomb plate which can enhance CHF to the largest extent in saturated downward-facing flow boiling condition and investigate the enhancement mechanism, downward-facing flow boiling experiments were conducted at same flow rate (640 kg/(m^2·s)) using different honeycomb plates.

5.4.1 CHF values of honeycomb plates with different raw particle sizes

Figure 5-19 shows the CHF values of solid and three porous honeycomb plate with different metal particle diameters at 640 kg/(m^2·s). As mentioned before, the hole diameter and hole pitch of the four plates are same which is 1.7 mm and 2.5 mm, respectively. CHF value increases as the metal particle diameter increases, but the CHF value of honeycomb plate whose metal particle diameter is 20μm is almost the same with that of honeycomb plate whose metal particle diameter is 100μm which means the water

supply ability of these two kinds of porous honeycomb plates are almost the same. The reason why the water supply ability through 5μm porous plate is weaker than that of 20 μm and 100μm porous plate is believed to that the permeability of 5μm porous plate is too small.

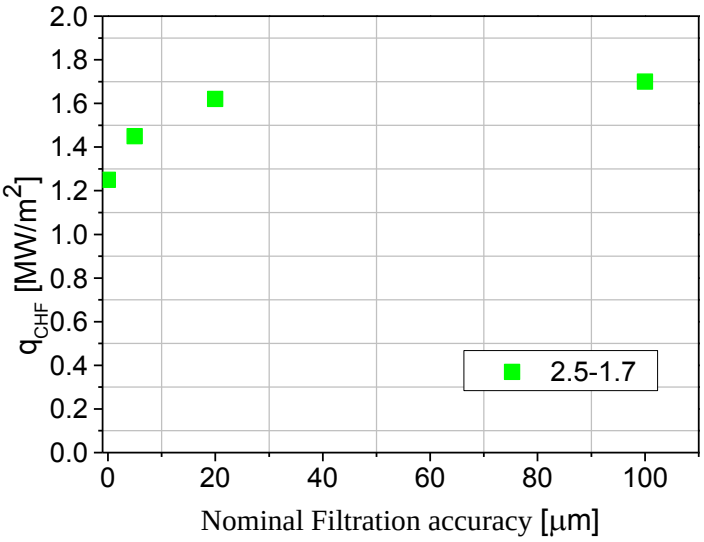

Figure 5-19: CHF values of solid and three porous honeycomb plates at 640 kg/(m^2·s).

5.4.2 CHF values of honeycomb plates with different hole diameters and pitches

As mentioned above, to find a honeycomb structure which can enhance CHF most and investigate the enhancement mechanism, nine honeycomb plates with different hole diameters or pitches were designed and manufactured. Flow boiling experiments were conducted using these honeycomb plate at same flow rate which is 640 kg/(m^2·s) to exclude the flow rate influence on CHF. As mentioned, to clarify the water supply ability through the metal porous media, solid honeycomb plate experiments were also conducted at same flow rate (640 kg/(m^2·s)).

Table 5-4 shows the information of the nine kinds of honeycomb plates and their CHF values at 640 kg/(m^2·s). From this table we can get some important conclusions. It is noted

that the CHF value of bare surface at this flow rate is about 1Mw/m^2.

Firstly, in general, for honeycomb plate with same hole diameter and hole pitch, all CHF values of porous plates are higher than that of solid honeycomb plates due to additional water supply through the metal porous media. But the CHF increase ratios of them are different.

Secondly, the highest CHF value is obtained by using the porous honeycomb plate with 1.7 mm hole diameter and 2.5 mm pitch.

Thirdly, not all honeycomb plates can get a higher CHF value than that of the bare surface at this flow rate. Among nine porous honeycomb plates, CHF values of seven of them are higher than of the bare surface. Among the solid honeycomb plates, CHF values of only two of them are higher than that of the bare surface. The CHF values of some solid honeycomb plates are even very low.

Table 5-4: CHF values of all honeycomb plates at 640 kg/(m^2·s).

Number of holes	pitch/diameter	Hole Diameter (mm)	Hole pitch (mm)	CHF of porous plate Mw/m^2	CHF of solid plate Mw/m^2
149	1.47	1.7	2.5	1.65	1.3
149	2.5	1.0	2.5	0.9	0.04
67	2.35	1.7	4.0	0.7	0.61
295	1.8	1.0	1.8	1.44	0.81
216	1.24	1.7	2.1	1.36	1.12
85	1.33	2.4	3.2	1.33	1.00
52	1.45	2.9	4.2	1.25	0.91
105	1.76	1.7	3.0	1.46	0.67
52	1.75	2.4	4.2	1.18	0.73

The experimental results of these honeycomb plates can be explained and analyzed from two aspects: boiling area percent and additional water supply through porous media.

As mentioned before, if we attach a honeycomb plate on the copper boiling surface, there will a reduction of the boiling area due to the structure and very low thermal conductivity of stainless steel. The boiling area is only the total area of the holes. The actual boiling area equals the total hole area which is smaller than that of copper surface. Figure 5-20 is the photo of a porous plate with a 1.7 mm hole diameter and 2.5 mm pitch. Bubbles will only grow and come out from the holes. At this condition, the total hole area is only 37.6% of the copper surface area. Decrease in boiling area may have a negative effect on CHF.

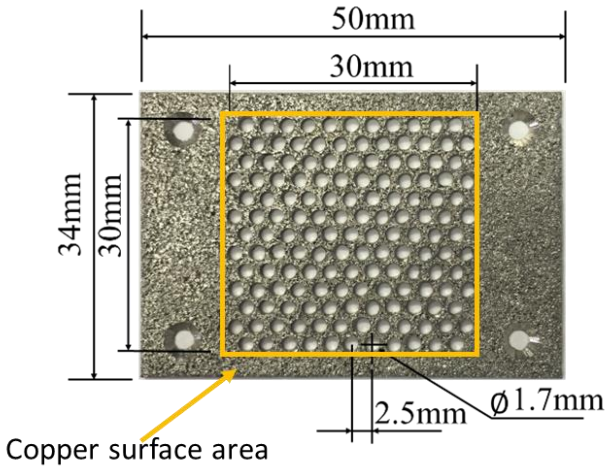

Figure 5-20: Photo of the porous plate with 1.7 mm hole diameter and 2.5 mm pitch.

Here we define a parameter - boiling area ratio, which equals the ratio of total hole area and copper heat surface area. It is noted that for honeycomb plates which have same pitch/diameter, the boiling area ratios of them are same.

Figure 5-21 shows the relationship between CHF values of all honeycomb plates and boiling area ratio. CHF values of solid honeycomb plates have strongly relationship with

boiling area percent. In general, CHF values of solid honeycomb plates increase as boing area percent increase. It is noted that even though the solid honeycomb plate with 1.7 mm hole diameter and 2.5 mm hole pitch has same boiling area ratio with the solid honeycomb plate with 2.9 mm hole diameter and 4.2 mm hole pitch, CHF of the former is much higher than that of the latter. The hole diameter of the latter is large and number of the hole is small, so the size of bubbles coming out from the hole is big. As a result, the heat surface is easily be covered by the bubbles and CHF happen earlier.

The CHF values of porous honeycomb plates do not show strongly relationship with boiling area percent due to additional water supply through the porous media as porous media area decreases as boiling area percent increases. It is noted that CHF of two of porous honeycomb are lower than that of bare surface. The common of these two porous honeycomb plates is that both of their boiling area percent are lower than 20%, which are 13% and 16.9 %, respectively.

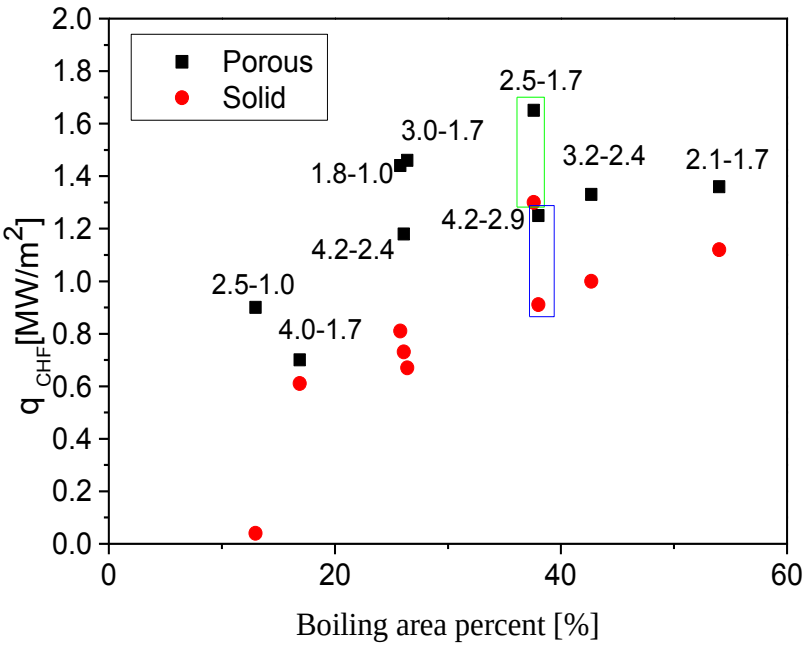

Figure 5-21: Relationship between CHF values and boiling area percent.

Next, additional water supply through porous media is analyzed. It is believed that CHF difference between porous honeycomb plate and solid honeycomb plate whose hole diameter and hole pitch are same is due to additional water supply through metal porous media. Larger difference in CHF between the porous honeycomb plate and solid honeycomb plate which have same hole diameter and pitch, more water is supplied through the metal porous media.

Figure 5-22 shows CHF values of four kinds of honeycomb plates which have same hole diameter (1.7 mm) but different pitches change as the boiling area percent. It can be seen that the both of the CHF values of solid plates first increase and then decrease as the boiling area percent increases. Even though the boiling area percent of solid honeycomb plate with of 2.1 mm pitch is higher than that of the solid plate with 2.5 mm pitch, the CHF value of the former is lower than the latter. The reason is that bubbles easily coalesce with each other and produce a vapor film which will prevent water supply to the heat surface when the hole pitch is too small. As a result, CHF will happen earlier even though the boiling area is higher. The CHF values of porous plates are higher than that of solid plates with same hole diameter and hole pitch due to the additional water supply through the metal porous media. As the hole pitch increase, the porous media area will increase. As a result, water supply ability through porous media will increase. So even though the CHF value of solid honeycomb plate with 3.0 mm pitch is smaller than that of solid honeycomb plate with 2.1 mm pitch, the CHF value of porous honeycomb plate with 3.0 mm pitch is higher than that of porous honeycomb plate with 2.1 mm pitch due to a stronger water supply ability through the porous media. It is noted that the CHF value of the porous honeycomb plate with 4.0 mm pitch is very low. This is due to its too small boiling area ratio. When the boiling area ratio is too small, the CHF value of porous

honeycomb plate will be limited by too small boiling area.

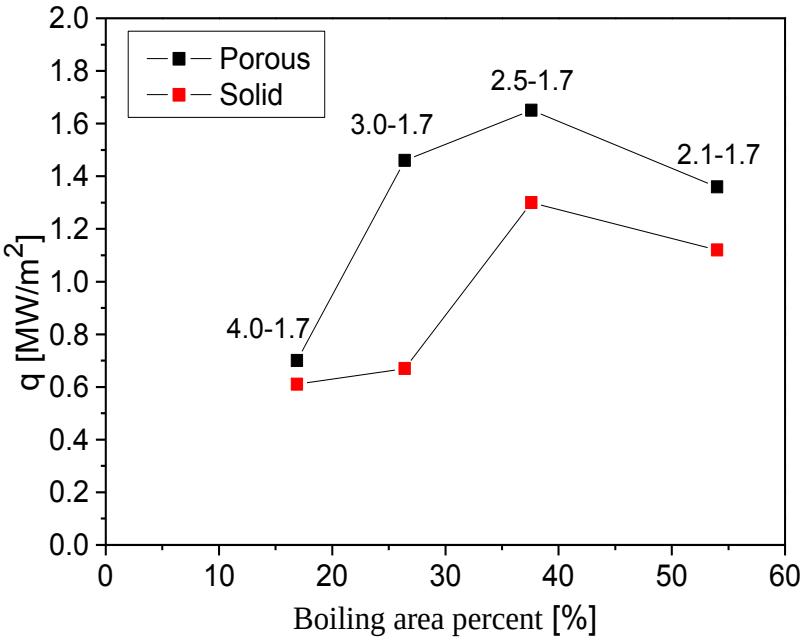

Figure 5-22: CHF values of honeycomb plates with 1.7 mm hole diameter.

Figure 5-23 shows CHF values of two kinds of honeycomb plates which have same hole diameter (1.0 mm) change as the boiling area percent. Both of the CHF values of porous plates and solid plates increase as the boiling area percent increase. CHF values of porous plate with 1.8 mm hole pitch are higher than that of porous plate with 2.5 mm pitch due to a high boiling are ratio. CHF value of the solid honeycomb plate with 2.5 mm pitch is very low due to its small hole diameter and low boiling are ratio. It is noted that CHF of porous plate with 1.0 mm hole diameter and 2.5 mm hole pitch is much smaller than that of porous plate with 1.7 mm hole diameter and 2.5 mm hole pitch. The reason is that it is hard for water supply through the perimeter of the hole and there is a big boiling area ratio reduction when the hole diameter is reduced from 1.7 mm to 1.0 mm.

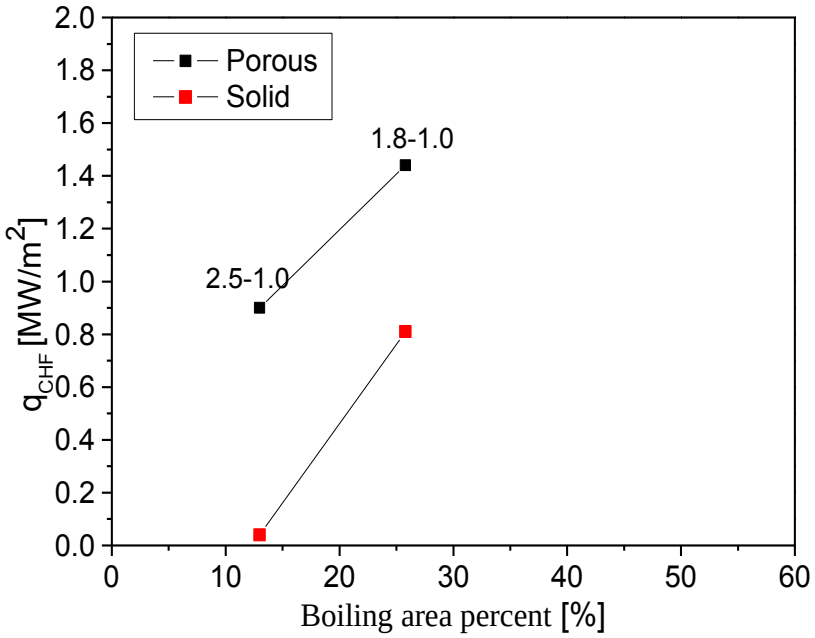

Figure 5-23: CHF values of honeycomb plates with 1.0 mm hole diameter.

Figure 5-24 shows the change CHF values of two kinds of honeycomb plates which have same hole diameter (2.4 mm) as the boiling area percent.

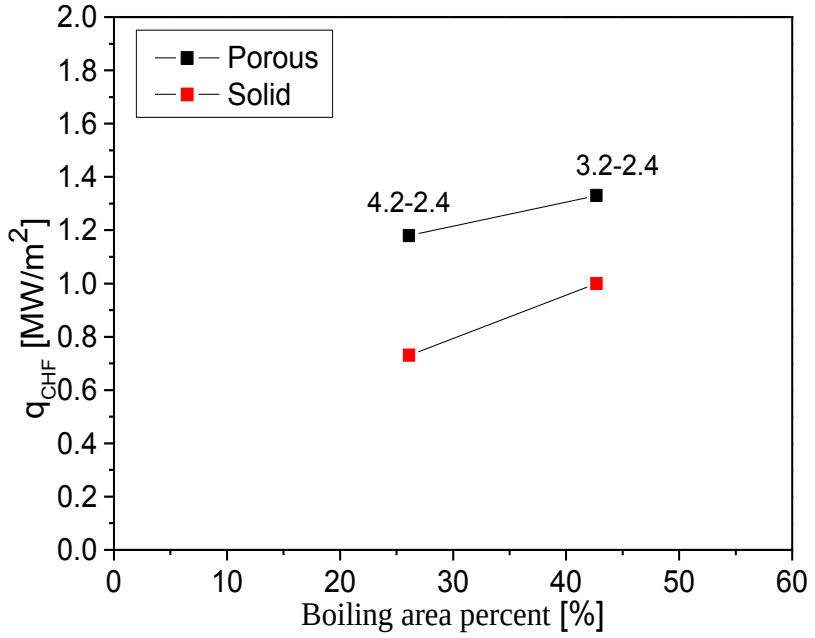

Figure 5-24: CHF values of honeycomb plates with 2.4 mm hole diameter.

The tendency is similar to that of honeycomb plate with 1.0 mm hole diameter while the CHF difference between porous plates and solid plates are smaller than that of 1.0 mm hole diameter condition.

Comparing CHF values difference between porous plates and solid plates, it can be concluded: for porous honeycomb plate, there are two water supply ways: from the perimeter of the holes and from the porous media. Water supply through the porous media is more important for a small hole diameter comparing to a large hole diameter condition. Water supply through the perimeter become to the main way when the pitch/hole ratio is small.

5.5 Summary of honeycomb experiment

Downward-facing experiments using same honeycomb plates at different flow rates and using different honeycomb plates at same flow rates were conducted. It is found that saturated downward-facing flow boiling CHF can be enhanced by attaching a metal porous honeycomb plates (1.7 mm hole diameter, 2.5 mm hole pitch) on the heat surface at all flow rates, but the CHF enhancement effect decreases as the flow rate increases. CHF enhancement of porous honeycomb plate is due to honeycomb structure as well as additional water supply through porous media. Among all the honeycomb plates, the porous honeycomb plate (100μm) with 1.7mm hole diameter, 2.5mm pitch can obtain a maximum enhancement effect at 640 kg/m^2-s due to a relatively high boiling area percent and a suitable hole diameter. The roles of two water supply ways of porous honeycomb plates were analyzed. It is found that water supply through the porous media is more important for a small hole diameter comparing to a large hole diameter condition and water supply through the perimeter become to the main way when the pitch/ratio is small.

6 Irradiation Experiment

To research whether RISA irradiation effect can enhance CHF of bare surface or honeycomb in saturated downward-facing flow boiling condition as the surface wettability will increase after being irradiated or there is any other irradiation effect on heat transfer and CHF in flow boiling condition, irradiation experiment of bare surface and porous honeycomb were conducted. Test sections and porous honeycomb plate were irradiated and then downward-facing flow boiling experiments were conducted just after irradiation. The irradiation experiment were conducted at Takasaki Advanced Radiation Institute of Japan. So the downward-facing experiment loop was moved there before the irradiation experiment. To research whether there is any difference between different kinds of irradiation, two types of irradiation sources (Gamma-ray irradiation and electron beam irradiation) were used.

6.1 Irradiation facility

6.1.1 Gamma-ray irradiation facility

Figure 6-1 shows the photo of Gama-ray irradiation experiment. The Gamma-ray source is C_O^{60}. The test sections of bare surface and honeycomb were fixed on a shelf and put in the Gamma-ray irradiation room as shown in figure 6-1. The porous honeycomb plates used in the Gamma-ray irradiation experiment were also put on the shelf to be irradiated. The dose rate is 15 kGy per hour. The total irradiation dose of copper surface and porous honeycomb plate is envisaged to be around 1000 kGy. However, due to the schedule of Gamay-ray irradiation room, the irradiation dose is not exactly 1000 kGy.

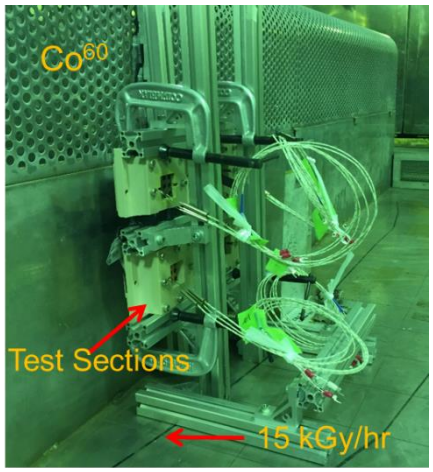

Figure 6-1: Photo of the Gamma-ray irradiation facility.

6.1.2 Electron beam irradiation facility

The electron beam irradiation and flow boiling experiments were both conducted at Takasaki Advanced Radiation Institute of Japan. The schematic layout of the electron beam irradiation facility is as shown in figure 6-2. After being emitted from the heated filaments, electrons are accelerated through a vacuum tube by high voltage and then pass through the metallic window to irradiate the copper surface. There is a beam scanner before the window to expand the irradiation area.

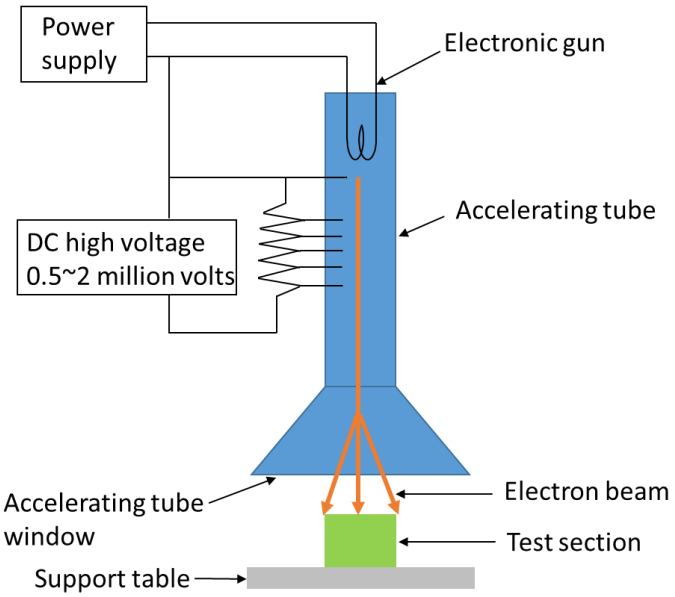

Figure 6-2: The schematic diagram of the electron beam irradiation facility.

The irradiation parameters is as shown in Table 1. The accelerating voltage and electronic current of the electron beam are 2Mev and 1mA, respectively.

Table 6-1: The parameter of the electron beam irradiation.

Accelerating voltage	Electronic current	Sweep speed	Dose rate
2Mev	1mA	200Hz(5ms)	~1.5 kGy/s

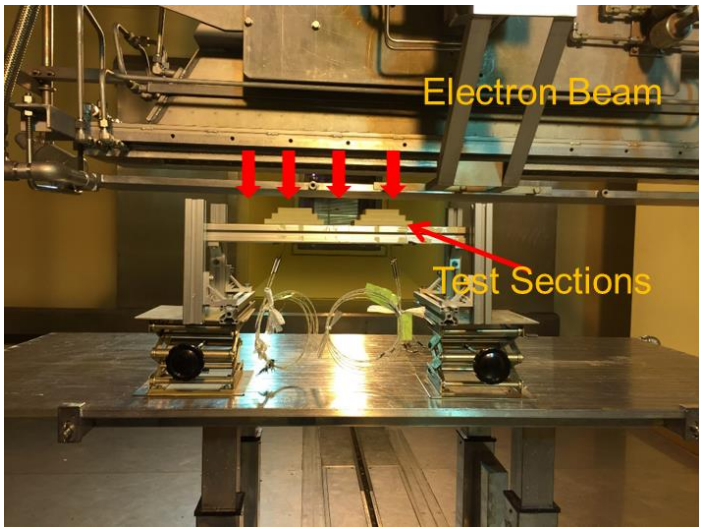

Figure 6-3: Photo of the electron beam irradiation facility.

6.2 Experiment procedure

For bare surface irradiation experiments, the experiment procedure is as below:

1. Polishing the copper surface of the bare surface test section using P1200 sandpaper; cleaning it using acetone and distilled water; starting irradiation.
2. Stopping irradiation; installing the bare surface test section on the flow channel.
3. Adding distilled water into the loop, heating the water to saturation condition and degassing for 30 minutes.
4. Adjusting the flow rate to target flow rate using the pump controller.
5. Increasing the output voltage of the slidac (Increasing the heat flux) step by step and keeping each stable state for at least 4 minutes;

6. CHF happens; shut down the heater power of the test section; saving data.

For honeycomb irradiation experiments, the experiment procedure is as below:

1. Polishing the copper surface of the honeycomb test section using P1200 sandpaper; cleaning it using acetone and distilled water; starting irradiation.
2. Stopping irradiation; installing the honeycomb test section on the flow channel.
3. Adding distilled water into the loop, heating the water to saturation condition and degassing for 30 minutes.
4. Adjusting the flow rate to target flow rate using the pump controller.
5. Increasing the output voltage of the slidac (Increasing the heat flux) step by step and keeping each stable state for at least 4 minutes;
6. CHF happens; shut down the heater power of the test section; saving data.

6.3 Gamma-ray irradiation experimental results

To verify the surface wettability of copper surface and metal porous plate be increased by Gamma-ray irradiation, a copper sample and a metal porous plate were irradiated and then the droplet tests were conducted. The Gamma-ray irradiation dose is around 1000KGy. After the test pieces were taken out from the irradiation room, droplet tests were conducted immediately. It was found that the static contact angle of copper surface and porous honeycomb plate decreases significantly after Gamma-ray, implying an increase in surface wettability after being irradiated by 1000 kGy irradiation. Figure 6-4 shows the contact angle change of porous plate (raw particle size: 100μm) after Gamma-ray irradiation from approximately 91 degrees to 0 degree. Figure 6-5 shows the contact angle change of copper surface after Gamma-ray irradiation from approximately 99 degrees to 15 degree.

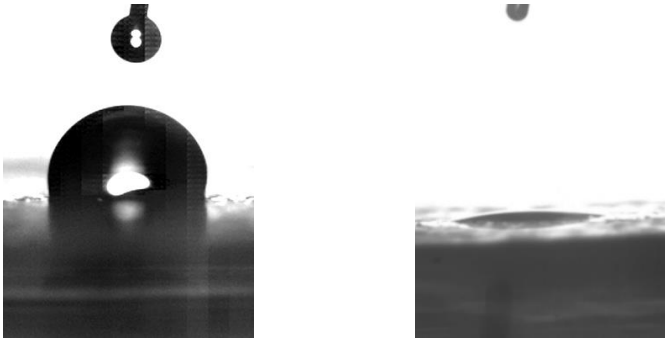

91°±6° 0°

Before irradiation After irradiation

Figure 6-4: Static contact angle of porous plate before and after Gamma-ray irradiation.

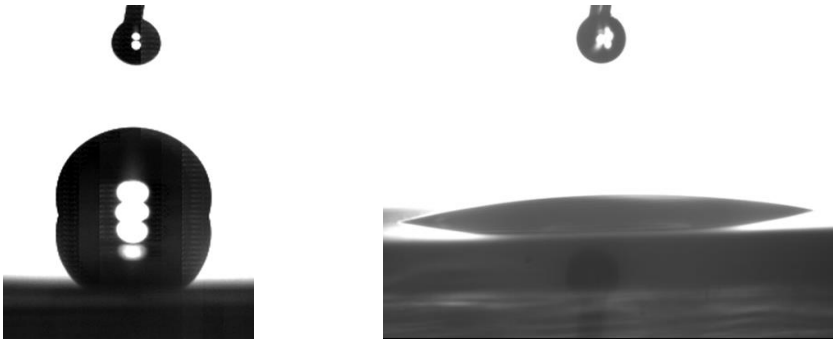

99°±1° 15°±2°

Before irradiation After irradiation

Figure 6-5: Static contact angle of bare surface before and after Gamma-ray irradiation.

To investigate whether the CHF of bare surface can be enhanced by RISA effect or CHF values of porous honeycomb can be further enhanced by RISA effect in saturated downward-facing flow boiling condition, three cases of experiments as shown in Table 6-2 were conducted. The flow rates in the three cases are all 640 kg/(m^2·s). The porous honeycomb plate (raw particle size: 100μm) with a 1.7 mm hole diameter and 2.5 mm pitch was used.

Table 6-2: Three cases of the Gamma-ray irradiation experiments.

Case 1	BARE(G-1035kGy)
Case 2	Cu (G-960kGy)+ HC
Case 3	Cu (G-645kGy) + HC(G-2040kGy)

Figure 6-6 shows the boiling curves of bare surface before and after about 1000 kGy Gamma-ray irradiation. CHF does not have an increase after the Gamma-ray irradiation. At low heat flux condition, the wall superheat has a little increase compared with that of non-irradiation condition. As the heat flux continues to increase, the two boiling curves come close.

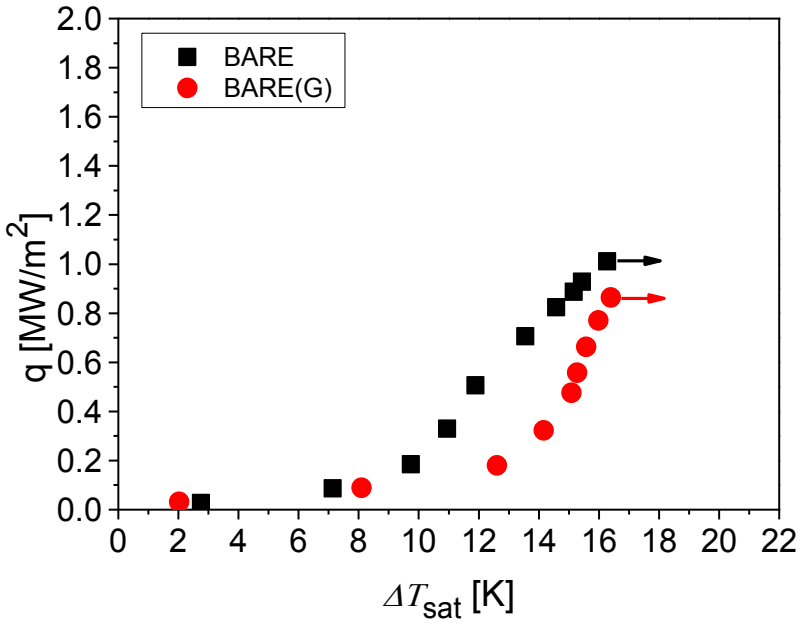

Figure 6-6: Boling curves of bare surface before and after Gamma Irradiation at 640kg/(m^2·s).

This result means that CHF in saturated downward-facing flow boiling cannot be enhanced just by surface wettability increase unlike pool boiling condition. On one hand, water supply ability in saturated downward-facing boiling is strong enough due to the high mass flow rate (640 kg/(m^2·s). On the other hand, comparing to water supply ability, bubble removal which will leave space for water supply to the heat surface is more important for downward-facing flow boiling CHF. So CHF value does not increase even though the surface wettability increase a lot after Gamma-ray irradiation.

Figure 6-7 shows the boiling process of bare surface after Gamma-ray irradiation at 640kg/(m^2·s). Compared with the boiling process of non-irradiation at this flow rate in figure 4-6, the number of nucleation sites decrease at low heat flux after irradiation, this is why the wall superheat at low heat flux shows a little increase after irradiation.

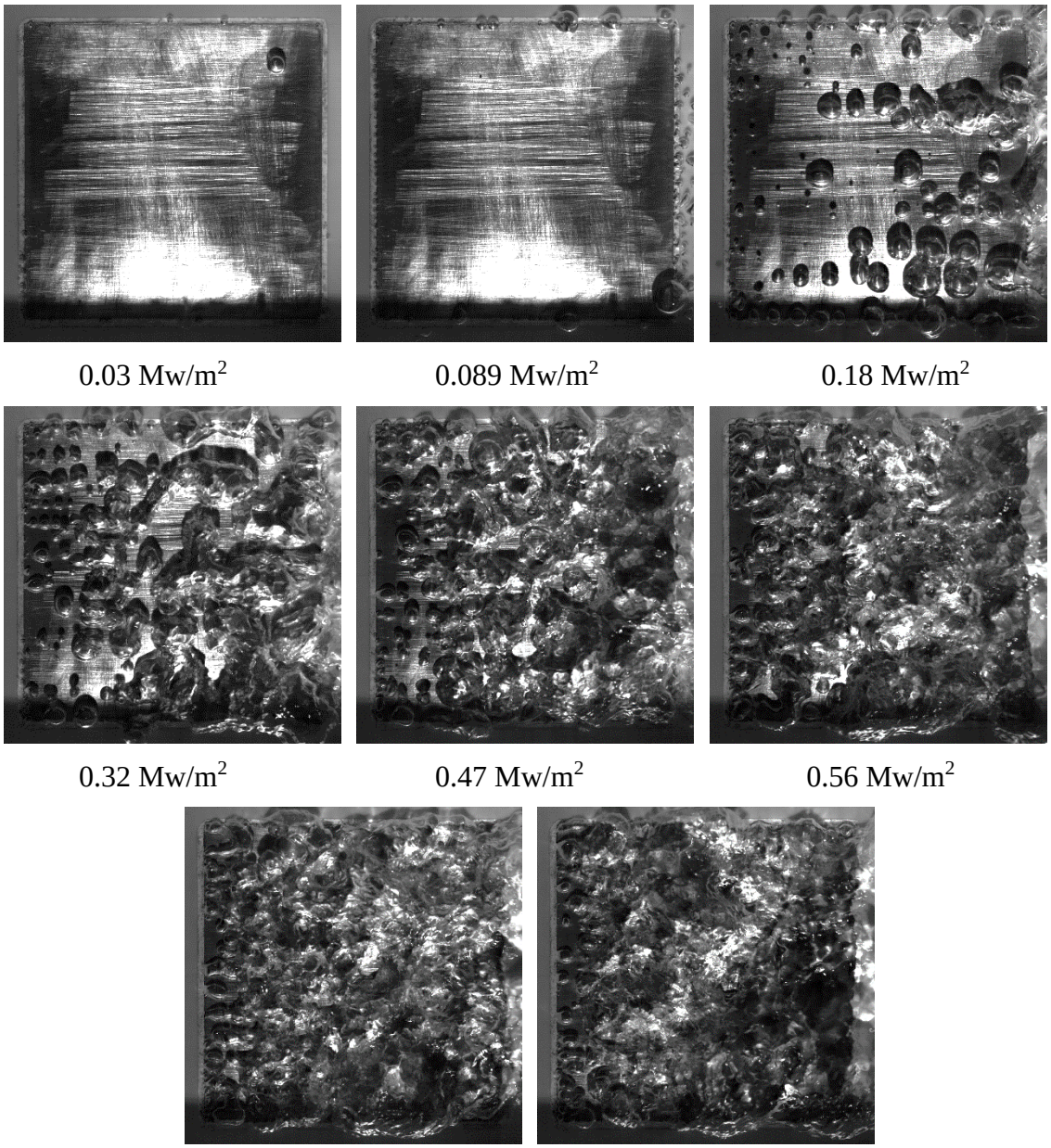

0.03 Mw/m^2 0.089 Mw/m^2 0.18 Mw/m^2

0.32 Mw/m^2 0.47 Mw/m^2 0.56 Mw/m^2

0.86 Mw/m^2 CHF

Figure 6-7: Boling process of bare surface after Gamma irradiation at 640kg/(m^2·s).

Figure 6-8 shows the boiling curves of porous honeycomb plates before and after Gamma-ray irradiation at 640kg/m^2-s. It can be seen that CHF values do not have any increase no matter just the copper surface is irradiated by Gamma-ray or both of the copper surface and the porous plate are irradiated by Gamma-ray while the wall superheat also increases after Gamma-ray irradiation like bare surface condition. For porous honeycomb plate, the water supply ability is very strong due to the high mass flow rate and water supply through the porous media. As the CHF of porous honeycomb plate happens at a high heat flux, many bubbles generate on the heat surface near CHF condition. Slowing down coalescing of bubbles and leaving space for water supply to the heat surface is more important for downward-facing flow boiling CHF. So CHF values of porous honeycomb plates cannot be further increased even though the surface wettability of copper surface and porous plate increase a lot after Gamma-ray irradiation.

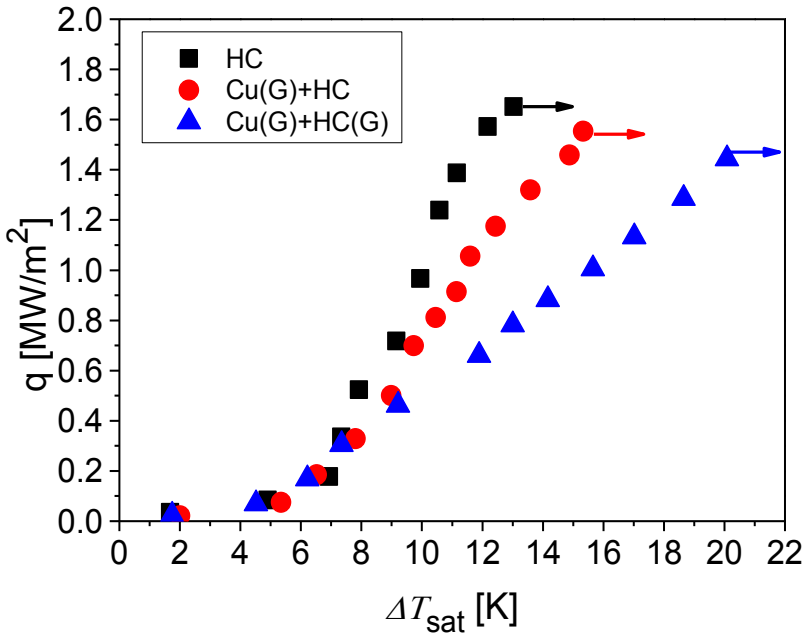

Figure 6-8: Boling curves of honeycomb surface before and after Gamma Irradiation at 640kg/(m^2·s).

6.4 Electron beam irradiation experimental results

As like the Gamma-ray irradiation experiment, we first researched electron beam irradiation on CHF of bare surface and porous honeycomb plate using 1000 kGy irradiation dose. The two cases of the electron beam irradiation experiments are as shown in table 6-3. The mass water flow rate adopted is 320 kg/(m^2·s) and the raw particle size of the porous plate is 5μm. We want to research whether RISA effect can enhance CHF when the flow rate is not so high and permeability of the porous plate is small as there is no CHF enhancement in the Gamma-ray irradiation experiment.

Table 6-3: Two cases of the electron beam irradiation experiments.

Case 1	BARE(E-1000kGy)
Case 2	Cu (E-1000kGy)+ HC(1000kGy)

Also, we did the droplet test just after the electron beam irradiation like in Gamma-ray irradiation experiment. Figure 6-9 shows the contact angle change of porous plate (raw particle size: 5μm) from approximately 100 degrees to 0 degree after 1000kGy electron beam irradiation.

91°±6° 0°

Before irradiation After irradiation

Figure 6-9: Static contact angle of porous plate before and after electron beam irradiation.

Figure 6-10 shows the contact angle change of copper surface from approximately 100 degrees to 30 degree after 1000kGy electron beam irradiation.

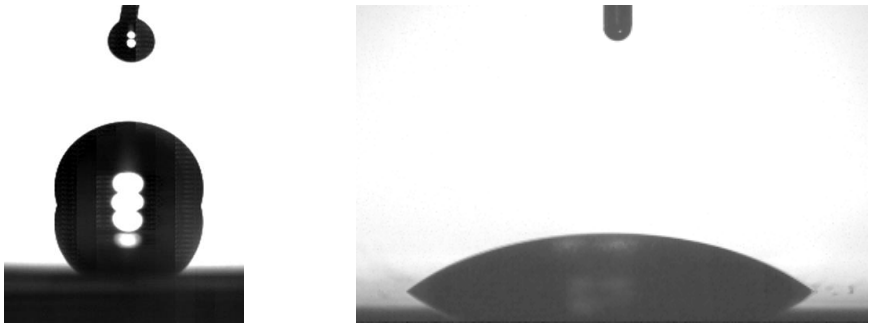

99°±1° 29°±4°

Before irradiation After irradiation

Figure 6-10: Static contact angle of bare surface before and after electron beam irradiation.

It can be seen that that the static contact angle of both bare surface and metal porous plate decreases significantly, implying an increase in surface wettability after the electron beam irradiation as like the surfaces being irradiated by Gamma-ray irradiation.

The downward-facing boiling experiments were conducted just after the electron beam irradiation as like the Gamma-ray irradiation experiment. Figure 6-11 shows the boiling curves of bare surface and porous honeycomb plate before and after electron beam irradiation at 320 kg/(m^2·s). It is unexpected that both CHF values of bare surface and honeycomb plate have a big decrease after electron beam irradiation. Even though the boiling curves are very close before and after electron beam irradiation, the CHF values of two cases after electron beam irradiation are just about half compared with that of non-irradiation conditions. These experimental results are very different with that of Gamma-ray irradiation experiments.

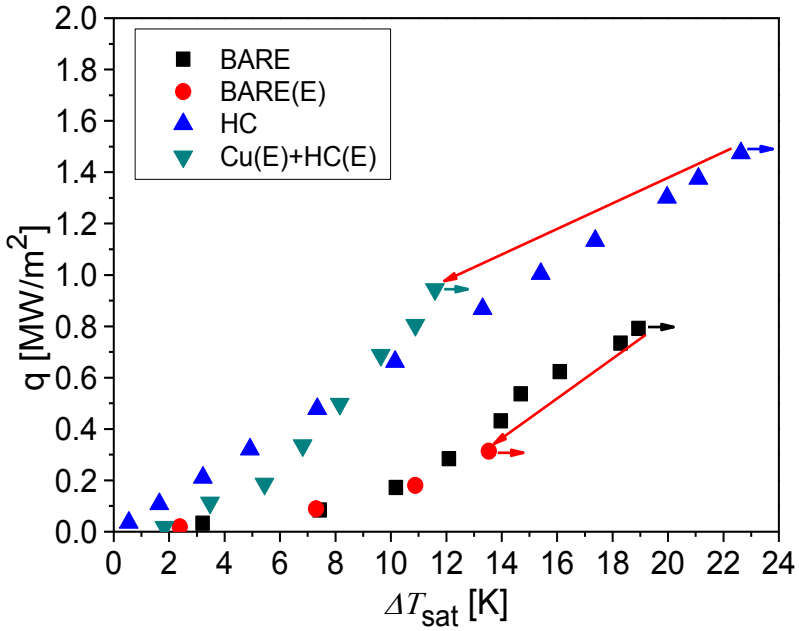

Figure 6-11: Boiling curves before and after electron beam irradiation at 320kg/(m^2·s).

Boiling videos of bare surface are used to find the reason of CHF degradation. Figure 6-12 shows the boiling process of the bare surface after 1000 kGy electron beam irradiation at 320kg/(m^2·s). Comparing with the boiling process of non-irradiation bare surface condition at same flow rate in figure 4-5, it can be seen that many more small bubbles generated from the surface which means the number of nucleation sites increases after the copper surface being irradiated by electron beam irradiation. At the same low heat, the heat surface area covered by the bubbles after irradiation is larger than that of non-irradiation condition. For irradiation condition, the heat surface uncovered by the bubbles reduce more rapidly as the heat flux increases than that of non-irradiation condition. As a result, CHF happened much earlier after the copper surface being irradiated by electron beam. This means that electron beam irradiation not only increased the surface wettability but also changed the surface structure of copper surface.

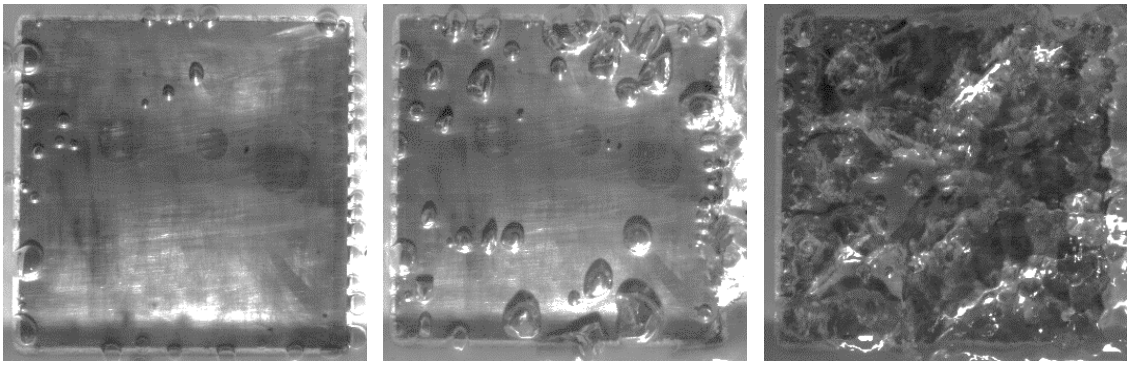

0.019 Mw/m^2 0.09 Mw/m^2 0.18 Mw/m^2

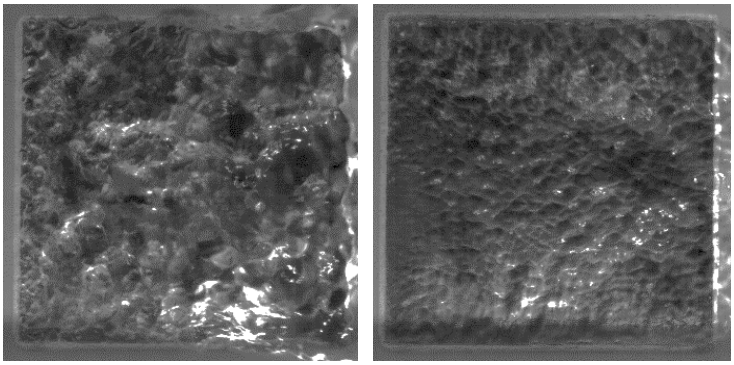

0.31 Mw/m^2 CHF

Figure 6-12 Boling process of bare surface after 1000 kGy electron beam irradiation at 320kg/(m^2·s) .

As the copper surface of honeycomb test section was also irradiated by electron beam irradiation, it is believed that the CHF degradation of honeycomb is also due to surface change of copper surface by electron beam irradiation.

Based on the electron beam experimental results and boiling phenomena, it is believed that the electron beam irradiation has another effect on copper surface and influences the CHF in saturated downward-facing flow boiling in addition to RISA effect. So then we focus on investigating electron beam effect on CHF of bare surface in saturated downward-facing conditions using different irradiation does.

6.4.1 CHF values under different electron beam irradiation doses

Based on above electron beam irradiation experimental results, it is believed that that electron beam irradiation may change the surface structure of copper heat surface which lead to the degradation of CHF in downward-facing flow boiling condition. Then, different electron beam irradiation doses (300kGy, 1000kGy, and 3000kGy) were used to investigate the irradiation effect on CHF of bare surface saturated downward-facing condition. The experiments are also all conducted at 320kg/(m^2·s).

The boiling curves of the non-irradiated and irradiated experiments are shown in figure 6-13. As it can be seen, the boiling curves are very close to each other which means there is no big difference in heat transfer efficient before and after electron beam irradiation. However, the CHF values have very big difference. All the CHF values decrease after irradiation.

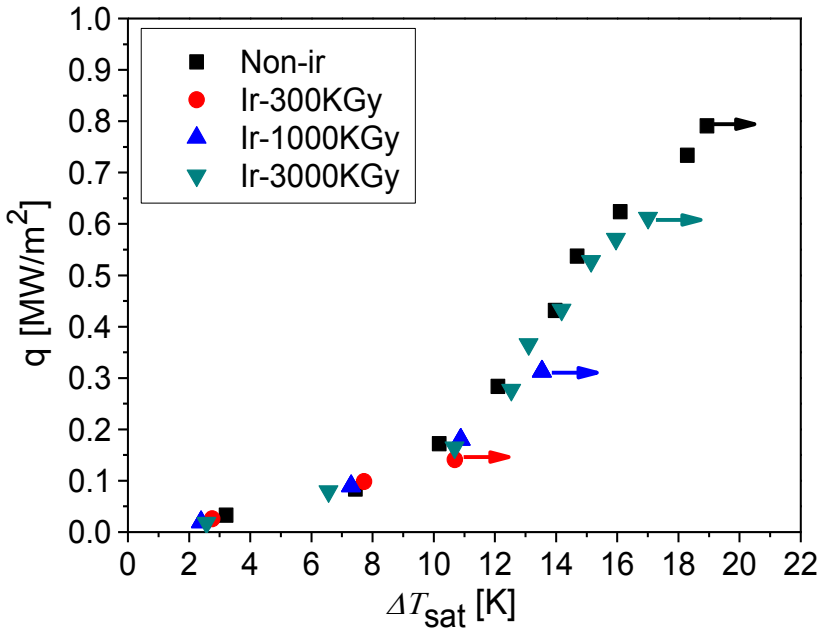

Figure 6-13: Boling curves of bare surface after different irradiation doses at 320kg/(m^2·s).

Figure 6-14 shows the CHF values change as irradiation dose increase. The CHF values decrease by 82%, 61%, and 23% at 300, 1000, and 3000 kGy, respectively. The CHF value at 300 kGy is 0.14 MW/m^2, which is very low.

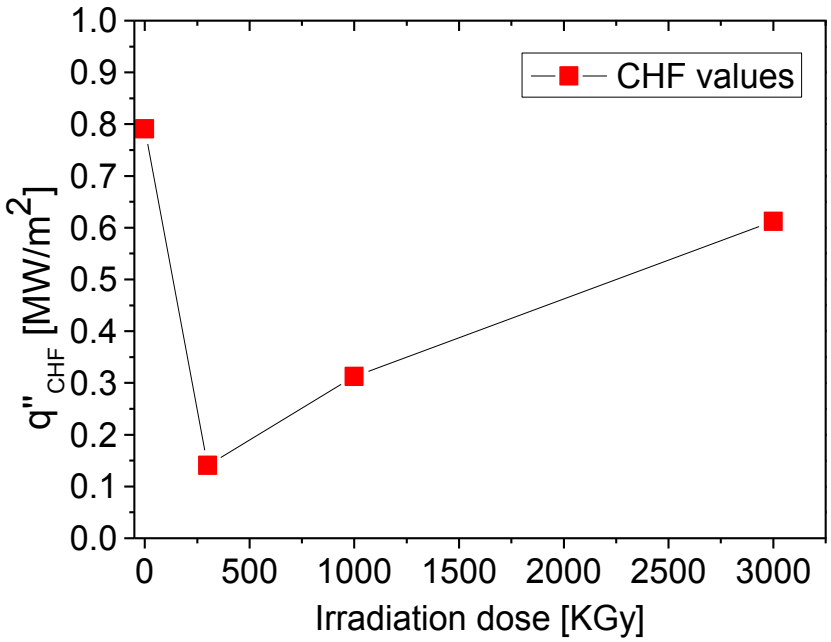

Figure 6-14: CHF values change as irradiation doses at 320kg/(m^2·s).

It is noted that CHF values decrease more at low irradiation dose condition. Again, the boiling videos are used to find the reason. Figure 6-15 shows the boiling process of bare surface after 300 kGy electron beam irradiation at 320kg/(m^2·s). It can be seen that at same low heat flux condition, many more tiny bubbles generated on the copper heat surface than the non-irradiation condition in figure 4-5 or 1000 kGy condition in figure 6-12. For example, many tiny bubbles generated on the copper heat surface and almost covered the heat surface when the heat flux is around 0.098 Mw/m^2 which is a very low heat flux. As a result, CHF happens at a very low heat flux and the CHF value is lower than that of irradiated 1000 kGy condition.

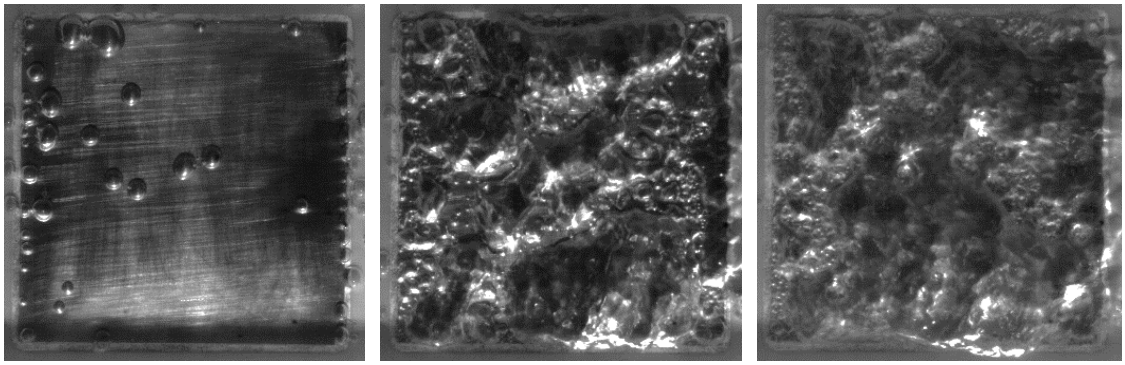

0.025 Mw/m^2 0.098 Mw/m^2 0.14 Mw/m^2

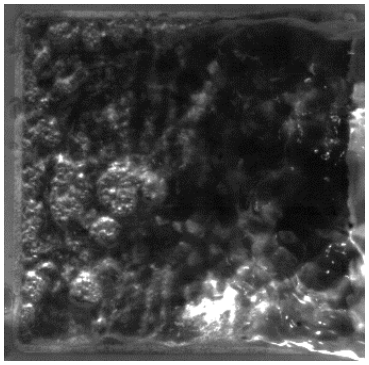

CHF

Figure 6-15: Boling process of bare surface after 300 kGy electron beam irradiation at 320kg/(m^2·s).

Figure 6-16 shows the boiling process of bare surface after 3000 kGy irradiation. It can be seen that there are not many tiny bubbles generated on the surface at low heat flux as irradiated 300 kGy condition. The boiling phenomenon is similar to that of non-irradiated condition. Big bubbles are generated on the heat surface and taken away quickly. The heat surface is not uncovered by the bubbles until a higher heat flux. As a result, the CHF value of this condition is only decreased by 23% compared with that of non-irradiated condition.

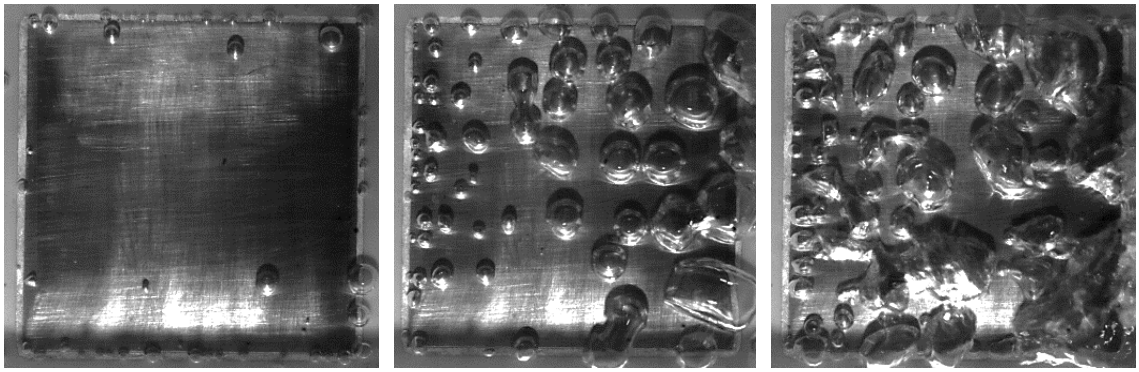

0.018 Mw/m^2 0.08 Mw/m^2 0.16 Mw/m^2

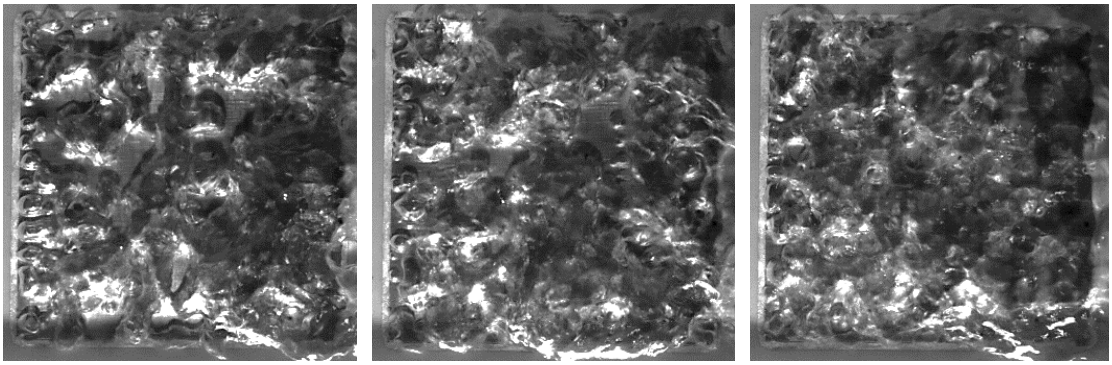

0.27 Mw/m^2 0.37Mw/m^2 0.52 Mw/m^2

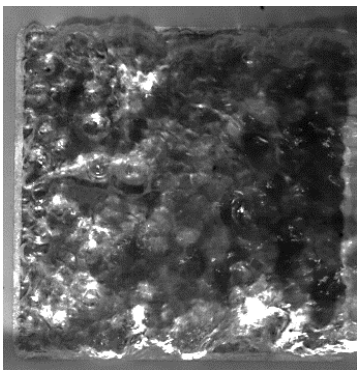

CHF

Figure 6-16: Boling process of bare surface after 3000 kGy electron beam irradiation at 320kg/(m^2·s).

In order to investigate the phenomena encountered for the low dose irradiation more deeply and check the repeatability of the experiment, a new bare surface test section was manufactured and the irradiation experiments were repeated with lower irradiation doses. Also, the non-irradiation experiment was conducted before that for comparison. The copper surface was irradiated at 30kGy, 100kGy, 300kGy and 1000kGy. The experiments are all conducted at 320kg/(m^2·s) which is same as before.

Figure 6-17 shows the boiling curves of the new test section before and after electron beam irradiation. It is similar to the old section that the heat transfer efficiency of these five conditions are almost the same but there is a big difference in CHF value. For the non-irradiation case, the CHF value is around 0.8 MW/m^2 which is almost same as that of old test section without irradiation. All CHF values for the irradiated cases are decreased. The CHF values are decreased by 62%, 70%, 46%, and 46% at 30kGy, 100kGy, 300kGy and 1000kGy, respectively, compared to that of non-irradiated surface.

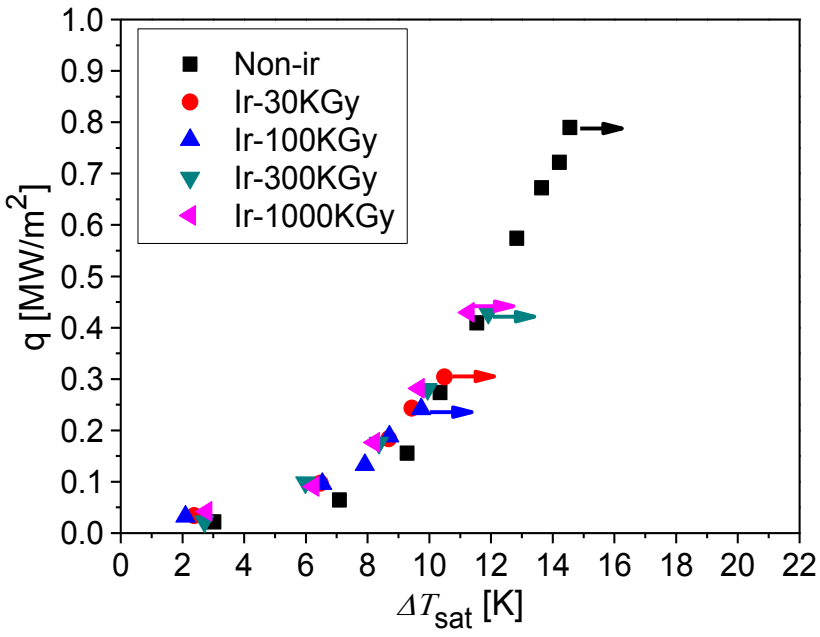

Figure 6-17: Boling curves of new surface after different irradiation doses at 320kg/(m^2·s).

Figure 6-18 shows the CHF values of new test section change as irradiation dose increase. The tendency is similar as that of old test section. CHF values also decrease more at lower irradiation doses conditions. CHF values decrease by 62%, 70%, 46%, and 46% at 30, 100, 300, and 1000 kGy, respectively, compared to that of the non-irradiated surface.

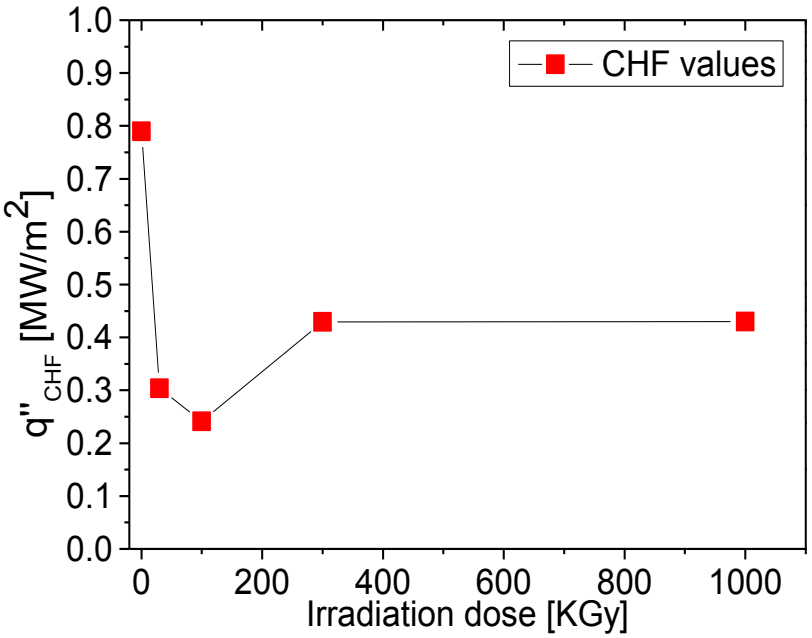

Figure 6-18: CHF values change of the new test section as irradiation doses at 320kg/(m^2·s).

Figure 6-19 shows the boiling process of new bare surface test section without irradiation condition at 320kg/(m^2·s) flow rate. It is similar to that of old test section without irradiation at 320kg/(m^2·s) flow rate. Big bubbles generated on the heat surface and were taken away by water quickly. The heat surface was not uncovered by the bubbles until a high heat flux. As a result, CHF happens when the heat flux is around 0.8 MW/m^2 which is higher than irradiation condition.

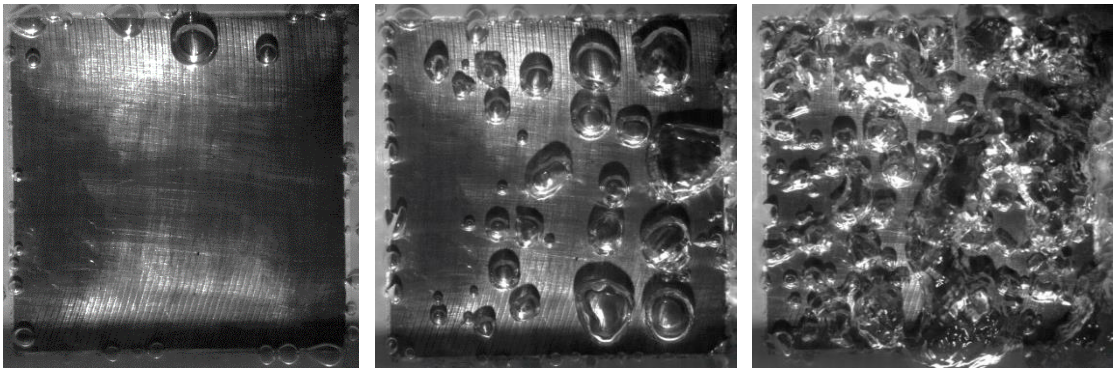

0.02 Mw/m^2 0.06 Mw/m^2 0.16 Mw/m^2

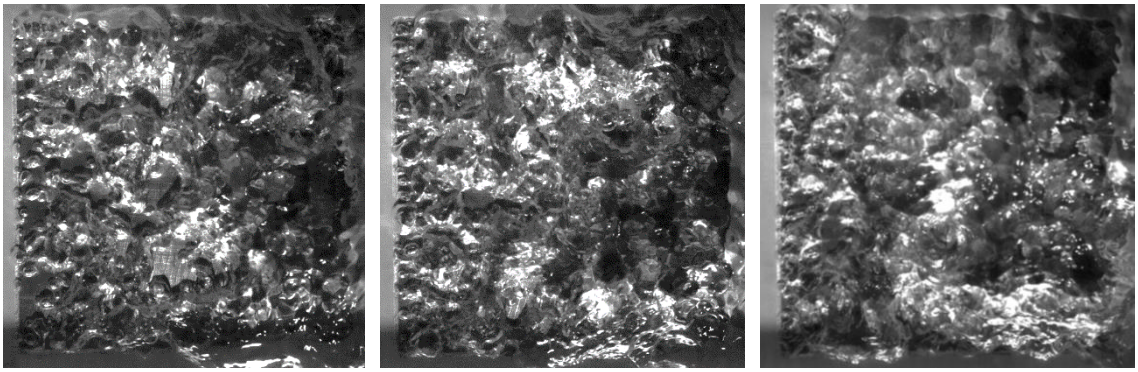

0.27 Mw/m^2 0.41 Mw/m^2 0.57 Mw/m^2

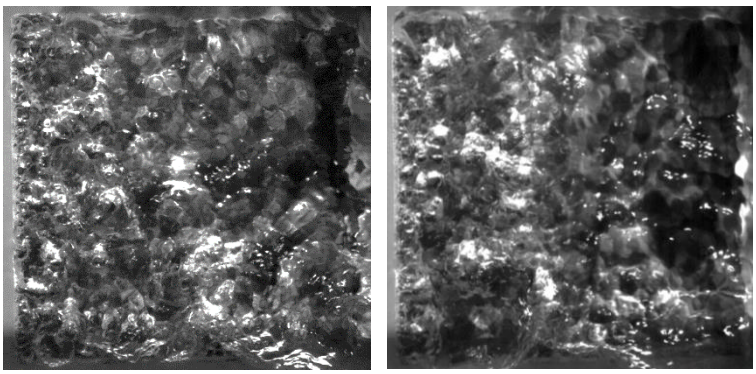

0.57 Mw/m^2 CHF

Figure 6-19: Boling process of new test section without irradiation at 320kg/(m^2·s).

Figure 6-20 and Figure 6-21 shows the boiling process of new bare surface test section after 30 kGy and 100 kGy irradiation. As it can be seen, many tiny bubbles are generated on the heat surface at similar low heat flux for these two doses conditions. As a result, the CHF values of this two conditions are very low.

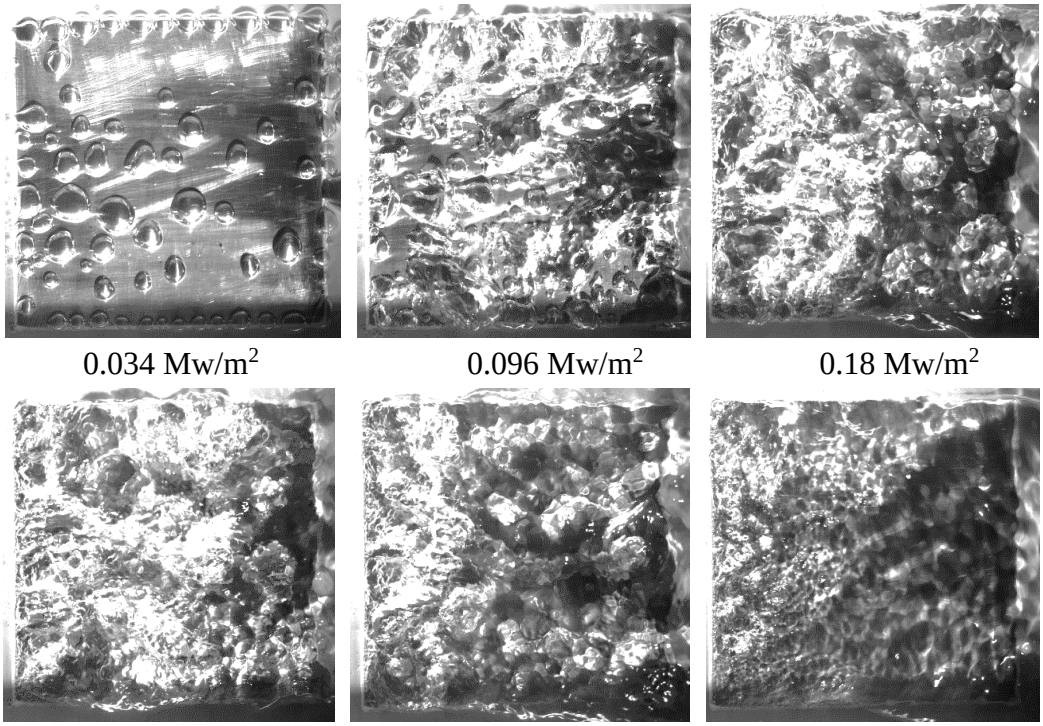

0.034 Mw/m^2 0.096 Mw/m^2 0.18 Mw/m^2

0.24 Mw/m^2 0.3 Mw/m^2 CHF

Figure 6-20: Boling process of new test section after 30 kGy irradiation at 320kg/(m^2·s).

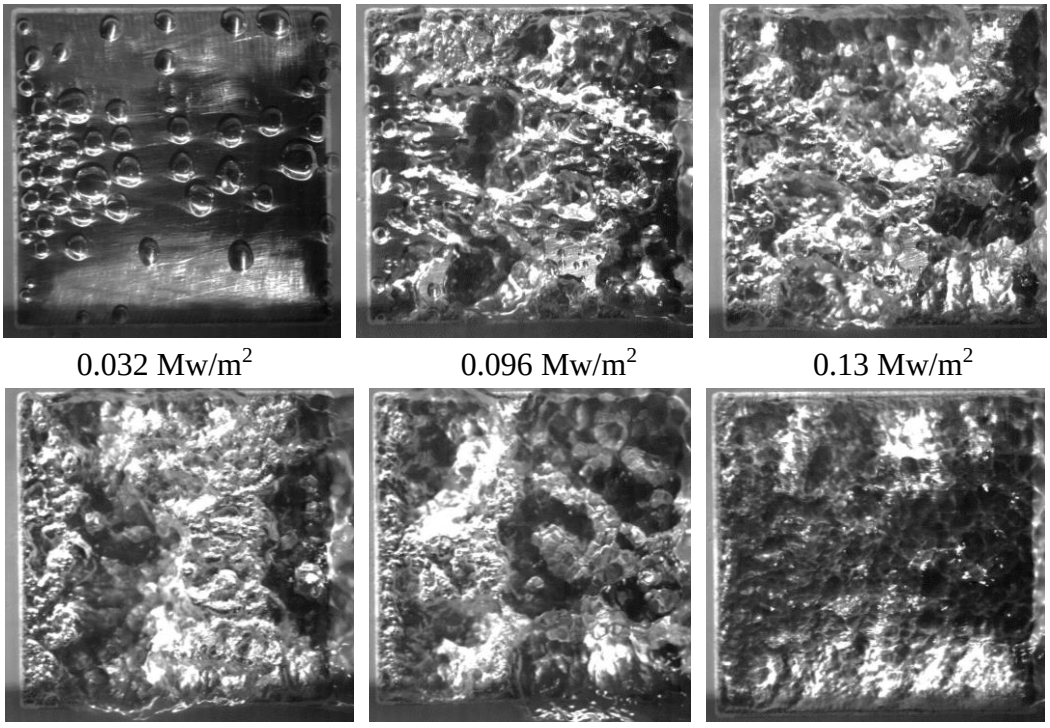

0.032 Mw/m^2 0.096 Mw/m^2 0.13 Mw/m^2

0.18 Mw/m^2 0.24 Mw/m^2 CHF

Figure 6-21: Boling process of new test section after 100 kGy irradiation at 320kg/(m^2·s).

Figure 6-22 and Figure 6-23 shows the boiling process of new bare surface test section after 300 kGy and 1000 kGy irradiation. Comparing with that of non-irradiation condition, the nucleation sites number at same low heat flux of these two conditions increase. So the heat surface area uncovered by the bubbles at same low heat flux condition is smaller than that of non-irradiation condition, and CHF values of these two conditions decrease. The CHF values of this two conditions are about half of that non-irradiation condition. The nucleation sites number at same low heat flux of these two conditions are less than that of 30 kGy and 100 kGy irradiation condition. As a result, CHF values of these two conditions are smaller than that of non-irradiation condition but a little higher than that of 30 kGy and 100 kGy conditions.

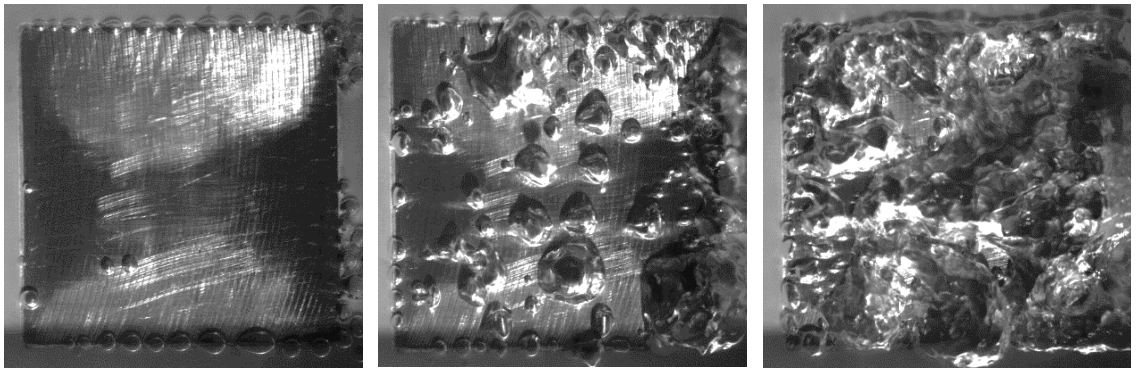

0.023 Mw/m^2 0.098 Mw/m^2 0.17 Mw/m^2

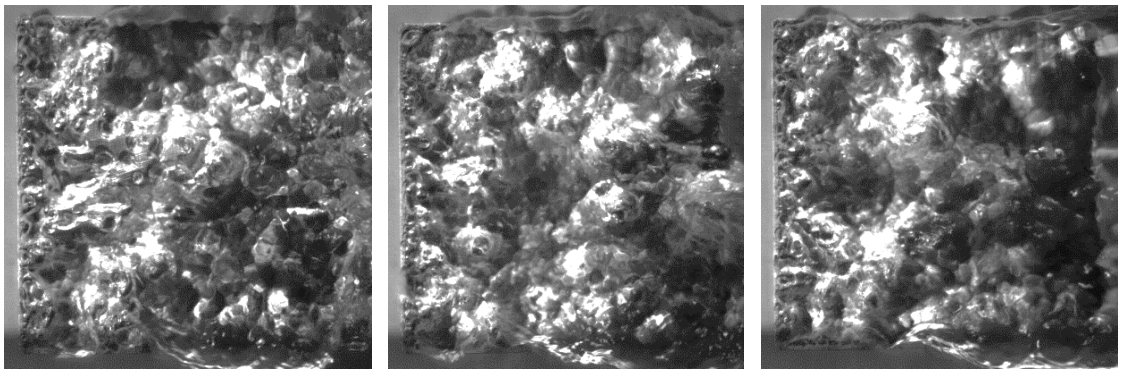

0.28 Mw/m^2 0.43 Mw/m^2 CHF

Figure 6-22: Boling process of new test section after 300 kGy irradiation at 320kg/(m^2·s).

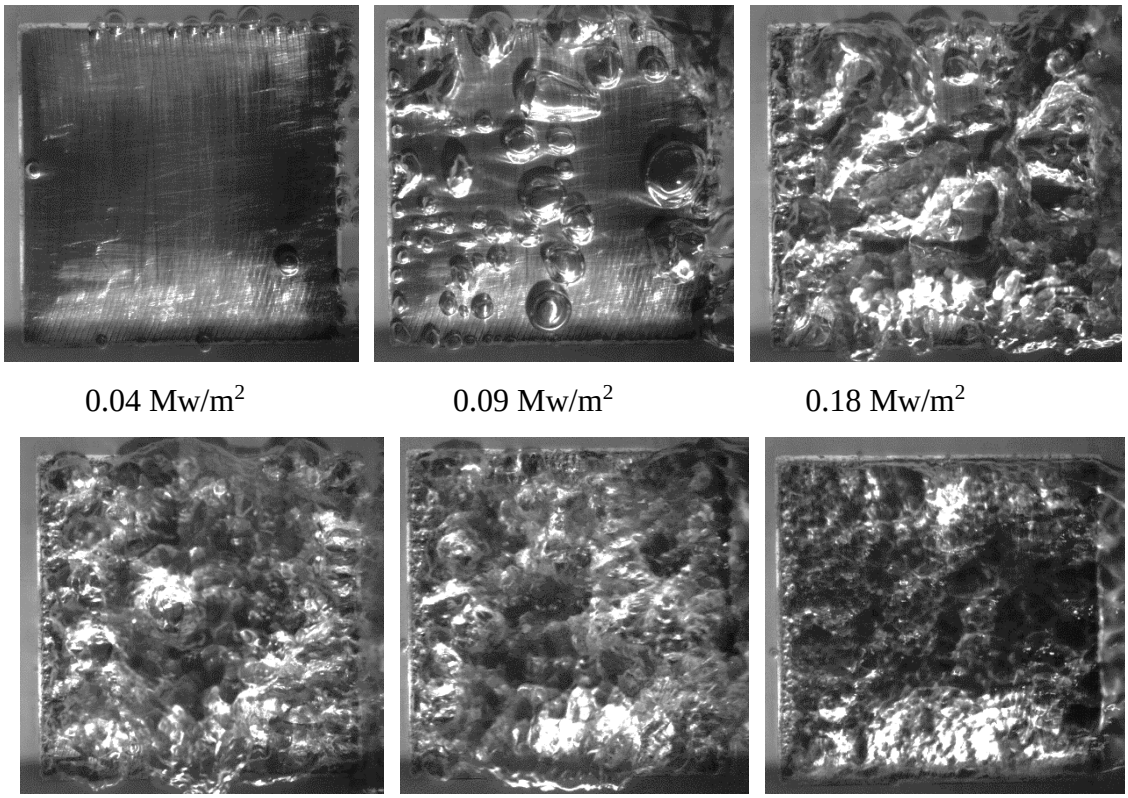

0.04 Mw/m^2 0.09 Mw/m^2 0.18 Mw/m^2

0.28 Mw/m^2 0.43 Mw/m^2 CHF

Figure 6-23: Boling process of new test section after 1000 kGy irradiation at 320kg/(m^2·s).

From the boiling phenomena, the reason of CHF degradation in saturated downward-facing flow boiling after electron beam irradiation is due to many more nucleation sites generating at same low heat flux compared to that of non-irradiation condition. More bubbles generate at low heat flux condition, more heat surface area covered by bubbles, earlier CHF happens. Compared to high irradiation dose conditions, low dose electron beam irradiation can generated more nucleation sites on the copper heat surface. As a result, CHF values in saturated downward-facing flow boiling decrease more at low irradiation dose than that of high irradiation dose condition.

6.4.2 Relation between CHF and nucleation site density in saturated downward-facing flow boiling

Griffith and Wallis found that re-entrant type cavities on the boiling surface are stable, easily activated nucleation sites [33]. It is widely believed that increasing the nucleation site density can enhance the nucleate boiling heat transfer and enhance CHF. Much work has been done for increasing the nucleate site density on the boiling surface, such as polishing, etching, and using coatings. Kurihara and Myers [34] showed that the nucleate boiling enhancement from the roughening was the result of increased active nucleation site density. Ammerman et al. [35] used a microporous coating to enhance flow boiling heat transfer and obtained an increase in both heat transfer coefficient and CHF. They attributed the enhancement to the increase in nucleation site density and bubble departure frequency. Chang [36] reported that the microporous coated surface containing numerous active augmented pool boiling heat transfer coefficients by 30% and increased CHF by about 100%. It is noted that You et al. [8] conducted the pool boiling experiment using nanofluids and obtained significant CHF enhancement (~200%), but the heat transfer coefficients did not show significant change. They cannot explain the CHF enhancement reason but they found that the average size of departing bubbles increases and the bubble frequency decreases significantly in nanofluids compared to those in pure water.

From our experimental results and observation of the boiling phenomena, we can find that a high nucleation site density does not necessarily imply high boiling heat transfer efficiency and CHF enhancement for saturated downward-facing flow boiling. From our observations, low dose irradiations of the boiling surfaces generated excessive number of nucleation site densities that led to a decrease in CHF.

As it is impossible to count the nucleation sites number on the heat surface near CHF condition as too many bubbles constantly covering the heat surface. The number of nucleation sites of the all cases at same low heat flux (around 0.08 Mw/m^2) was counted by carrying out high-speed imaging. During the recording time (0.3 s), all the nucleation sites that produced bubbles were counted. Figure 6-24 shows the relationship between the CHF values and the number of nucleation sites at approximately the same, low heat flux (around 0.08 Mw/m^2). From this graph, we can clearly see that low dose irradiation can generate considerably many more nucleation sites at similar heat fluxes and that an inverse relationship exists between the CHF values and the nucleation site density.

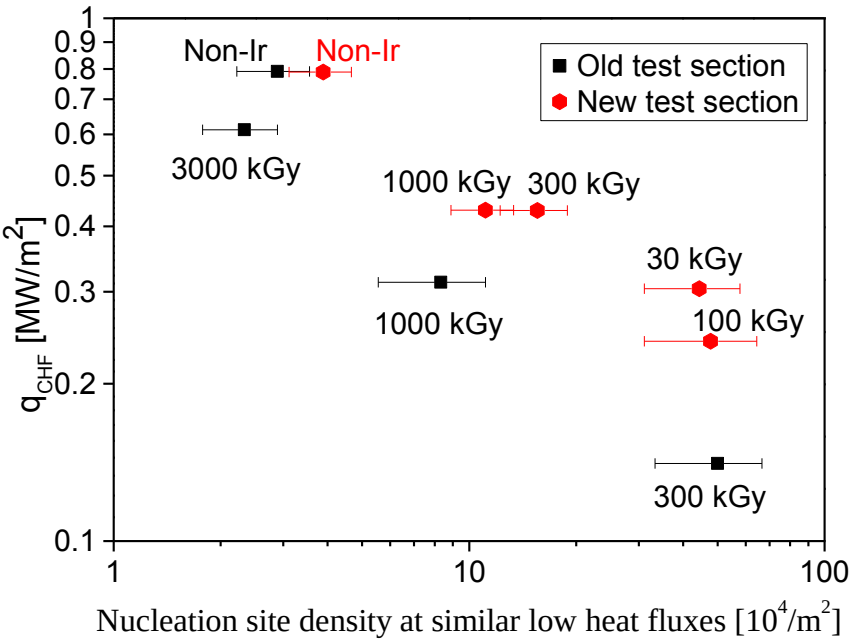

Figure 6-24: Relationship between nucleation site density at similar low heat fluxes and CHF values.

Considering the boiling phenomena, the reason why an increase in nucleation site density may lead to CHF reduction in saturated downward-facing flow boiling can be explained by concentrating on the following two-aspects：boiling surface coverage ratio

and bubble removal ability.

On one hand, if more nucleation sites generate at the same heat flux condition, the area covered by bubbles will increase. Here we define a parameter- bubble coverage area S_b, which represents the surface area covered by bubbles:

$$S_b = N\pi r_a^2 \tag{6-1}$$

N is the nucleation sites number, r_a is the average bubble departure radius. If the heat flux taken away by vaporization is the same at one moment, the vapor volume produced on the boiling surface V which can be expressed by below equation should be the same:

$$V = N \times \frac{4}{3}\pi r_a^3 \tag{6-2}$$

So the average bubble diameter has below relationship with the nucleation sites number at the same heat flux condition,

$$r_a \propto N^{-\frac{1}{3}} \tag{6-3}$$

So we can get:

$$S_b \propto N^{\frac{1}{3}} \tag{6-4}$$

As the nucleation site numbers increase at low irradiation doses conditions, the bubble covering area increases. This will make water supply to the heat surface harder and lead to CHF happen earlier.

On the other hand, for downward-facing flow boiling, bubble removal is very

important. If bubble cannot be removed quickly, a vapor film will be produced on the heat surface, CHF will soon happen. For downward-facing flow boiling condition, bubble removal is strongly depends on drag force.

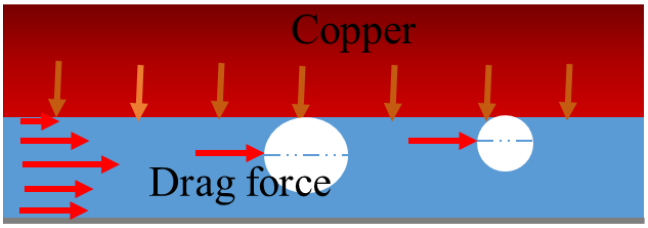

Figure 6-25: Diagram of drag force and velocity distribution in the channel.

The drag force on single bubble can be calculated using below equation:

$$F_D = \frac{1}{2}\rho_l u^2 C_D A \tag{6-5}$$

Where:

F_D = drag force [N]

ρ_l =density of the liquid [kg/m^3]

u =speed of the bubble relative to the fluid [m/s]

C_D = drag coefficient

A =cross sectional area [m^2]

If the shape of bubble is assumed to be spherical, the cross sectional area can be expressed as below:

$$A = \pi r_a^2 \tag{6-6}$$

According to equation 6-3, if more nucleation sites are generated at low heat flux in saturated down-ward-facing condition, the bubble sizes will decrease. So we can get:

$$A \propto N^{-\frac{2}{3}} \tag{6-7}$$

Besides, the velocity in the channel cross-section is not the same due to wall friction. The velocity near the wall is lower than that in the center. The velocity distribution in the cross-section can be expressed as below:

$$\frac{u}{u_{max}} = \left(\frac{y}{h}\right)^{1/} \tag{6-8}$$

Where；

u_{max} = maximum velocity in the channel [m/s]

y = distance from the channel wall [m]

h = half of the channel height [m]

If we use average bubble radius representing distance from the channel wall, we can get:

$$u \propto r_a^{\frac{1}{7}} \tag{6-9}$$

Substituting equation 6-3 into equation 6-9, we can get:

$$u \propto N^{-\frac{1}{21}} \tag{6-10}$$

Subtitling equation 6-7 and equation 6-10 into equation 6-5, we can get that;

$$F_D \propto N^{-0.76} \tag{6-11}$$

According to equation 6-11, if the nucleation sites number on the surface increases,

the drag force imposed on each bubble become smaller. The bubble removal ability in downward-facing flow boiling decrease at same water flow rate.

Equation 6-4 reveals that the boiling coverage area increase as nucleation sites number increase. Equation 6-11 reveals that bubble removal ability decrease as nucleation sites number increase. These above two aspects make water supply water to the boiling surface, which is very important for downward-facing flow boiling CHF. That is why all CHF values have an inverse relationship with nucleation site density in saturated downward-facing flow boiling condition.

6.4.3 Discussion of electron beam irradiation on copper surface

From the boiling phenomena, it is found that many more nucleation sites will be generated at same heat flux after electron beam irradiation, especially at low dose irradiation condition. One potential reason of this is that electron beam irradiation destroys the copper surface or tiny oxide layer and creates more cavities which can become nucleation sites as seen in figure 6-26.

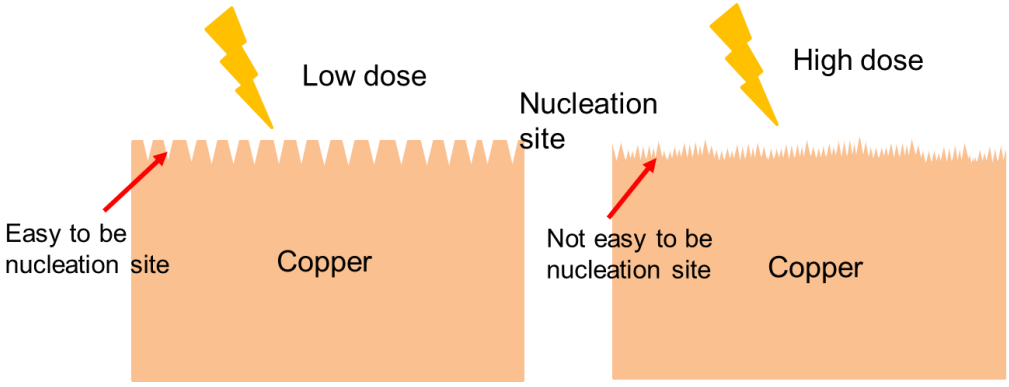

Figure 6-26: Assumption of electron beam irradiation effect on copper surface.

At low dose condition, many small cavities that can be nucleation sites are generated. However, as the irradiation style is scanning, the surface will be irradiated by too times

and the surface may be become smooth again if the irradiation dose is too high. As a result, number of cavities which can be nucleation sites on the copper surface decrease at high dose irradiation condition compared to low irradiation dose condition.

To verify the assumption, Scanning Electron Microscope (SEM) is used to observe the copper surface condition before and after electron beam irradiation. Four small copper test pieces were manufactured and the surface of them are polished using sandpaper. Then three of them were irradiated by 30 kGy, 300 kGy and 3000 kGy electron beam irradiation respectively. After the electron beam irradiation, the surfaces of four copper test pieces were observed using SEM.

Figure 6-27 shows the SEM images of the non-irradiated surface and irradiated copper surfaces. The magnification times is 4000 times. This is the largest magnification times can be used due to the performance of the SEM we used. As seen in figure 6-27, it is hard to find the difference between the four surfaces in small cavities on the copper surface. From these images, we cannot even distinguish the cavities which can be nucleation sites due to magnification times. The size of cavities which can be nucleation sites in saturated flow boiling condition is believed to be much smaller than 10μm. Thus, more work is needed with the help of advanced surface observation equipment to verify the assumption about electron beam effect on copper surface structure.

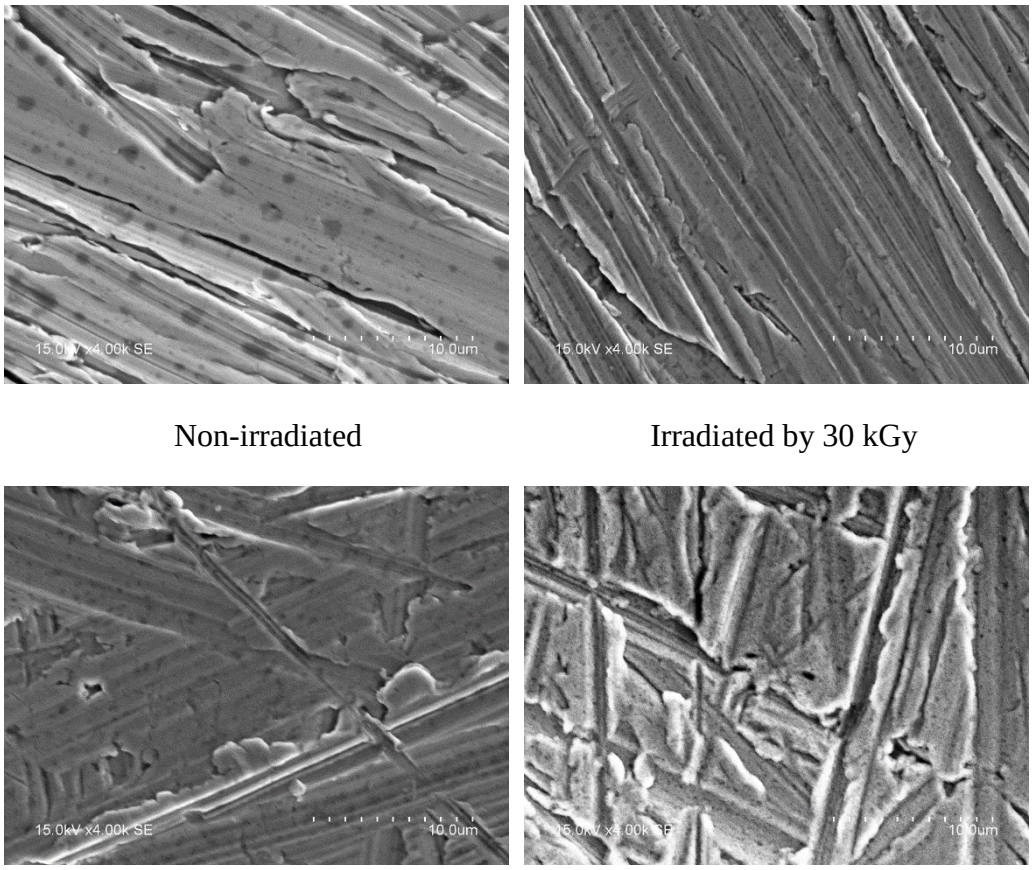

Non-irradiated Irradiated by 30 kGy

Irradiated by 300 kGy Irradiated by 3000 kGy

Figure 6-27: SEM images of non-irradiated and irradiated copper surfaces.

6.5 Summary of irradiation experiment

Experimental research about irradiation effect of Gamma-ray irradiation and electron beam irradiation on CHF in downward-facing flow boiling were conducted.

CHF values of bare surface and porous honeycomb plates do not have any increase at 640kg/m^2-s after the surfaces being irradiated by Gamma-ray even though the surface wettability of copper surface and metal porous plate increased significantly due to RISA effect. This experimental result reveals that CHF in saturated downward-facing flow boiling cannot be enhanced just by surface wettability increase unlike pool boiling

condition. On one hand, water supply ability in saturated downward-facing boiling is strong enough due to the high mass flow rate. On the other hand, comparing to water supply ability, bubble removal which will leave space for water supply to the heat surface is more important for downward-facing flow boiling CHF.

Surface wettability also increased significantly after the surfaces being irradiated by electron beam. However, this study found that CHF values in downward-facing flow boiling decrease after the surfaces are irradiated by electron beam while the heat removal is almost the same. CHF values of bare surface decrease more at the low irradiation doses range (30-300kGy) compared to high irradiation doses range (1000-3000kGy). The main reason is that low dose electron beam irradiation can generate many more nucleation sites on the boiling surface which increases the bubble coverage area and decreases bubble removal ability. In this case, water supply to the boiling surface becomes difficult and CHF occurs at low heat flux. This is contrary to traditional opinion that high nucleation density will increase nucleate boiling heat transfer and enhance CHF.

7. Conclusion and future work

7.1 Conclusion

There is a strong need to find a way to enhance the CHF for IVR strategy due to the nuclear plant power increase in recent years. Previous research about enhancing CHF in downward-facing flow boiling condition is rare. In this study, experimental research about enhancing CHF in saturated downward-facing flow boiling by attaching a metal porous honeycomb plate on the heat surface and irradiation effect were conducted.

For using a metal porous honeycomb plate to enhance CHF in saturated downward-facing flow boiling, below conclusions are obtained:

1. CHF in saturated downward-facing flow boiling can be enhanced by attaching a metal porous honeycomb plate with a 1.7 mm hole diameter and 2.5 mm pitch on the heat surface at all four flow rates (160-1280 kg/m^2-s), but the CHF increase ratios decrease as the flow rate increases, from approximately 2.4 at lowest flow rate to around 1.1 at highest flow rate.

2. CHF enhancement of porous honeycomb plate is due to honeycomb structure which can slow down coalescing of bubbles as well as additional water supply through the porous media. At highest flow rate (1280 kg/m^2-s), both of these two enhancement effects become weak.

3. The boiling area reduces and equals to the total hole area of the honeycomb plate when a honeycomb plate is attached on the heat surface. This has a negative effect on CHF in downward-facing flow boiling. If the hole area of the honeycomb plate is too low

(less than 20%), CHF of porous honeycomb plates may be lower than that of bare surface.

4. There are two water supply ways for porous honeycomb plate: from the perimeter of the holes and from the porous media. Water supply through the porous media is more important for a small hole diameter comparing to a large hole diameter condition. Water supply through the perimeter become to the main way when the pitch/hole ratio is small.

5. Among different honeycomb plates, the porous honeycomb plate with a 1.7mm hole diameter, 2.5mm hole pitch (100μm raw particle size) can obtain a maximum enhancement effect due to a relative high boiling area ratio and a suitable hole diameter.

For irradiation effect on CHF in saturated downward-facing flow boiling, below conclusions are obtained:

1. CHF values of bare surface does not have any increase at 640kg/m^2-s after the boiling surface being irradiated by around 1000 kGy Gamma-ray even though the surface wettability of copper surface increased significantly due to RISA effect. This experimental result reveals that CHF in saturated downward-facing flow boiling cannot be enhanced just by surface wettability increase. On one hand, water supply ability in saturated downward-facing boiling is strong enough due to the high mass flow rate (640 kg/(m^2·s). On the other hand, comparing to water supply ability, bubble removal which will leave space for water supply to the heat surface is more important for downward-facing flow boiling CHF.

2. CHF values of porous honeycomb plates cannot be further increased at 640 kg/m^2-s after the copper surface being irradiated by Gamma-ray or both of the copper surface and porous plate being irradiated by Gamma-ray even though the surface wettability of

copper surface and metal porous plate increased significantly due to RISA effect. The reason is similar to that of bare surface case.

3. Surface wettability of copper surface and metal porous plate both increase significantly after the surfaces being irradiated by 1000 kGy electron beam. However, this study found that CHF values of bare surface and porous honeycomb plates in saturated downward-facing flow boiling decrease a lot whereas heat removal almost remains the same after the surfaces being irradiated by 1000 kGy electron beam at 320 kg/m^2-s due to more nucleation sites generated on the copper boiling surface by electron beam irradiation.

4. The CHF values of bare surface at 320kg/m^2-s decrease more in the low electron beam irradiation dose range (30 – 300 kGy) than in the high electron beam irradiation dose range (1000 – 3000 kGy). This is mainly because low dose electron beam irradiation can generate considerably more nucleation sites on the copper boiling surface than high dose electron beam irradiation, which increases the bubble surface coverage area and decreases the bubble removal ability. In this case, water supply to the boiling surface becomes difficult and the CHF occurs at a low heat flux. It is found that CHF values have an inverse relationship with nucleation site density in saturated downward-facing flow boiling condition which is contrary to the traditional opinion that a high nucleation density increases nucleate boiling heat transfer and enhances the CHF.

7.2 Future work

This study shows that CHF enhancement by attaching a metal porous honeycomb

plate on a small heat surface in saturated downward-facing flow boiling is feasible. The out surface of the reactor vessel is hemispheric and the area is really large. Can CHF be enhanced by attaching a metal porous honeycomb plate on the heat surface when the heat surface is downward-facing hemispheric and the heat surface size is very large? If it can be enhanced, to what extent it will be enhanced? Future work is needed to answer these questions.

Many studies have shown that radiations can change the mechanical properties of metallic materials, such as hardness, embrittlement, and susceptibility to environmentally induced cracking. For convenience, most previous experimental studies on heat transfer and CHF related to nuclear reactors have been conducted using an electric heater without any irradiation. Therefore, the effect of irradiation on heat transfer and CHF has not received sufficient attention even though it is vital to the safety of the reactor. In this study, CHF in downward-facing flow boiling degraded a lot after the copper surface being irradiated by electron beam, especially at low dose condition. To verify the assumption about electron beam effect on copper surface structure, more work is needed with the help of advanced surface observation equipment. Research about irradiation effect on CHF in flow boiling with other surface material (for example, Zirconium alloy) should be continually conducted as it is important to the safety of the reactor.

Acknowledgement

It is a great pleasure for me to study in the department of Nuclear Engineering and Management at the University of Tokyo. The study time is very enjoyable and exciting.

I would like to thank Professor Koji Okamoto for his excellent guidance and help. He is so wise, knowledgeable and experienced. He gives me a lot of assistance and guidance about my research. It is my pleasure to be his student.

I would like to thank my committee members for taking the time out of their busy schedules to attend my presentations and for providing suggestions regarding my research.

I would like to thank Associate Professor Nejdet Erkan and Dr. Abdul R. Khan for their assistance and help during my research. Associate Professor Nejdet Erkan gives me a lot of helpful advices.

I would like to thank Mr. Haiguang Gong for his assistance in doing experiments.

I would like to thank all members of Okamoto laboratory. They give me a lot of help during the past three years.

Finally, I am very thankful and grateful to my family members for their support and love.

References

1. Nuclear safety in light water reactors: Severe accident phenomenology[M]. Academic Press, 2011.

2. Theofanous T G, Liu C, Additon S, et al. In-vessel coolability and retention of a core melt[J]. Nuclear Engineering and Design, 1997, 169(1-3): 1-48.

3. Dinh T N, Tu J P, Salmassi T, et al. Limits of coolability in the AP1000-related ULPU-2400 configuration V facility[C]//10th International Topical Meeting on Nuclear Reactor Thermal Hydraulics, NURETH10, Oct. 2003: 5-11.

4. Zuber N. Hydrodynamic aspects of boiling heat transfer (thesis)[R]. California. Univ., Los Angeles; and Ramo-Wooldridge Corp., Los Angeles, 1959.

5. Haramura Y, Katto Y. A new hydrodynamic model of critical heat flux, applicable widely to both pool and forced convection boiling on submerged bodies in saturated liquids[J]. International Journal of Heat and Mass Transfer, 1983, 26(3): 389-399.

6. Theofanous T G, Dinh T N, Tu J P, et al. The boiling crisis phenomenon: Part II: dryout dynamics and burnout[J]. Experimental Thermal and Fluid Science, 2002, 26(6): 793-810.

7. Rohsenow W M, Griffith P. Correlation of maximum heat flux data for boiling of saturated liquids[R]. Cambridge, Mass.: Massachusetts Institute of Technology, Division of Industrial Cooperation,[1955], 1955.

8. You S M, Kim J H, Kim K H. Effect of nanoparticles on critical heat flux of water in pool boiling heat transfer[J]. Applied Physics Letters, 2003, 83(16): 3374-3376.

9. Trisaksri V, Wongwises S. Critical review of heat transfer characteristics of nanofluids[J]. Renewable and sustainable energy reviews, 2007, 11(3): 512-523.

10. Wu J M, Zhao J. A review of nanofluid heat transfer and critical heat flux enhancement—research gap to engineering application[J]. Progress in Nuclear Energy, 2013, 66: 13-24.

11. Ahn H S, Kim M H. A review on critical heat flux enhancement with nanofluids and surface modification[J]. Journal of Heat transfer, 2012, 134(2): 024001.

12. Kim H. Enhancement of critical heat flux in nucleate boiling of nanofluids: a state-of-art review[J]. Nanoscale research letters, 2011, 6(1): 415.

13. Cooke D, Kandlikar S G. Effect of open microchannel geometry on pool boiling enhancement [J]. International Journal of Heat and Mass Transfer, 2012, 55(4): 1004-1013.

14. Honda H, Wei J J. Enhanced boiling heat transfer from electronic components by use of surface microstructures [J]. Experimental Thermal and Fluid Science, 2004, 28(2): 159-169.

15. Ahn H S, Lee C, Kim H, Jo H J, Kang S H, Kim J, Shin J, Kim M H. Pool boiling CHF enhancement by micro/nanoscale modification of zircaloy-4 surface [J]. Nuclear Engineering and Design, 2010, 240(10): 3350-3360.

16. Coursey J S, Kim J, Boudreaux P J. Performance of graphite foam evaporator for use in thermal management [J]. Journal of Electronic Packaging, 2005, 127(2): 127-134.

17. Hwang G S, Kaviany M. Critical heat flux in thin, uniform particle coatings [J]. International Journal of Heat and Mass transfer, 2006, 49(5): 844-849.

18. Li C, Peterson G P. Parametric study of pool boiling on horizontal highly conductive microporous coated surfaces [J]. Journal of Heat Transfer, 2007, 129(11): 1465-1475.

19. Ahn H S, Lee C, Kim J, Kim M H. The effect of capillary wicking action of micro/nano structures on pool boiling critical heat flux [J]. International Journal of Heat and Mass Transfer, 2012, 55(1): 89-92.

20. Mori S, Utaka Y. Critical heat flux enhancement by surface modification in a saturated pool boiling: A review[J]. International Journal of Heat and Mass Transfer, 2017, 108: 2534-2557.

21. Liter S G, Kaviany M. Pool-boiling CHF enhancement by modulated porous-layer coating: Theory and experiment [J]. International Journal of Heat and Mass Transfer, 2001, 44(22): 4287-4311.

22. Jaikumar A, Kandlikar S G. Enhanced pool boiling for electronics cooling using porous fin tops on open microchannels with FC-87 [J]. Applied Thermal Engineering, 2015, 91: 426-433.

23. Mori S, Okuyama K. Enhancement of the critical heat flux in saturated pool boiling using honeycomb porous media [J]. International Journal of Multiphase Flow, 2009, 35(10): 946-951.

24. Rainey K N, Li G, You S M. Flow boiling heat transfer from plain and microporous

coated surfaces in subcooled FC-72[J]. Journal of Heat Transfer, 2001, 123(5): 918-925.

25. Imai Y, Koga T, Takamasa T, et al. Radiation Induced Surface Activity Phenomenon: 1st Report—Surface Wettability on Metal Oxides[C]//10th International Conference on Nuclear Engineering. American Society of Mechanical Engineers, 2002: 979-982.

26. Koga T, Imai Y, Takamasa T, et al. Radiation Induced Surface Activity Phenomenon: 2nd Report—Radiation Induced Boiling Enhancement[C]//10th International Conference on Nuclear Engineering. American Society of Mechanical Engineers, 2002: 975-977.

27. Okamoto K, Akiyama H, Madarame H, et al. Experimental study on radiation induced boiling enhancement for stainless steel plate[C]//10th International Conference on Nuclear Engineering. American Society of Mechanical Engineers, 2002: 929-932.

28. Gong H, Khan A R, Erkan N, et al. Critical heat flux enhancement in downward-facing pool boiling with radiation induced surface activation effect[J]. International Journal of Heat and Mass Transfer, 2017, 109: 93-102.

29. Zhang H, Mudawar I, Hasan M M. Experimental assessment of the effects of body force, surface tension force, and inertia on flow boiling CHF[J]. International Journal of Heat and Mass Transfer, 2002, 45(20): 4079-4095.

30. Was G S. Fundamentals of radiation materials science: metals and alloys[M]. Springer, 2016.

31. Zinkle S J, Was G S. Materials challenges in nuclear energy[J]. Acta Materialia, 2013, 61(3): 735-758.

32. Katto Y, Kurata C. Critical heat flux of saturated convective boiling on uniformly heated plates in a parallel flow[J]. International Journal of Multiphase Flow, 1980, 6(6): 575-582.

33. Griffith P, Wallis J D. The role of surface conditions in nucleate boiling[R]. Cambridge, Mass.: Massachusetts Institute of Technology, Division of Industrial Cooperation,[1958], 1958.

34. Kurihara H M, Myers J E. The effects of superheat and surface roughness on boiling coefficients[J]. AIChE Journal, 1960, 6(1): 83-91.

35. You S M. Enhancing small-channel convective boiling performance using a

microporous surface coating[J]. 2001.

36. Chang J Y, You S M. Enhanced boiling heat transfer from microporous surfaces: effects of a coating composition and method[J]. International Journal of Heat and Mass Transfer, 1997, 40(18): 4449-4460.